

**This PDF was created from the British Library's microfilm copy of the original thesis. As such the images are greyscale and no colour was captured.**

**Due to the scanning process, an area greater than the page area is recorded and extraneous details can be captured.**

**This is the best available copy**

DX

178814

**THE BRITISH LIBRARY**  
BRITISH THESIS SERVICE

**TITLE** THE DEVELOPMENT OF A CRYSTAL MODULATOR  
USING A MULTIPATH REFLECTION TECHNIQUE

**AUTHOR** Vassilis  
BOUGAS

**DEGREE** Ph.D

**AWARDING BODY** University of North London

**DATE** 1993

**THESIS NUMBER** DX178814

**THIS THESIS HAS BEEN MICROFILMED EXACTLY AS RECEIVED**

The quality of this reproduction is dependent upon the quality of the original thesis submitted for microfilming. Every effort has been made to ensure the highest quality of reproduction. Some pages may have indistinct print, especially if the original papers were poorly produced or if awarding body sent an inferior copy. If pages are missing, please contact the awarding body which granted the degree.

Previously copyrighted materials (journals articles, published texts etc.) are not filmed.

This copy of the thesis has been supplied on condition that anyone who consults it is understood to recognise that its copyright rests with its author and that no information derived from it may be published without the author's prior written consent.

Reproduction of this thesis, other than as permitted under the United Kingdom Copyright Designs and Patents Act 1988, or under specific agreement with the copyright holder, is prohibited.

C6.

ACADEMIC REGISTRY  
/ 1 JUL 1993  
RESEARCH

**THE DEVELOPMENT OF A CRYSTAL  
MODULATOR USING A MULTIPATH  
REFLECTION TECHNIQUE**

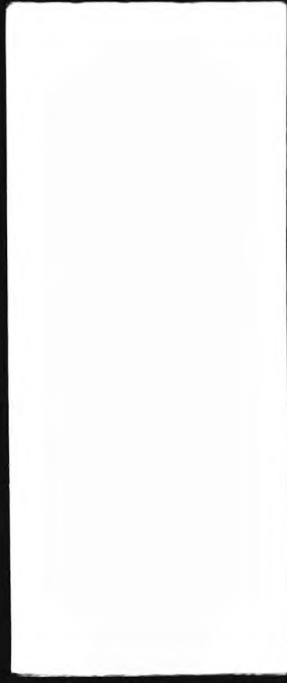
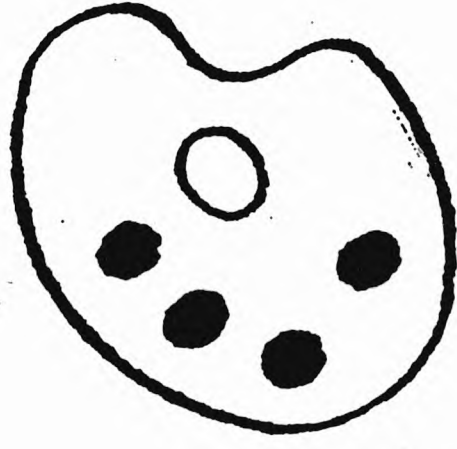
**VASSILIS BOUGAS**

A thesis submitted in partial fulfilment of the  
requirements of the University of North London  
for the degree of Doctor of Philosophy

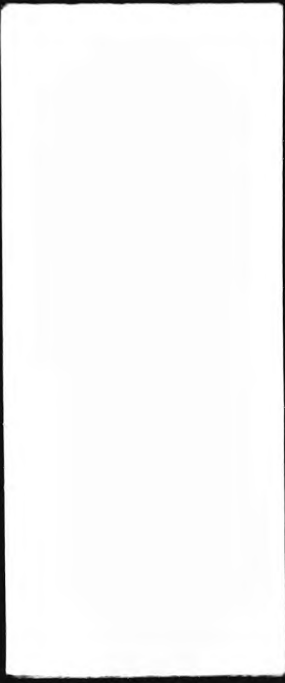
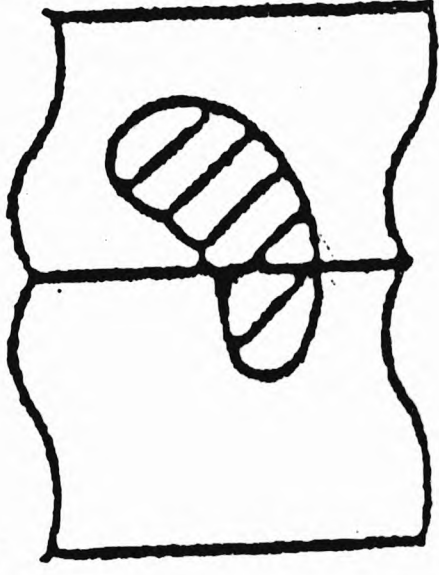
**THIS RESEARCH PROGRAMME WAS CARRIED OUT IN  
COLLABORATION WITH ELECTRO OPTIC DEVELOPMENTS LTD**

**JUNE 1993**

NUMEROUS ORIGINALS  
IN COLOUR



# VARIABLE PRINT QUALITY



#### ABSTRACT

An ADP lumped crystal transverse modulator has been developed, based upon a novel crystal cut, which operates at much lower driving voltages than presently available commercial state of the art modulators. With the latter, the modulation bandwidth is limited by the requirement for driving voltages in the range of 115V to 250V, which are difficult and expensive to produce using existing semiconductor technology. The reduction in driving voltage leads to an increased modulation bandwidth; low voltage wideband drivers are readily available. The modulator's novelty lies in a composite crystal scheme which allows a light beam to be reflected back and forth many times. The voltage requirement is reduced by a factor dependent on the number of times the light beam passes through the crystals. This modulator does not require a half wave plate and can therefore operate at any optical wavelength as is also the case with some of the existing designs. But in addition, unlike the existing designs, this novel modulator allows for multicolour multibeam operation. Using four ADP crystals (15.0mm length, 16.5mm width and 2.5mm thickness) a half wave voltage of 65V has been achieved after seven passes. The extinction ratios obtained were in the range of 50:1 to 100:1. A theory developed and supported by experimental results shows that the extinction ratio depends upon the angle of propagation of the light beam through the crystals. Improvements in this area are suggested. Finally, a technique for extending the operational bandwidth of any modulator is presented. The bandwidth of the multipath modulator was 70MHz.

## CONTENTS

### ABSTRACT

	PAGE
CHAPTER 1 INTRODUCTION	
1.1 The modulation of light and its applications	1
1.2 Types of modulators and switches	2
1.3 Current technology trends and justification for the present work	4
1.4 State of the art modulation systems	9
1.5 Aims, objectives and plan of thesis	12
CHAPTER 2 CRYSTAL OPTICS	
2.1 Introduction	15
2.2 The representation quadric	17
2.3 The index ellipsoid	19
2.4 The electro-optic effect	22
2.5 Application to modulators and the production of modulated light	23
2.5.1 Introduction	23
2.5.2 Phase modulation	24
2.5.3 Amplitude modulation	25
2.5.4 Polarisation modulation	26
CHAPTER 3 OVERVIEW OF MODULATORS AND CRYSTAL CUTS	
3.1 Choice of material	28
3.2 Existing crystal cuts	29
3.2.1 Longitudinal and transverse configurations	29
3.2.2 Longitudinal modulators, crystal class $\bar{4}2m$ (ADP)	29
3.2.3 Transverse modulators, crystal	32



class 42m (ADP)	
3.2.4 Transverse mode crystal cuts	35
3.2.4.1 45° z cut	35
3.2.4.2 45° y cut	38
3.2.4.3 45° y' cut	43
3.2.4.4 37° y' cut	45
CHAPTER 4 THE MULTIPATH REFLECTION TECHNIQUE	
4.1 Existing ADP transverse modulator crystal cuts - further comments	46
4.2 The multipath reflection technique	47
4.3 Multipath reflection technique crystal cuts	50
4.4 The (0°,45°,45°) cut	53
4.5 Calculation of the half wave voltage for the (0°,45°,45°) cut crystal	55
4.6 Calculation of the relative permittivity for the (0°,45°,45°) cut crystal	58
4.7 The composite modulator	59
CHAPTER 5 THE DESIGN OF MULTIPATH MODULATORS	
5.1 Basic considerations	66
5.2 Estimation of the modulator capacitance and bandwidth	71
5.3 Estimation of the transmission loss	72
5.4 Index matching oil considerations	73
5.5 Basic description of the modulator	75
5.5.1 The modulator body	76
5.5.2 The crystal case and the mounting of crystals	76
5.5.3 The mirror windows	81
5.5.4 Mirror alignment mechanics and considerations	82

## CHAPTER 6 EXPERIMENTAL

6.1 Tests performed before the assembly of the modulator	85
6.2 Assembly of the modulator	88
6.3 Initial set up and alignment procedures	89
6.4 Single pass operation, measurement of performance	91
6.4.1 Capacitance of the assembled modulator	91
6.4.2 Measurement of the half wave voltage	91
6.4.3 Dielectric strength tests	94
6.4.4 Transmission measurements	95
6.4.5 Extinction ratio measurements	96
6.5 Multipath operation	97
6.5.1 Initial set up and mirror alignment	97
6.5.2 Measurement of performance	100
6.5.2.1 Half wave voltage	100
6.5.2.2 Transmission measurements	102
6.5.2.3 Extinction ratio measurements	103
6.5.3 Discussions	104
6.5.4 An improved composite crystal scheme	105
6.5.5 Performance comparison of the six composite modulators	108
6.5.6 Second prototype, an improved modulator design	109
6.5.7 Measurement of performance of the second prototype	112
6.5.8 The extinction ratio of an electro-optic modulator	112
6.5.8.1 The characteristics of the laser light	113
6.5.8.2 The crystals	114
6.5.8.3 The engineering of the modulator	115

6.5.8.4	The correct alignment and use	117
6.5.9	The quest for better extinction ratio	117
6.5.10	Third prototype, a modulator with a better crystal alignment	120
6.5.11	Third prototype measurement of performance and conclusions	126
6.5.12	Performance with a reduced angle of incidence	129
6.5.13	An optimisation study for the angle of propagation of the laser beam	130
6.5.14	Discussion of the optimisation analysis results	134
6.5.15	The optimised modulator and its performance	139
CHAPTER 7 DOUBLE REFRACTION AND ASSOCIATED EFFECTS ON THE EXTINCTION RATIO OF (0°,45°,45°) MODULATORS		
7.1	The problem of double refraction	141
7.2	Double refraction in uniaxial crystals	142
7.3	Double refraction in (0°,45°,45°) crystals	143
7.4	The angle between the new and the old crystal polarisation directions	150
7.5	The effect of the rotation of axes in the modulator operation	154
7.6	The effect of spatial coherence in the modulator performance	164
7.7	The 45° y cut and 45° z cut modulators at oblique angle of incidence	168
7.8	Estimation of the extinction ratio for the (0°,45°,45°) cut modulator	169
7.9	Conclusions	170
CHAPTER 8 BEAM PROFILE AND TEMPERATURE STABILITY MEASUREMENTS		
8.1	Beam profile measurements	174
8.1.1	Introduction	174
8.1.2	Measurement method and results	175

8.1.3 Analysis of results and conclusions	176
8.1.4 Conclusions	182
8.2 Modulator temperature stability performance	182
8.2.1 Introduction	182
8.2.2 Method of measurement and results	184

CHAPTER 9 FREQUENCY RESPONSE OF AN ELECTRO-OPTIC MODULATOR

9.1 Introduction	189
9.2 A new bandwidth broadening technique	195
9.3 Experimental	201
9.4 Conclusions and suggestions for further work	205

CHAPTER 10 CONCLUSIONS AND SUGGESTIONS FOR FURTHER WORK

10.1 Discussion and conclusions	208
10.2 Suggestions for future work	212

ACKNOWLEDGEMENTS

REFERENCES

ADDITIONAL REFERENCES AND BIBLIOGRAPHY

## CHAPTER 1 INTRODUCTION

### 1.1 The modulation of light and its applications.

Since the invention of the laser by T. H. Maiman in 1960 the developments have been extremely rapid and although applications for lasers had a very slow start during the first decade it has become one of the major focuses in engineering. The applications of lasers have been multiplied to such an extent that new applications are being found almost every day<sup>(1)</sup>. Applications of the laser often require a means of controlling the amplitude, phase, frequency, or direction of a light beam at high speeds. This has led to a demand for special devices to achieve modulation and switching of an optical signal.

Applications of light modulators and switches<sup>(2,3)</sup> include wide band analogue optical communication systems, switching for digital information, recording on photographic film, information storage and processing, video disc mastering of photosensitised substrates. Other applications include ultra fast optical shuttering for selecting a single or multiple pulses from a mode locked train, pulse shaping, pulse slicing, pulse picking, beam deflection and scanning, frequency stabilisation, Q switching of lasers, colour separation and half tone screen generation for reprographics, high speed ellipsometry, DC to 30 GHz modulation systems. Finally modulators are also used for recorders in the entertainment industry that convert either real time

television camera or video tape recorder output to 35 or 70mm film, this allows electronic special effects and editing to be done before the picture is recorded, seismic recording for oil well exploration and others.

#### 1.2 Types of modulators and switches.

Although in many cases the same device can function as either a modulator or a switch a device is considered to be a modulator if its primary function is to impress information on a light wave by temporarily varying one of its properties. A switch on the other hand changes the spatial position of the light, or else turns it on and off. There are several types of modulators and switches and in general they can be divided in a number of ways. Probably the most important division is according to how the optical characteristics are changed. This can be done by the application of a force field to a material which can be mechanical, electrical, magnetic or without any of these three. Mechanical shutters, choppers, moving mirrors, elasto-optic and acousto-optic modulators are based on the application of mechanical forces or stress waves to a material through which a light beam propagates. The two basic types of acousto-optic modulators are the Bragg and the Raman-Nath configurations. Electro-optic modulators work with the principle that an external electric field modifies the polarising properties of the medium. They can be further subdivided<sup>(4)</sup> into Pockels, Kerr, Franz-Keldysh and Stark modulators according to the nature and physical origin of the electro-optic effect. Magneto-optic modulators are based onto

the principle that the presence of a magnetic field may also affect some optical processes in a medium. They can further be sub-divided into Zeeman, Cotton-Mouton, Voigt, Kerr and Faraday modulators. Finally passive or Dye modulators and switches may be accomplished by placing a saturable absorber in a laser cavity. They have the great advantage of being extremely simple but of limited life time and variability in the timing of the onset of laser action<sup>(5)</sup>. Modulators can be also classified relative to their size, as lumped or integrated. The first type is used to modulate powerful laser beams while the second type is used in fibre optic communications and in the field of optical computing. Also according to which particular property or parameter of the optical signal is changed, modulators can be further divided into amplitude or intensity, phase, frequency and polarisation modulators. It has to be mentioned that in principle any modulator can be operated as any of the above types depending on the arrangement of input and output ports.

Finally modulation of laser light is usually accomplished either internally or externally. Internal modulation is accomplished by directly influencing the source, for example by either placing a saturable dye absorber or a Pockel cell inside the laser cavity. External modulation is applied only after the radiation has emerged from the laser cavity. Internal modulation has the advantage of involving less source power, however switching at high enough rates is often limited by the external circuitry.

### 1.3 Current technology trends and justification for the present work.

Electro-optics is considered one of the fastest moving technologies in the history of electronics. Because of the very broad scope of the electro-optics field it is common practice to consider two distinct technologies as two separate areas of study, speed of progression and applications. The first area encompasses the traditional techniques and components to manipulate and process a laser beam or any other optical wave. This technology requires prisms, lasers, mirrors, lumped electro-optic modulators and detectors which occupy space and are relatively slow in terms of speed and bandwidth. These limitations were soon appreciated and as a result the concept of integrated optics emerged. The essential difference between the two technologies is that integrated optics are concerned with the transmission and manipulation of optical signals through waveguide structures and not through-the-air optical paths. The flourishing of integrated optics over the last 15 years is responsible for the development of the integrated lasers, modulators, switches, couplers, lenses and many others. The state of the art in high speed electro-optic modulators has long surpassed the 100GHz barrier at experimental stage. Integrated modulators offering bandwidths in excess of 20 GHz are now commercially available. Their applications are widespread in the field of telecommunications.

On the other hand external optical bulk modulators with




tens of MHz bandwidths but with high optical power handling capability have a multitude of applications in present and future. Their importance is evident from the requirements for high coherence, stability and power throughput, qualities which cannot be offered by semiconductor lasers and high speed integrated modulators. In the nineteen sixties and early seventies several workers have contributed to the development of these modulators mostly employing crystals of the XDP family and other electro-optic materials. It is surprising that nearly 20 years after their development they still remain today as the most useful electro-optic modulators. Although between 1960 and 1970 the design of XDP modulators was a challenging subject, it has not excited a great deal of interest for research and development. The reasons being that the bandwidth these devices offer was enough for most applications and there was also availability of high voltage drivers at the moderate frequencies of interest. The advent of the laser recorder and optical recording media has brought the need for higher speeds. Bulk electro-optic modulators are ideally suited to wideband modulation of video information in laser imaging recorders, for use as high speed light shutters for digital information recording, modulation on optical data links, light modulation for large area display systems and phase modulation in FM spectroscopy. Also, demands for multiwavelength or multicolour modulation and modulation of a white light beam for large area displays stimulated an increasing interest over the last years. Unfortunately, since the time of their development electro-optic engineers have run out of ideas and

the technology has reached a dead end or what others might say a state of the art limit of performance which beyond the technology cannot go.

The basic model of an electro-optic modulation system consists of the electro-optic modulator and the driving electronics unit. In general the bandwidth of the system is limited because of the modulator's capacitance and the driver's capabilities to produce large voltage swings at high frequencies. Low capacitance modulator designs require high driving voltages in the order of 400V so the system is limited by the capabilities of the driver. High capacitance modulators require relatively low voltages and in this case the bandwidth is limited due to both the crystals capacitance and the driver as well. State of the art Ammonium Dihydrogen Phosphate (ADP) modulators utilising the longest available crystals from the crystal boule have capacitances of 180pF and voltage requirements of 115 volts at 633nm for 100% modulation. Although the capacitance of such a modulator limits the frequency response to 50MHz this can be extended with special broadbanding techniques and bandwidths of 200MHz at least in theory are possible. Presently what is not possible and does not exist is a suitable driver to produce 115V from DC to 200MHz. The signal level (90V) of the existing drivers is just enough to produce less than 80% modulation from DC to 50MHz.

There are two obvious solutions to the problem. One is to try to develop a high voltage driver the other is to develop



a low voltage modulator. Considering the first solution the engineer is faced with the problem of non availability of semiconductors with the required voltage and power handling capabilities and speed of response. On the other hand this might look as just the right sort of application for large high power transmitting valves. An electro-optic modulator driver must be DC coupled, capable of a flat response, stable, differential throughout and thermally compensated so that gain temperature time effects typical of large signal amplifiers are minimised. Valves generate a lot of heat which make them more prone to drift, they require replacement quite often and their reliability is not great. The characteristics of valves change slightly with time so they have a need for periodic retuning. Also direct coupling between valves is not easy to design. This is the reason why all the television valve video amplifiers have been replaced with transistorised equivalent units. The unique feature of response down to DC means that the output of the modulator can be in the ON state as long as the input is held high. Drifts of the operating point show up in the output as a signature or thermal tail which affects the overall repeatability of the input output transfer function. This is particularly essential in analog imaging recorders for tight correlation between the video input signal and resultant exposure time. Valves would be more appropriate and retain their superiority over transistors in narrowband high frequency applications where large signal power is required.

On the other hand high performance differential output

amplifiers covering DC to relatively high frequencies exist. These are solid state amplifiers, feature rugged design stable operation and durability. The use of broadband transistors ensures a high degree of operational reliability, virtually eliminating any need for periodic tuning. For these reasons all the reputable electro-optic systems manufacturers have switched to all solid state drivers and have developed a wide range of products. Even though these products are not able to cope as already said, with the increasing bandwidth demands at such voltage and power levels.

At the same time demands for larger, brighter and sharper images on both TV and computer screens in applications from desk top publishing to medical imaging require technological advances in all aspects of colour and monochrome monitor designs. Advances with important new RF modules and new transistor families whose characteristics are optimised for horizontal deflection applications have been introduced recently by Motorola, Philips and other leaders in the field. For example the CR 2424 module can produce a 50V output voltage over a bandwidth of 145MHz. These developments show the current trend and technological limits of the today's semiconductor industry. These devices are ideally suited as drivers for electro-optic modulators not only from output level considerations but from capacitance considerations as well, if only, one had modulators that would operate at 50V.

Necessary developments in the electrooptic modulators field should be done by appreciating these developments and

tailoring the specifications of a new modulator within the above limitations, which more simply means that about 50V is a critical voltage level that the design should be based around . To utilise the availability of the existing solid state devices it has been decided to design and investigate how such a low voltage (50V) modulator can be produced and made practically realisable. As it will be shown this can be only achieved with a new crystal cut and a new technique, the multipath reflection technique. It will be also explained in following sections that such a low voltage modulator is not feasible with the existing modulator designs and crystal cuts.

#### 1.4 State of the art modulation systems.

This Thesis describes research at the University of North London on lumped crystal modulators which are based on the first order electro-optic or Pockels effect. These modulators make use of a number of doubly refracting crystals and with the application of an external electric field the characteristics of the optical irradiance e.g. amplitude, phase, frequency and state of polarisation are altered by introducing the modulator in the beam. Electro-optic modulators have been available for many years. They are the most popular among all the other types of modulators. The reasons being that they offer speed and optical efficiency. They are superior to acousto-optic modulators in terms of bandwidth<sup>(6)</sup> and also because electric fields are easier to generate than magnetic fields, electro-optic devices are

usually preferred to magneto-optic devices. They have found use in many applications requiring amplitude or phase modulation of CW or pulsed lasers.

As the state of the art in laser beam recorders advances, the need for broader modulation bandwidth and higher laser throughputs increases. The present state of performance is limited by the capacitance of the modulator which ultimately limits the bandwidth and also by the high power requirements necessary to drive the modulator efficiently i.e. to the highest modulation depth. This is because it is extremely difficult to change high voltages at high speeds. The situation becomes even more complicated when one considers that these necessary voltage changes have to be done across a reactive load, in this case a significant amount of capacitance. Capacitive loads have been known to give engineers severe problems and have caused the death of countless number of output stages and transistors. To overcome the problem, commercial modulators use sophisticated drivers employing expensive transistors and complicated circuitry to achieve reliable operation. The cost of the modulator-driver system becomes prohibitively expensive, <sup>at</sup> tens of thousands of pounds and the maximum bandwidth offered by the best commercial systems presently known to us is 100MHz. Even with such expensive systems 100% modulation is not possible and the size and weight ratio between the modulator and the driver is very unequal. Figures of 30kg and 480 x 230 x 450mm (length x height x depth) for the driver and 50mm diameter x 220mm length and less than a 1kg for the modulator

are typical for the most advanced systems in the market. The design of electronic drivers for electro-optic modulators is a very complex task. The very long modulator units available are the result of the electro-optic engineers effort to reduce the half wave voltage of the device down to a value below the upper limit of voltage and power characteristics at the frequencies of interest available from the today's semiconductor devices.

Increasing the length of the modulator to decrease the half wave voltage is not a new idea, Peters in 1965 was the first to construct a modulator 16 inches long by using 8 crystals yielding to a half wave voltage of 50 volts. Unfortunately this method of reducing the driving voltage is not without problems. It comes at the expense of introducing a number of difficulties and undesirable effects in the design, construction and operation of the modulator. First a very long modulator presents assembly problems and is not very practical to use since the device has to be introduced at a point in the laser beam without always the necessary space being available. There is also an upper limit to the maximum length of the crystals that can be sliced out from the crystal boule. This is a geometric limitation imposed by the dimensions of the boule. But even if this was not a problem, using very long crystals results in unstable operation, drift of the operating point due to thermal gradients within the crystal material itself. As a result it is impossible to compensate satisfactorily<sup>(7)</sup>, also very long unstrained crystals are practically unobtainable<sup>(8)</sup>. Using a

large number of short crystals to construct a long modulator would also suffer from the same effects as above since not only there are always small differences in the dielectric properties and characteristics between different boules but also within the same boule itself. This is the reason why parts of adjacent crystal pieces should always be chosen for making a modulator so that they are matching each other as closely as possible. Other problems would arise from the difficulty of aligning and cutting all the boules to be used for the same modulator at exactly the same angles with respect to the crystal axes. Reducing the height of the crystals reduces also the half wave voltage but this aperture reduction would also preclude large diameter laser beams through the modulator without beam forming optics.

Finally, quite often it is not always the half wave voltage or the bandwidth of the modulator-driver system that controls the choice of a particular system and determines its superiority over other systems for a specific application. Other parameters and considerations such as extinction ratio, optical transmission, crystal quality, piezo-optics effects, dielectric constants, temperature dependence of birefringence, ease of alignment and use, size, cost, optical power handling capability, wavelength of operation capacitance, repeatability of characteristics, life, stability etc. could be equally or even more important also. The aims of this research are primarily as stated above, to reduce the half wave voltage and increase the bandwidth while keeping the other parameters within acceptable levels.



### 1.5 Aims, objectives and plan of thesis.

A novel crystal cut will be described and the design of amplitude modulators based on this new cut will be given in full detail. The main feature of this cut is that unlike all the other known cuts reported in the literature, it permits a multipath reflection technique to be used and as a result to reduce dramatically the power requirements needed for full modulation of the laser beam carrier. A number of Ammonium Dihydrogen Phosphate (ADP) crystals were available for this research which was broadly aimed at:

- a. developing a high frequency low voltage electrooptic modulator with voltage requirements attainable from existing semiconductors.
- b. designing, building, optimising and fully characterising such low voltage modulators based on the novel crystal cut and the multipath reflection technique.
- c. examining the high frequency behaviour of the modulator and by employing <sup>relevant</sup> techniques and network structures extend the moderate bandwidth of the prototypes into the very high frequencies spectrum.

Chapter 2 contains the necessary background and theory applicable to light modulators, chapter 3 contains an overview of all the crystal cuts known and their limitations when used for light modulation. The new modulator theoretical

and experimental work is described in sections 4 to 9. Chapter 4 contains the theory of the novel crystal cut and the composite modulator schemes. The modulator design and its engineering aspects are discussed in chapter 5. Chapter 6 contains most of the experimental work and the optimisation process. Chapter 7 contains a theoretical investigation of double refraction at oblique angles of incidence and the associated effects in the modulator performance, in particular to the extinction ratio. Chapter 8 contains the experimental work related to the beam profile and temperature stability performance of the modulator. Chapter 9 examines the frequency response of electrooptic modulators, various techniques used and their limitations. A new technique is also presented which overcomes the above limitations to a certain extent and results to an increased modulation bandwidth.

Finally discussions, conclusions and suggestions for further work are included at the end.

## CHAPTER 2 CRYSTAL OPTICS AND APPLICATION TO MODULATORS

### 2.1 Introduction.

According to Maxwell's electromagnetic theory, light is a simultaneous propagation of electric and magnetic fields. Although Maxwell postulated his theory more than 100 years ago, scientists are still solving and investigating his equations. The tremendous computing power available today makes this type of research possible. Fortunately the already existing knowledge is enough to explain the propagation of a plane light wave in a dielectric medium. Maxwell's four equations give the relations in space and time between the vector quantities  $E$ , the electric field strength, and  $H$ , the magnetic field strength. From a more practical point of view we are interested in relations which describe the behaviour of substances under the influence of a field. These relations are known as the material equations and can be derived from the four basic Maxwell equations. They are given by:

$$j = \sigma E \quad 2.1$$

$$D = \epsilon E \quad 2.2$$

$$B = \mu H \quad 2.3$$

where:

$\sigma$  is the specific conductivity tensor

$\epsilon$  is the dielectric or permittivity tensor

$\mu$  is the magnetic permeability tensor

$j$  is the electric current density vector

$D$  is the electric displacement vector

$B$  is the magnetic induction vector

The above equations describe the effect of the field on material objects. In the case of a dielectric medium we have  $j=0$  and  $\sigma=0$ . If a medium is isotropic there are linear relations between  $D$  and  $E$  and between  $B$  and  $H$ . In such a case the four vectors are related by scalar constants or tensors of a zero rank. If a medium is magnetically isotropic but electrically anisotropic then we have to consider substances whose electrical excitation depends on the directions of the electric field. The permittivity of such a medium depends on the direction of propagation of the wave and except in certain special directions,  $D$  is not parallel to  $E$ . To specify the vector  $D$  we choose three mutually perpendicular axes  $OX$ ,  $OY$ ,  $OZ$  and give the components of the vector along them. The relationship between the excitation  $D$  and the field strength  $E$  is now given by:

$$D_1 = \epsilon_{11}E_1 + \epsilon_{12}E_2 + \epsilon_{13}E_3 \quad 2.4$$

$$D_2 = \epsilon_{21}E_1 + \epsilon_{22}E_2 + \epsilon_{23}E_3 \quad 2.5$$

$$D_3 = \epsilon_{31}E_1 + \epsilon_{32}E_2 + \epsilon_{33}E_3 \quad 2.6$$

The dielectric constant is now a symmetric tensor of rank two. Many crystal properties are represented by tensors<sup>(9)</sup>. Electrical conductivity, thermal conductivity and others are represented by a second rank tensor. The electro-optic properties can be represented by a third rank tensor and the elasto-optic ones by a fourth rank tensor. Equations 2.4, 2.5 and 2.6 can be written in a more convenient method.

$$D_1 = \sum_{j=1}^3 \epsilon_{1j} E_j \quad 2.7$$

$$D_2 = \sum_{j=1}^3 \epsilon_{2j} E_j \quad 2.8$$

$$D_3 = \sum_{j=1}^3 \epsilon_{3j} E_j \quad 2.9$$

The vector D can be also expressed by using any other set of orthogonal axes. A different set of axes gives a different set of coefficients for the dielectric tensor. However both tensors equally well represent the same physical quantity (the permittivity of the crystal) therefore there must be some relation between them<sup>(9)</sup>. The following equation gives the coefficients of the new tensor in terms of the old one.

$$T_{ij} = a_{ik} a_{jl} T_{kl} \quad 2.10$$

where  $a_{ik}$  and  $a_{jl}$  are the direction cosines between the new and the old set of axes.

## 2.2 The representation quadric.

It can be also shown that every tensor can be geometrically represented by a surface usually an ellipsoid<sup>(9)</sup>. Therefore the ellipsoid or the representation quadric or the indicatrix as it is known can be used to describe any physical property associated with this tensor. All tensors used in this work are of a second or third rank and symmetrical. An important property of the indicatrix is the possession of principal axes mutually perpendicular. If this set of axes is chosen to express the physical quantity the tensor takes its simplest form. Thus when the tensor,

$$S_{ij} = \begin{vmatrix} S_{11} & S_{12} & S_{13} \\ S_{12} & S_{22} & S_{23} \\ S_{31} & S_{32} & S_{33} \end{vmatrix} \quad 2.11$$

is transformed to its principal axes it becomes

$$\begin{vmatrix} S_1 & 0 & 0 \\ 0 & S_2 & 0 \\ 0 & 0 & S_3 \end{vmatrix} \quad 2.12$$

The representation quadric also takes its simplest form which is:

$$S_1 x_1^2 + S_2 x_2^2 + S_3 x_3^2 = 1 \quad 2.13$$

By comparing with the standard equation of a quadric

$$\frac{x^2}{a^2} + \frac{y^2}{b^2} + \frac{z^2}{c^2} = 1 \quad 2.14$$

it is obvious that the semi axes of the representation quadric are of lengths

$$a = \frac{1}{\sqrt{S_1}}, \quad b = \frac{1}{\sqrt{S_2}}, \quad c = \frac{1}{\sqrt{S_3}} \quad 2.15$$

The representation quadric is shown in fig 2.1

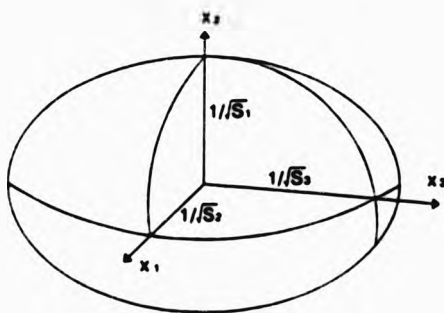


Fig. 2.1 The representation quadric.

The effect of the crystal symmetry on the physical property of the crystal is to reduce the number of the independent components of the associated tensor<sup>(9)</sup>. The crystals used for this work were uniaxial and belonged to the tetragonal system  $\bar{4}2m$ . The tensor referred to the principal axes has two independent coefficients and takes the form:

$$\begin{vmatrix} S_1 & 0 & 0 \\ 0 & S_1 & 0 \\ 0 & 0 & S_1 \end{vmatrix} \quad 2.16$$

### 2.3 The index ellipsoid.

It can be also shown that Maxwell's equations lead to the conclusion that not one but two waves of different velocity may in general be propagated through a crystal with a given normal direction<sup>(10)</sup>. The indicatrix is one the most convenient methods of representing the optical characteristics of the crystal. These figures represent geometrically the three dimensional variations in their directions of vibration of the indices of refraction of all waves passing through uniaxial crystals. This ellipsoid is mostly known as the index ellipsoid or the ellipsoid of the wave normals or the fresnel ellipsoid and is shown in fig 2.2. It is given by

$$\frac{x^2}{n_x^2} + \frac{y^2}{n_y^2} + \frac{z^2}{n_z^2} = 1 \quad 2.17$$

The semi axes of the index ellipsoid are equal to the principal refractive indices  $n_x$  and  $n_y$ . For a given wave

normal direction within the crystal, one can draw a plane<sup>(11)</sup>, shown in fig. 2.3, which contains the wave normal and the optic axis. This is called a principal plane and in general it is an ellipse. Suppose that a wave of light moves in the direction ON, parallel to its wave normal. The light in the wave vibrates parallel to TQ and has a refractive index between  $n_o$  and  $n_e$  given by the length OQ. Another wave also moves along ON, but this wave vibrates normal to the principal plane and has an index of refraction equal to the radius of the circular equatorial section of the indicatrix. This wave has an index of  $n_o$ .

In general the direction of propagation of a wave does not coincide with the propagation directions of its component rays. Moreover it is believed from a consideration of electromagnetic theory that a ray vibrates in a direction perpendicular to its wave normal. Accordingly the vibration direction of a ray need not be at right angles to the ray path. To obtain the direction of the rays for the wave moving along ON a normal is drawn from ON tangent to the indicatrix. The line from O to P, the point of tangency, gives the direction of the rays in the wave. The phase difference  $\Gamma$  or retardation or natural birefringence between the two waves is given by:

$$\Gamma = \frac{2\pi}{\lambda} l \Delta n \quad 2.18$$

where:

$l$  is the length of the wave inside the crystal

$\lambda$  is the wavelength

$\Delta n$  is the refractive index difference of the two waves.



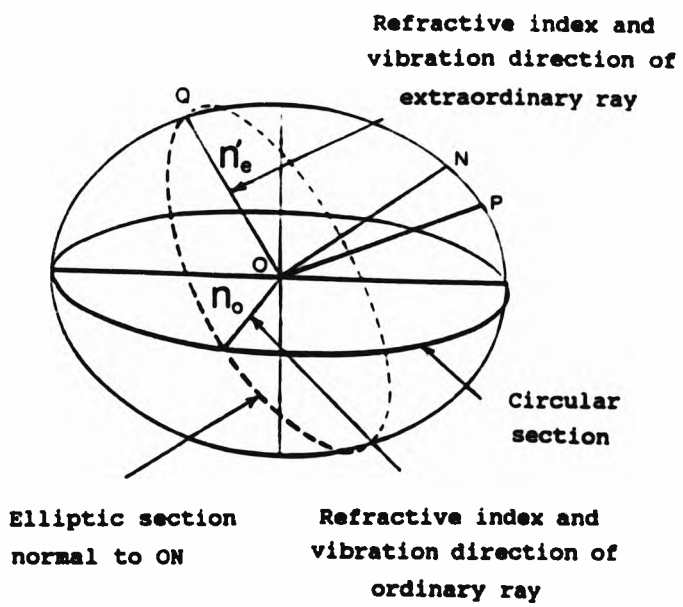


Fig. 2.2 The index ellipsoid.

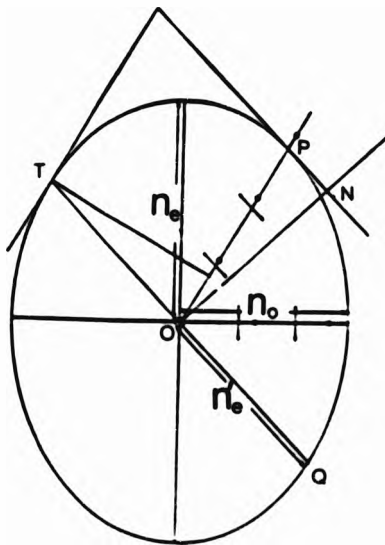


Fig. 2.3 Principal plane, wave, ray and polarisation directions.

#### 2.4 The electro-optic effect.

The electro-optic effect describes the behaviour of D under the influence of an electric field. Therefore the electro-optic effect may be regarded as a change in the optical dielectric tensor of a crystal upon the application of an electric field. When this change is linear to the applied electric field, it is called linear electro-optic or Pockels effect. In general the application of a field changes the permittivity and dielectric constant and hence the refractive index<sup>(9)</sup>. The effect can be simply described as a small change in the shape, size and orientation of the index ellipsoid. New principal axes are induced and these have now a different length. Because of this uniaxial crystals become biaxial.

In its most general form the electro-optic effect is conveniently expressed as a change in the coefficients of the index ellipsoid. Denoting the principal axes of the ellipsoid by x, y, z the field free ellipsoid is given by equation 2.17. When an electric field is applied the ellipsoid becomes<sup>(4)</sup>

$$x^2(n_x^{-2} + \sum r_{1j}E_j) + y^2(n_y^{-2} + \sum r_{2j}E_j) + z^2(n_z^{-2} + \sum r_{3j}E_j) + 2yz \sum r_{4j}E_j + 2zx \sum r_{5j}E_j + 2xy \sum r_{6j}E_j = 1 \quad 2.19$$

where:  $j=x,y,z$

$E_{x,y,z}$  are the components of E,

$r_{ij}$  are the first order electro-optic coefficients.

The coefficients  $r_{1j}$ ,  $r_{2j}$ ,  $r_{3j}$  do not affect the orientation of the ellipsoid axes, they only cause a change in the

respective index by an amount  $\Delta n_i$ , such that

$$(n_i + \Delta n_i)^{-2} = n_i^{-2} - 2n_i^{-3} \Delta n_i + \dots = n_i^{-2} + \sum_j r_{ij} E_j \quad 2.20$$

Thus for small changes,  $\Delta n_i$  can be approximated by

$$\Delta n_i = -\frac{1}{2} n_i^3 \sum_j r_{ij} E_j \quad 2.21$$

The coefficients  $r_{ij}$ ,  $r_{ji}$ ,  $r_{ij}$ , on the other hand cause a rotation of the ellipsoid axes, in addition to affecting their lengths. These changes can be determined by transforming the ellipsoid to a new coordinate system, whose axes coincide with the principal axes of the new ellipsoid.

## 2.5 Application to modulators and the production of modulated light.

### 2.5.1 Introduction.

Electro-optic light modulation is the impression of information on a light wave as a result of a change in the refractive index induced by the electro-optic effect. Depending on the crystal cut and orientation, the state of polarisation of the input wave, the arrangement of input and output ports and the direction of the applied field, the change of refractive index can lead to phase modulation (PM), amplitude or intensity modulation (AM, IM), frequency or wavelength modulation (FM, WM), polarisation modulation (PLM) and their derivatives such as amplitude or intensity shift keying (ASK, ISK), phase shift keying (PSK), frequency shift keying (FSK) etc.

### 2.5.2 Phase modulation.

A beam of light entering a crystal comes out with a phase

$$\phi = \phi_0 + \frac{2\pi L}{\lambda_0} n_o \quad 2.22$$

Application of an electric field changes the output phase to

$$\phi = \phi_0 + \frac{2\pi L}{\lambda_0} (n_o - \Delta n) \quad 2.23$$

Assuming that  $E=V/d$  and  $\Delta(1/n^2) = -2\Delta n/n_o^3$  then equation 2.23 becomes

$$\phi = \phi_0 + \frac{2\pi n_o L}{\lambda_0} \left(1 + \frac{n_o^2 r}{2d} V\right) \quad 2.24$$

where:  $\phi_0$  is the phase of the wave entering the crystal  
 $n_o$  is the refractive index for an ordinary wave

$r$  is the linear electro-optic coefficient associated with the directions of propagation and polarisation of the wave and the direction of the applied field. In general it is a function of all the non vanishing electro-optic coefficients of the material.

If the electric field is of the form

$$V = V_o \sin \omega_m t \quad 2.25$$

then the equation 2.24 can be written as

$$\phi = \phi_0 (1 + m_p \sin \omega_m t) \quad 2.26$$

This is the equation of a phase modulated signal with carrier

$$\Phi_o = \phi_o + \frac{2\pi n_o L}{\lambda_o} \quad 2.27$$

and modulation index

$$m_\phi = \frac{\pi n_o^3 L r V_o}{\lambda_o c \Phi_o} \quad 2.28$$

In general because two waves will propagate through the crystal then both waves will be individually modulated. Recovering of only one of the phase modulated waves can be done using an analyzer at the output, along the polarisation direction of the component to be recovered.

### 2.5.3 Amplitude modulation.

The use of an analyzer at the output in a direction different from the two polarisation directions of the crystal, will convert the phase modulated light into amplitude modulated. This is achieved as the result of interference between the two propagating waves. It can be shown that maximum interference occurs when the two components have equal amplitudes and the analyzer direction is at  $45^\circ$  with the crystal axes. This is achieved by placing the modulator at  $45^\circ$  between a crossed polariser analyzer combination. The phase difference of the waves coming out of the crystal is

$$\Delta\phi = \phi_x - \phi_y \quad 2.29$$

In a compensated design  $\phi_x$  is equal and of opposite sign to  $\phi_y$ , therefore

$$\Delta\phi = 2\phi_x = \frac{2\pi L}{\lambda} \Delta n = \frac{2\pi L}{\lambda} r n_o^3 \frac{V}{d} \quad 2.30$$

The transmitted electric field is

$$E = \frac{E_0}{2} [\cos(\omega t + \Delta\phi) - \cos(\omega t - \Delta\phi)] = -E_0 \sin\Delta\phi \sin\omega t \quad 2.31$$

The irradiance of the transmitted beam after the analyzer is given by averaging  $E^2$  over a complete period

$$\begin{aligned} I &= \frac{\omega}{2\pi} \int_0^{\frac{2\pi}{\omega}} E^2 dt \\ &= I_0 \sin^2 \Delta\phi \\ &= I_0 \sin^2 \frac{2\pi L}{\lambda} r n_o^3 \frac{V}{d} \\ &= \sin^2 \frac{\pi}{2} \frac{V}{V_\pi} \end{aligned} \quad 2.32$$

where  $V_\pi$  (also written as  $V_{\lambda/2}$ ) is the voltage required to turn the intensity from maximum to minimum and is known as the half wave voltage. The ratio of the maximum intensity over the minimum intensity is defined as the extinction ratio of the modulator.

Clearly the modulation is not linear and the effectiveness of the modulation process can be enhanced by biasing the modulator with a fixed retardation of  $\pi/2$  which corresponds to 50% transmission. This can be achieved by the inclusion of a quarter wave plate or a DC voltage bias.

#### 2.4.4 Polarisation modulation.

Polarisation modulation can be obtained from the amplitude modulation set up by removing the analyzer at the output port. The incident wave is resolved into two waves of equal

amplitude polarised along the crystal vibration directions. The emergent polarisation state will depend on the superposition of the two waves. As the phase difference changes the output polarisation goes from vertically polarised at zero bias to circular polarisation with half of the half wave voltage applied and to horizontal polarisation with the full half wave voltage applied. All the other states of polarisation for biasing voltages in between the above values are elliptical.

## CHAPTER 3 LIGHT MODULATION WITH UNIAXIAL ADP CRYSTALS

### 3.1 Choice of material.

The modulators described in this Thesis employ Ammonium Dihydrogen Phosphate (ADP) as the electro-optic material. Although research on the piezoelectric, piezo-optic and electro-optic properties of the XDP family of crystals started in 1943 by Benno et al<sup>(12)</sup> even at <sup>the</sup> present time they remain the most available and produce the most useful range of commercially available electro-optic modulators (Conoptics and Quantum Technology at USA and Electro-optic Developments at UK). In particular ADP is the earliest electro-optic material of all in the XDP family of crystals to be used<sup>(13)</sup> for light modulation long before the first laser was demonstrated. ADP is still very popular and remains the most widely used of all the other materials available. The reasons being that ADP is easily grown in large strain-free crystal boules and exhibits good transmission characteristics between 200nm to 1200nm with very low absorption<sup>(14)</sup>. Homogeneity is also very good and generally excellent crystals as large as 50mm in any direction can be obtained at a reasonable price. ADP also has large electro-optic coefficients. The main disadvantages are that:

- (a) ADP is extremely hygroscopic, crystal preparation and polishing has to be done in humidity levels less than 30%.
- (b) ADP is fragile, very easy to crack and scratched.
- (c) ADP shatters under a thermal shock

However it can be cut, polished and handled without



difficulty. Although other materials such as ADP, KDP and KD\*P have lower half wave voltages and better thermal stability ADP was preferred for its much lower cost.

### 3.2 Existing crystal cuts.

#### 3.2.1 Longitudinal and transverse configurations.

The design type of modulator determines the crystal cut. Modulators can be divided into two groups:

(a) Longitudinal - the modulating electric field is applied in the direction of propagation of the light beam.

(b) Transverse - the modulating electric field is applied at right angles to the direction of the light beam. Both types have advantages and disadvantages over each other.

#### 3.2.2 Longitudinal modulators, crystal class $\bar{4}2m$ (ADP).

The  $0^\circ$  z-cut crystal has the simplest orientation for a longitudinal modulator. Light is polarized along x or y axis and travels along the optic axis. The  $0^\circ$  z-cut modulator is shown in fig. 3.1. Since light propagates along the optic axis natural birefringence ( $n_o - n_e$ ) is not present so the operation of the modulator is not affected by changes caused by its temperature dependence. However the half wave voltage changes because it follows the temperature dependence of the  $r_{43}$  electro-optic coefficient. Compensation is not necessary

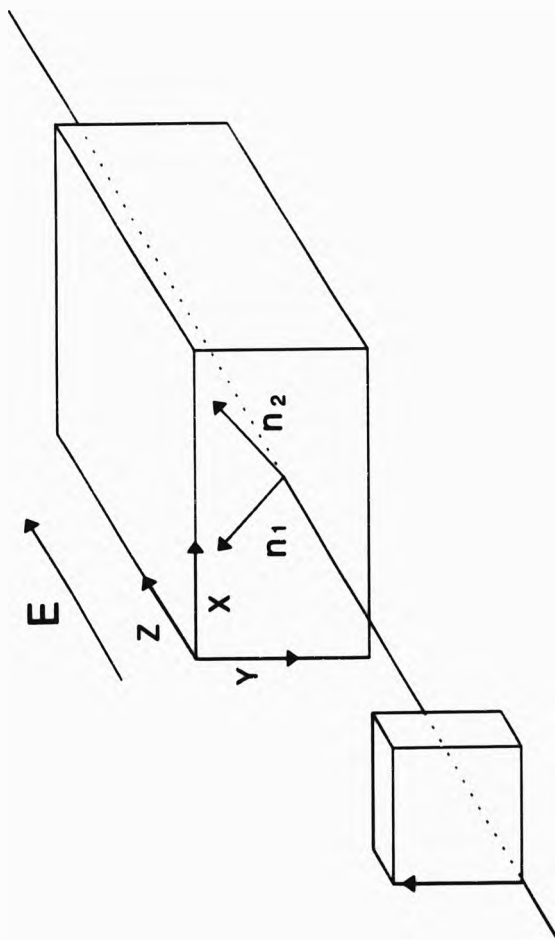


Fig. 3.1  $O_z$  cut longitudinal modulator.

with the  $0^\circ$  z-cut design so only one crystal is needed to make a modulator, resulting to high extinction ratios, small capacitance in the order of a few picofarads, and good beam profile. Because of the above, longitudinal modulators have found wide use in fast Q switching of high power laser beams. Other applications include cavity damping, pulse slicing and pulse selection. However, longitudinal modulators suffer from the electrode configuration required. This presents construction problems, limits the useful aperture of the device and distorts the electric field profile as compared to the ideal linear z direction field. Strong piezo-electric resonances are also present in the ADP  $0^\circ$  z-cut modulator. This piezoelectric contribution to the electro-optic effect causes ringing and oscillation in the pulse response of the modulator<sup>(9)</sup>. Although the longitudinal type of modulator does suffer from the general problems already mentioned its most serious disadvantage is that the halfwave voltage is independent of the crystal length. It is simply determined from the quantity  $n_o^3 r_{63}$ , which is purely a physical property of the crystal, the larger it is the smaller the halfwave voltage. Typical values for the half wave voltage are 4-14KV. Pockels<sup>(15)</sup> carried out the first work on this crystal cut and Billings and Carpenter<sup>(16,17,18)</sup>, were the first to use it to report the first light modulator.

The retardation is given by:

$$\Gamma = 2 \frac{\pi}{\lambda} n_o^3 r_{63} V_z \quad 3.1$$

### 3.2.3 Transverse modulators, crystal class $\bar{4}2m$ (ADP).

Alternatively to the longitudinal mode of operation we can use the transverse mode in which the electric field is applied normal to the direction of the light propagation. With such an arrangement the electrodes do not block or interfere with the beam and most importantly the induced retardation can be increased by the factor  $l/d$  also known as the aspect ratio. More simply, the half wave voltage is proportional to the width of the crystals used and inversely proportional to their length. This explains, in a way, the long and thin nature of most of the low voltage designs. Aspect ratios of 20-80 are common for existing commercial modulators yielding to half wave voltages in the region of 115-500V at 633nm typically.

Although the transverse mode of operation is very desirable for reasons already explained this significant improvement of the voltage requirements is to be outweighed by a number of problems that the electro-optic engineer faces when he designs and attempts to materialise such a modulator. In general the ordinary and the extraordinary rays travel in different directions and they do not always lie in the same plane of incidence. On emergence they are not coincident and as a result interference is restricted only in the area of overlap of the two rays. Also because the two wave normals are associated with different refractive index values there is a contribution to the overall phase difference between them by the crystals natural birefringence ( $n_o - n_e$ ). This

contribution is strongly temperature dependent and even small changes of the ambient temperature can cause a significant shift of the operating point. The modulator becomes very temperature sensitive and this is to be avoided by all means.

From the above it is clear that a form of stabilisation or compensation is absolutely necessary. Ways of doing this have been proposed by Peters<sup>(20)</sup> and Ley<sup>(23, 24)</sup>. Both of them suggested different crystal cuts suitable for transverse mode of operation and the necessary compensating schemes to achieve stable conditions independent of temperature changes. There are problems however. For all designs a composite crystal scheme is required to recombine the two beams and eliminate any temperature drift effectively. For this reason all the crystals needed to make a modulator must be cut from the same boule, handled and polished together to achieve the very tight mechanical tolerances required. Exact surface conditions, excellent parallelism and flatness of the crystal faces must be met. The crystals must be also properly aligned with respect to each other for best results. All the above make the task of transverse modulator design complicated and difficult to manufacture. Even if all the above requirements are met to the tightest tolerance, composite crystal lengths longer than 80mm are being found experimentally to show some temperature dependence<sup>(7)</sup>.

All the designs call for either two or four crystals for efficient compensation. Using more than one crystal increases the transmission loss through the modulator because of

Fresnel losses associated with various material interfaces that exist, air-crystal for dry modulators or liquid-crystal for modulators immersed in an index matching fluid. Extinction ratio is also strongly affected by the number of crystals used. Two-crystal designs tend to give higher extinction ratios, typically 500:1, when compared with four-crystal designs that tend to give something lower, 100:1 to 250:1. For comparison purposes, it is noted that longitudinal one crystal modulators have extinction ratios better than 1000:1. This difference should not be related only to the number of crystals used but also to the fact that in  $0^\circ$  z-cut longitudinal modulators double refraction is not present. Despite the higher extinction ratios that can be obtained from the two crystal designs, these necessitate a half wave plate for proper compensation. This has the effect of making the modulator wavelength dependent i.e. the modulator can only be used at the design wavelength of the half wave plate.

Nevertheless, transverse modulators are designed to give low voltage operation and as a result demanding less power from the driving electronics for efficient modulation. The longitudinal modulator driver system is always frequency limited by the capabilities of the high voltage driver, usually up to a few KHz. The low voltage transverse modulator designs are frequency limited up to a few tens of MHz by the capabilities of the driver and the capacitance of the crystals as well.

### 3.2.4 Transverse mode crystal cuts.

#### 3.2.4.1 45° Z cut.

This cut was initially suggested for electro-optic modulation by Peters<sup>(19)</sup> in 1963. Two years later he constructed the first compensated modulator overcoming the problems the initial uncompensated design suffered from<sup>(20)</sup>. This modulator used a number of crystal pairs separated by a half wave plate. This is shown in fig. 3.2. The electric field was applied along the z-axis and light propagated at 45° to  $\bar{x}$  and y axes. When light travels along or normal to the optic axis double refraction is not present but in the case of the 45° z-cut a phase difference is developed between the two waves as they propagate through the crystal since they are associated with different refractive indexes. This is the contribution of the natural birefringence which in this case was eliminated with the inclusion of a half wave plate between the two crystals, with its fast and slow axes at 45° to the crystal z axis. The function of the plate is to rotate the plane of polarisation of the two waves by  $\pi/2$  so that the ordinary wave in the first crystal emerges the plate with its polarisation rotated and becomes an extraordinary wave in the second crystal. The same mechanism applies for the extraordinary wave which now becomes an ordinary wave in the second crystal.

Compensation can be also achieved by using the scheme shown in fig. 3.3. It has the advantage of keeping both

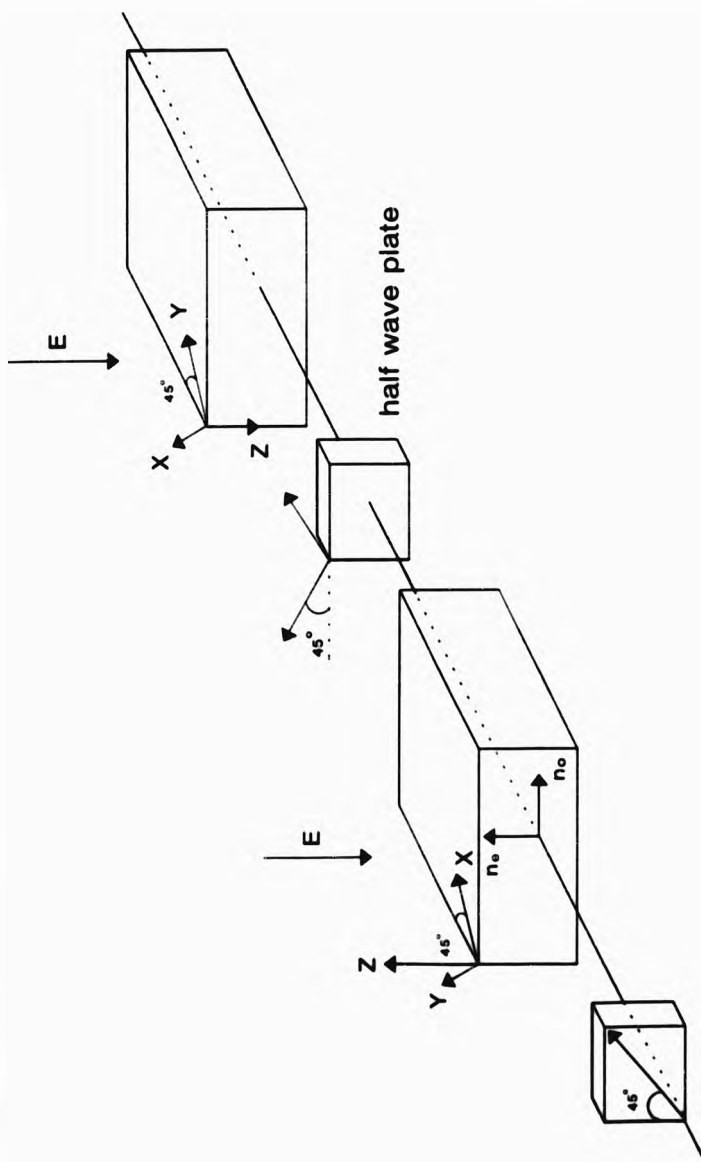


Fig. 3.2 45° z cut two crystal composite modulator.



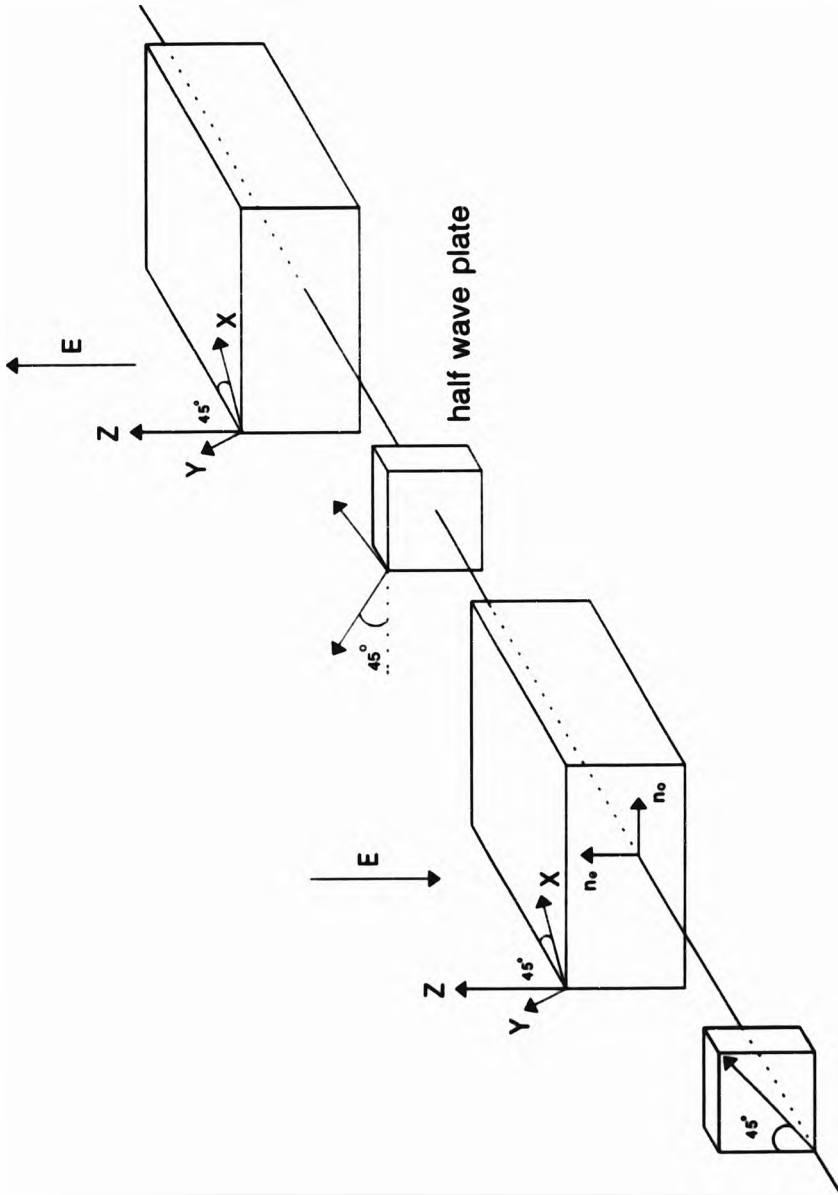


Fig. 3.3 45° z cut two crystal composite modulator.

crystals with the same orientation but it is unsuitable for travelling wave type of operation because the two fields have to be applied with a different polarity.

Alternatively to the schemes just described compensation can be achieved by rotating the second crystal by 90° with respect to the first crystal. This scheme does not use a half wave plate but is unsuitable for travelling wave type of operation. This is shown in fig. 3.4. Also this method presents engineering problems related with the application of the electric fields. These construction problems must be overcome in the design of practical devices. The XDP crystals are piezo-electric in this orientation and resonances cannot entirely be eliminated in the design. However, with this cut DK'P is usually preferred over ADP because of its higher value electro-optic coefficient, better extinction ratio and extended transmission into the infra-red. The phase retardation is given by :

$$\Gamma = \frac{\pi}{\lambda} n_o^3 r_{63} \frac{1}{d} V \quad 3.2$$

#### 3.2.4.2 45° y-cut.

This cut was initially described by Ley<sup>(11)</sup> in 1965. It takes advantage of the high value of  $r_{41}$  coefficient in ADP. The electric field is applied along the y-axis and light propagates in the x-z plane at 45° to x and z axes. In this orientation the crystal exhibits birefringence and double

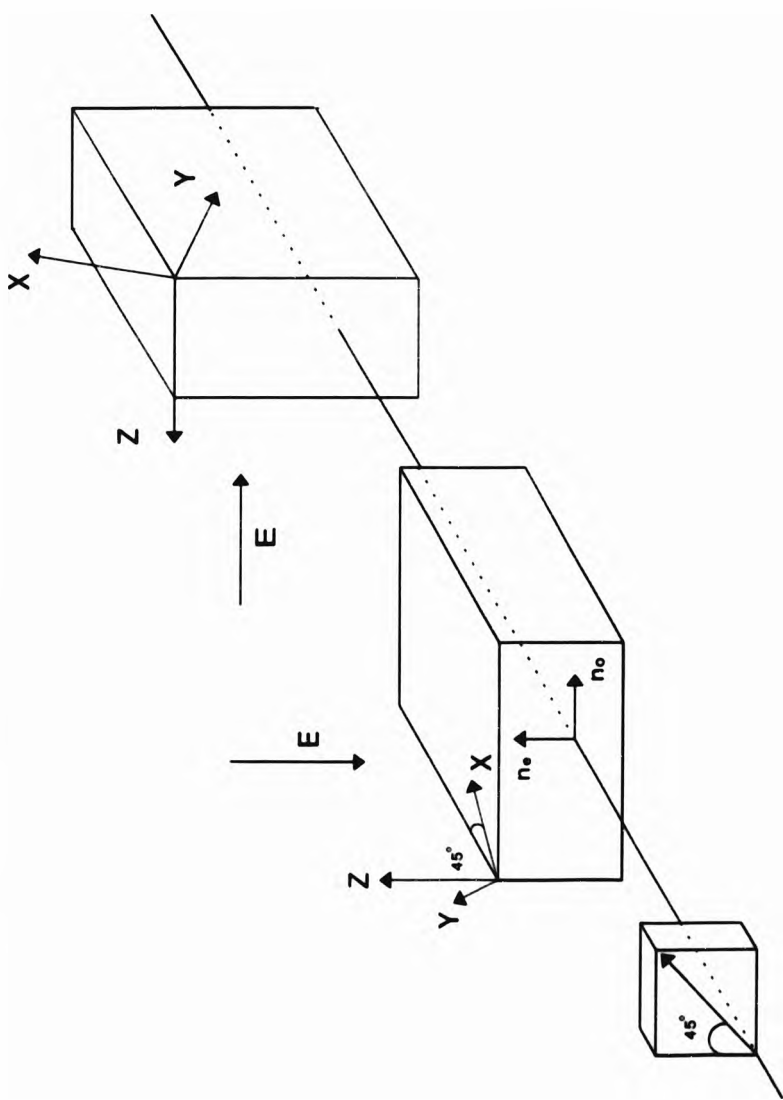


Fig. 3.4 45° z cut two crystal composite modulator.

refraction which both have to be compensated. Numerous ways and suggestions have been reported that cancel out the static or natural retardation and bring the two ray paths together again at the modulator output to permit the necessary interference between the two emergent light components. The phase retardation is given by:

$$\Gamma = \frac{\pi}{\lambda} n_{oo}^2 r_{41} V \frac{l}{d} \quad 3.3$$

$$\text{where: } \frac{1}{n_{oo}^2} = \frac{1}{2} \left( \frac{1}{n_o^2} + \frac{1}{n_e^2} \right) \quad 3.4$$

Compensation can be achieved with the following schemes:

1. Clayson's compensation scheme.

Clayson used two similar aligned crystals of identical length separated by a half wave plate<sup>(22)</sup>. This is shown in fig. 3.5.

2. Ley's compensation scheme.

Ley suggested three different schemes but only one of them eliminates natural birefringence effects<sup>(23,24)</sup>. This is shown in fig. 3.6. The use of the half wave plate produces the necessary cancellation. The combination of 45° x-cut and 45° y-cut crystals permits the two electric fields to be applied in the same directions in both crystals. This makes the modulator suitable for travelling wave type of operation

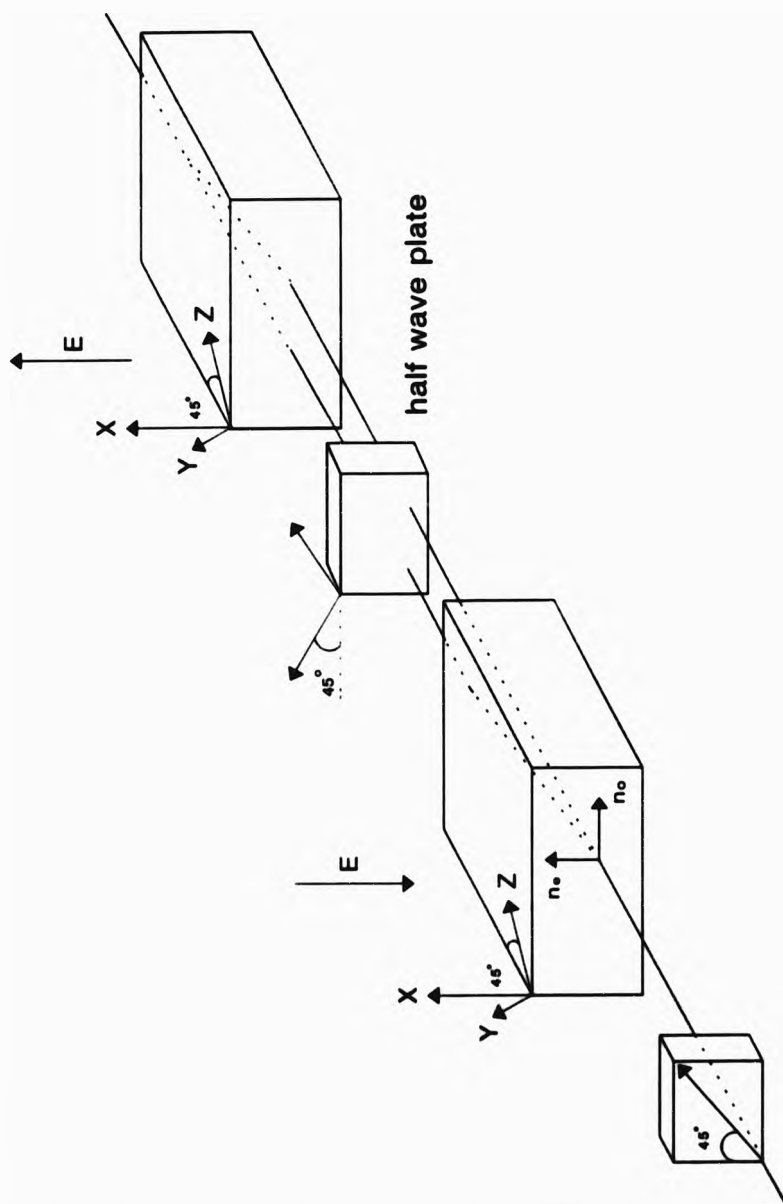


Fig 3.5 45° x cut two crystal composite modulator.

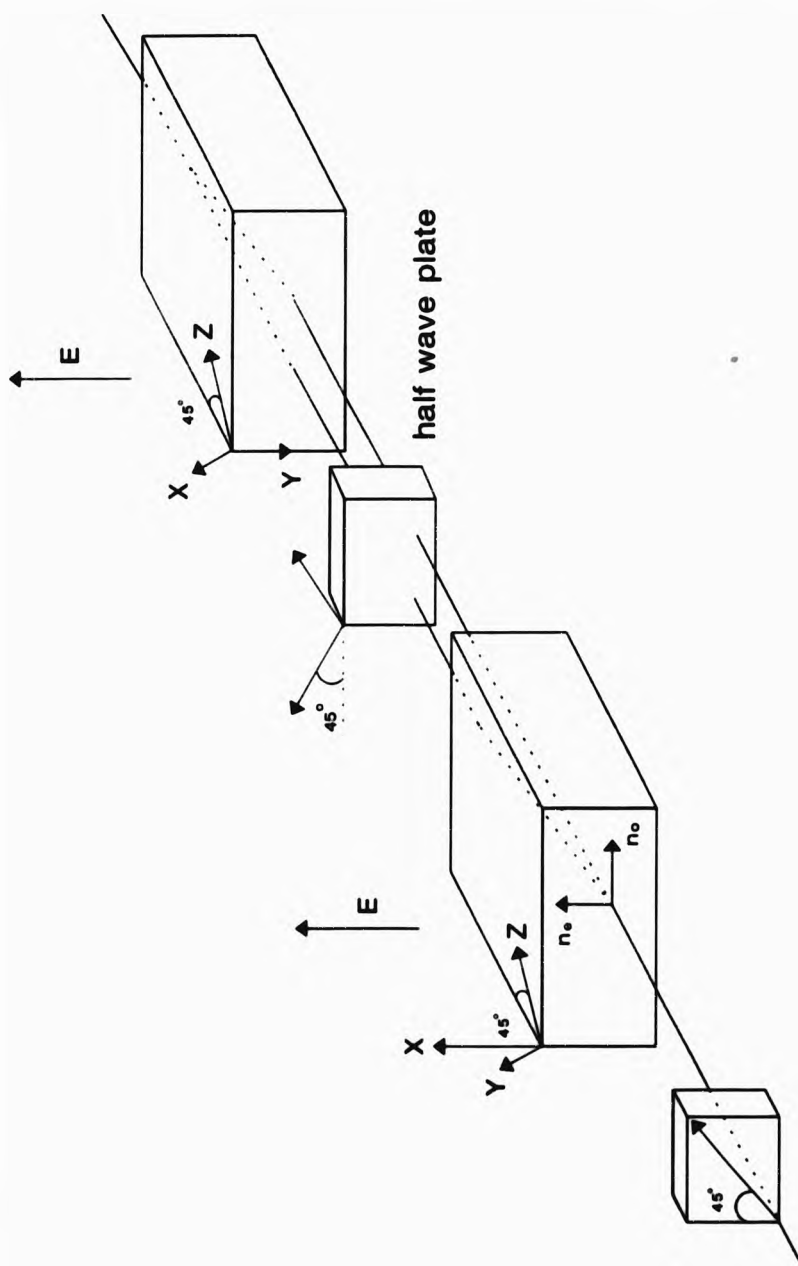


Fig. 3.6 45° x,y cut two crystal composite modulator.

since the two crystals can be incorporated in a continuous stripline.

### 3. Francois' and Librecht's compensation scheme.

The combined goals of temperature stabilisation, natural birefringence compensation, ray recombination and elimination of the half wave plate are achieved using this method<sup>(25)</sup>. The composite modulator comprises four identical 45° x-cut crystals. Two crystals are used end to end with the proper orientation to recombine the laterally separated components. A second pair identical to the first is then added in series but with a 90° degrees rotation to compensate the birefringence. The polarity of the applied field is adjusted in each crystal so that the electro-optic response adds. The composite modulator is shown in fig.3.7.

#### 3.2.4.3 45° y-cut.

This cut was described by Hookabe and Matsuo in 1970<sup>(26)</sup>. Light propagates in the direction 45° to the optic axis and 60° to the crystallographic x and y axes. The induced retardation is a function of both  $r_{41}$  and  $r_{63}$  electro-optic coefficients. The half wave voltage of this cut is considerably lower than that of the other two ADP cuts. The phase retardation is given by :

$$\Gamma = \frac{\pi}{\lambda} \frac{l}{d} \frac{1}{2\sqrt{2}} [r_{63}n_o^2 + (\frac{r_{63}}{2} + r_{41})n_{oe}^2] V \quad 3.5$$

Similar compensation arrangements to the 45° z-cut are

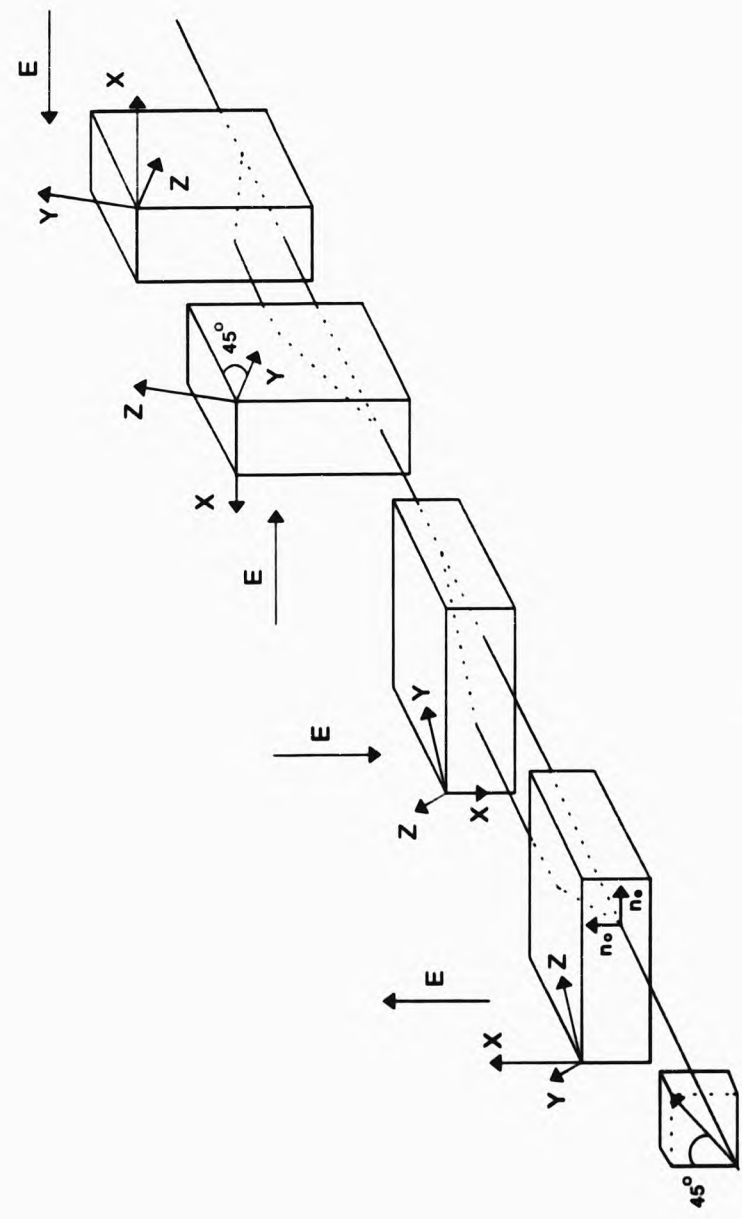


Fig. 3.7 45° x cut four crystal composite modulator.



required since natural birefringence and double refraction are present. Unfortunately, compensation without the use of the half wave plate is not possible with the  $45^\circ$   $y'$ -cut modulators. The  $45^\circ$   $y'$  cut modulators also suffer from strong piezoelectric resonances.

#### 3.2.4.4 $37^\circ$ $y'$ -cut.

This cut was described by Kalymnios in 1970<sup>(27)</sup>. Kalymnios extended the work of Hookabe and Matsuo and developed a general method of optimisation for electro-optic crystal modulators. The  $37^\circ$   $y'$ -cut is an optimisation of the  $45^\circ$   $y'$ -cut yielding to 5% reduction of the half wave voltage. The  $37^\circ$   $y'$ -cut is the most optimum cut resulting to the lowest half wave voltage that can be obtained from the ADP material. Again with this cut natural birefringence and double refraction effects are present. The same compensation methods used with the  $45^\circ$   $y'$ -cut are also applicable to this optimised cut.

## CHAPTER 4 THE MULTIPATH REFLECTION TECHNIQUE

### 4.1 Existing ADP transverse modulator crystal cuts - further comments.

All the composite and modulators employing the crystal cuts already discussed in section 3.3.4 suffer from one or more of the following disadvantages.

(a) A half wave plate is required. This degrades the modulator performance because of the plate's associated losses, wavelength and temperature dependence. Also deterioration of performance is to be expected at oblique angles of incidence since the plate does not function correctly any more.

(b) All the electric fields are not applied along the same direction, sets of electrodes orientated perpendicularly with respect to each other are required. This is not very desirable from a practical point of view.

(c) Combinations of  $45^\circ$  x and  $45^\circ$  y-cut crystals are required.

(d) The frequency response is not free from piezoelectric resonances for cuts using the  $r_{33}$  electrooptic coefficient. Flat frequency response is essential in some applications and also very critical for the design and reliable operation of the driving electronics. At the frequencies that

piezo-electric resonances occur the impedance of the modulator is reduced to a very low value and effectively short circuits the output of the driver usually with catastrophic effects. This by all means should be avoided.

(e) The second crystal or pair of crystals has to be placed with a  $90^\circ$  rotation with respect to the first one. This presents engineering problems.

#### 4.2 The multipath reflection technique.

For all transverse modulator designs the half wave voltage is proportional to the aspect ratio  $d/l$ . For reasons already explained in section 1.4 the physical length can not be further increased more than the usual length of the existing modulators but it would be possible to use the same modulator and pass the laser beam a number of times through the crystals so that the electro-optic effect acquired in its path is additive and hence the halfwave voltage of the device is correspondingly further reduced. This technique has the advantage of keeping the same physical length for the modulator but increases the effective length of interaction between the electrical and the optical waves. The multipath reflection technique should not be confused with the zig-zag modulators reported by Kaminow, Nesterova and Di Dinenico and Anderson<sup>(28,29,30)</sup>. The aim of the zig-zag techniques is to match the phase velocity between the laser beam and the electrical modulating wave, in other words to achieve velocity synchronisation and extend the bandwidth of the modulator

beyond the highest useful modulator frequency imposed by the transit time limitations in the electro-optic material. On the other hand the aim of the multipath reflection technique is to reduce the voltage and power requirements necessary for efficient modulation. The modulator has to be placed between two mirrors so that the beam is reflected forwards and backwards within the crystals. Effectively the two mirrors are the means for trapping the beam and forcing it to travel a longer path. The principle of the multipath reflection technique is shown in fig. 4.1.

Although the idea of the multipath reflection technique is quite simple, in practice there are three good reasons why the idea is impossible to be applied in all existing modulator designs. The first reason is simply that a very wide but thin aperture is required which is not possible to have with some of the described modulators. Specifically all the modulators employing a compensation scheme requiring a  $90^\circ$  rotation between the two crystals or pair of crystals are bound to have a square window type of aperture purely because of geometrical considerations. Increasing the width of the second crystal or pair to transform this square window into a parallelogram one also increases the half wave voltage dramatically. The multipath reflection technique also cannot be used with the modulators that incorporate a half wave plate for compensation purposes. In a multipath reflection set up the beam propagates at an angle through the modulator, thus the plate will not function correctly. This will have detrimental effects on the thermal stability of the device

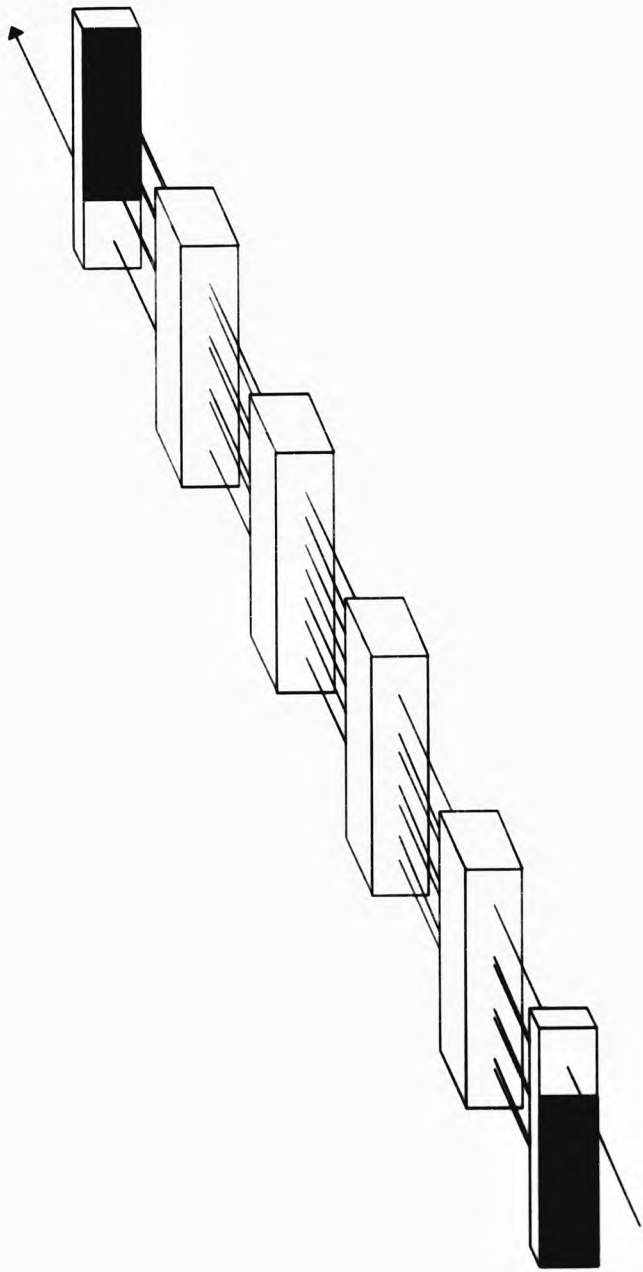


Fig. 4.1 The multipath reflection technique.

and will degrade the maximum extinction ratio. It is clear from the above that the resulting aperture of the composite modulator must meet certain geometrical conditions. It is also clear from fig. 4.1 that all the crystals have to be placed in the same plane in such a way that all the electric modulating fields are applied in the same direction and the resulting total aperture has exactly the same shape and dimensions with the crystals' end polished faces.

#### 4.3 Multipath reflection technique crystal cuts.

In general a crystal will permit two waves with mutually perpendicular polarisation directions to propagate. Light that falls on the crystal will be resolved into two components along OA and OE, fig. 4.2 a. These polarisation directions are at angles  $x$  and  $y$  with the horizontal. We can reasonably assume that both natural birefringence and double refraction will be present. The necessity for compensation implies that identical crystals have to be incorporated with the necessary orientation so that variations in optical path through the modulator can be observed through the use of polarisation and interference phenomena. In such an arrangement the orientation of any crystal can be derived from the positioning of the first crystal through appropriate rotations. From multipath reflection technique considerations only three rotations of the first crystal are permitted. These are:  $180^\circ$  around  $X_1$ , fig 4.2 b,  $180^\circ$  around  $X_2$ , fig 4.2 c and  $180^\circ$  around  $X_3$ , fig 4.2 d. Throughout the modulator only two fixed directions of polarisation should be allowed for

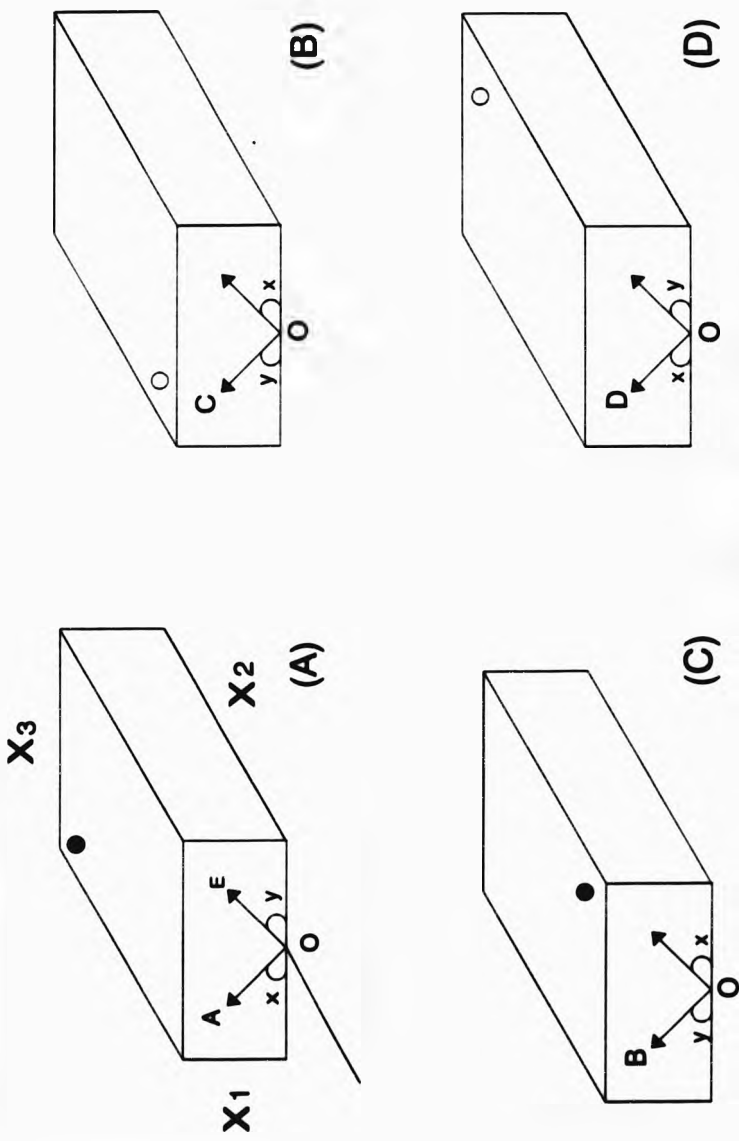


Fig. 4.2 Crystal rotations and directions.

proper interchange of roles of the two rays and for maximum interference to be observed. Maximum interference between the two rays will result to a high extinction ratio figure, which is a very important parameter of performance. From fig.4.2 we can see that OA, OB, OC, OD define one direction of polarisation in the four possible crystal orientations. It is easily understood that all these directions should be parallel i.e. OA//OB//OC//OD which more simply means that the two polarisation directions should be at an angle of 45° to the horizontal. This ensures that an incident wave will be resolved into two components polarised along OA and OB and these directions will not be altered or rotated at some point within the modulator. None of the cuts described in section 3.3.4 has its polarisation directions at 45° to the horizontal.

Two cuts suitable to be used with the multipath reflection technique are the (0°,45°,45°) cut<sup>(a)</sup> and the (45°,45°,45°) cut.<sup>(b)</sup> Both of these have been used by Kalymnios for double field operation<sup>(31)</sup>. Kalymnios has investigated the behaviour of the above XDP modulators under the influence of two orthogonal fields. He concluded that the two field XDP modulators are unlikely to find serious use in electro-optic light modulation. This is mainly due to the non linear distribution of the field in the crystal which ultimately restricts the light path to a very small central region of the modulator cross section. As already stated these cuts are also suitable to be used with the multipath reflection technique and it is more likely to find a use as a single field low voltage

(a) and (b) description according to the Standards on Piezoelectric crystals, Proceedings of the I.R.E., December 1949.



modulator since they do not suffer from the same limitation as the two field modulators. The behaviour and performance of the  $(0^\circ, 45^\circ, 45^\circ)$  multipath amplitude modulators will be examined. Although the  $(45^\circ, 45^\circ, 45^\circ)$  cut can also be used it will not be considered here since it employs the  $d_{36}$  piezoelectric coefficient and this would give rise to appreciable piezoelectric resonances, hence not a useful modulator.

#### 4.4 The $(0^\circ, 45^\circ, 45^\circ)$ cut.

Light propagates at  $45^\circ$  to the z-optic axis. Incident light is vertically polarised and is resolved into two components at an angle of  $45^\circ$  to the horizontal. Because the direction of propagation is not parallel or normal to the optic axis, light is doubly refracted into two rays which are transmitted with different velocities and polarised at right angles to each other. The  $(0^\circ, 45^\circ, 45^\circ)$  crystal is shown in fig. 4.3. The extraordinary ray lies and vibrates in the principal plane which is defined by the direction of propagation and the z-optic axis. The angle between the ordinary and the extraordinary ray is given by<sup>(32)</sup>:

$$\alpha = \tan^{-1} \frac{n_e^2 - n_o^2}{2(n_o^2 \sin^2 \omega + n_e^2 \cos^2 \omega)} \sin 2\omega \quad 4.1$$

where  $\omega$  is the angle which the normal to the wavefront makes with the optic axis. Substituting the values for  $n_e$ ,  $n_o$ , and  $\omega$  yields to:

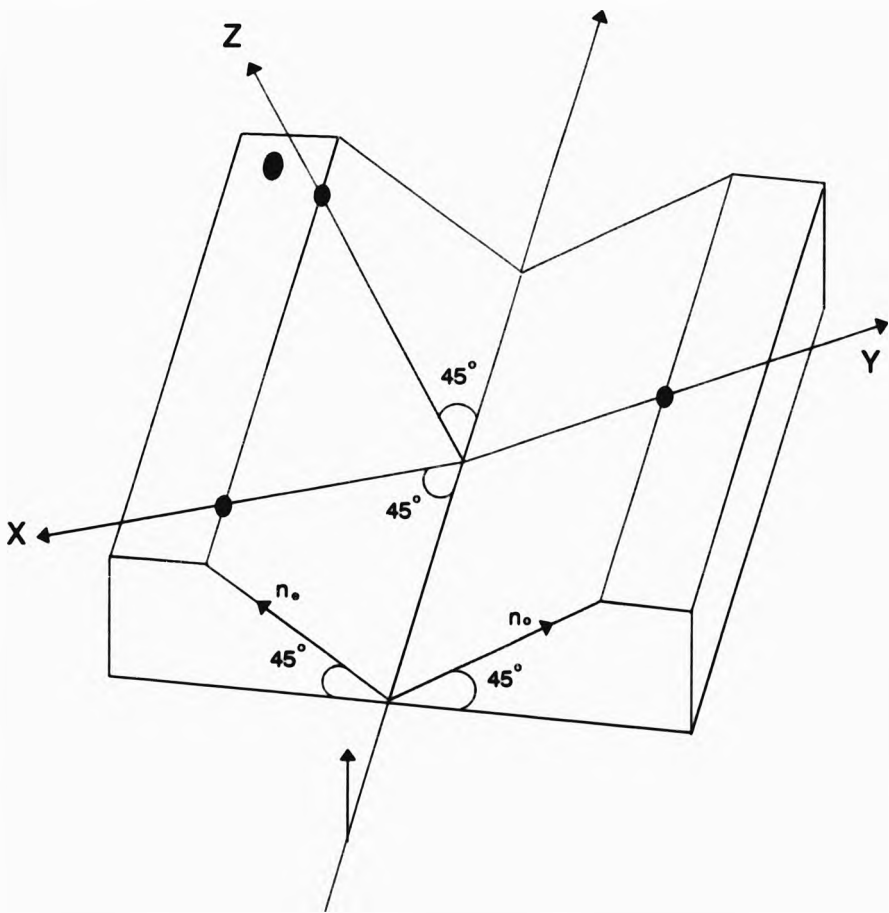


Fig. 4.3 The  $(0^\circ, 45^\circ, 45^\circ)$  cut crystal.

$$\alpha = 1.5^\circ \quad 4.2$$

The two refractive indexes are given by:

$$n'_o = n_o = 1.52 \quad 4.3$$

$$n'_e = \left( \frac{\sin^2 \omega}{n_o^2} + \frac{\cos^2 \omega}{n_e^2} \right)^{-\frac{1}{2}} = 1.50 \quad 4.4$$

4.5 Calculation of the half wave voltage for the  $(0^\circ, 45^\circ, 45^\circ)$  cut crystal.

The half wave voltage for this cut can be found using the general solution of the index ellipsoid outlined by Kalymnios<sup>(27)</sup>. We have,  $\varphi = 0^\circ$ ,  $\theta = 45^\circ$ ,  $\psi = 45^\circ$ . First the direction cosines are computed.

$$a_{11} = \cos \phi \cos \theta \cos \psi - \sin \phi \sin \psi = \frac{1}{2} \quad 4.5$$

$$a_{12} = \sin \phi \cos \theta \cos \psi + \cos \phi \sin \psi = \frac{1}{\sqrt{2}} \quad 4.6$$

$$a_{13} = -\sin \theta \cos \psi = -\frac{1}{2} \quad 4.7$$

$$a_{21} = -\cos \phi \cos \theta \sin \psi - \sin \phi \cos \psi = -\frac{1}{2} \quad 4.8$$

$$a_{22} = -\sin\phi \cos\theta \sin\psi + \cos\phi \cos\psi = \frac{1}{\sqrt{2}} \quad 4.9$$

$$a_{23} = \sin\theta \sin\psi = \frac{1}{2} \quad 4.10$$

$$a_{31} = \cos\phi \sin\theta = \frac{1}{\sqrt{2}} \quad 4.11$$

$$a_{32} = \sin\phi \sin\theta = 0 \quad 4.12$$

$$a_{33} = \cos\theta = \frac{1}{\sqrt{2}} \quad 4.13$$

Then the coefficients A, B, D, a, b, and d are computed. These are given by:

$$A = a_{11}a_{1m}S_{1m} = a_{11}a_{11}S_{11} + a_{12}a_{12}S_{22} + a_{13}a_{13}S_{33} = \frac{3}{4}S_{11} + \frac{1}{4}S_{33} \quad 4.14$$

$$B = a_{21}a_{2m}S_{1m} = a_{21}a_{21}S_{11} + a_{22}a_{22}S_{22} + a_{23}a_{23}S_{33} = \frac{3}{4}S_{11} + \frac{1}{4}S_{33} \quad 4.15$$

$$D = a_{11}a_{2m}S_{1m} = a_{11}a_{21}S_{11} + a_{12}a_{22}S_{22} + a_{13}a_{23}S_{33} = \frac{1}{4}S_{11} - \frac{1}{4}S_{33} \quad 4.16$$

$$a = a_{11}a_{1m}a_{2m}r_{1mn}E_r = [a_{12}a_{13}a_{11}r_{41} + a_{13}a_{12}a_{11}r_{41} + a_{13}a_{11}a_{12}r_{41} + a_{11}a_{13}a_{12}r_{41} + a_{11}a_{12}a_{13}r_{63} + a_{12}a_{11}a_{13}r_{63}]E_1 = -\frac{1}{4\sqrt{2}}r_{41}E_1 \quad 4.17$$

$$b = a_{21}a_{2m}a_{rn}r_{lmn}E_r = [a_{22}a_{23}a_{11}r_{41} + a_{23}a_{22}a_{11}r_{41} + a_{23}a_{21}a_{12}r_{41} + a_{21}a_{23}a_{12}r_{41} + a_{21}a_{22}a_{13}r_{63} + a_{22}a_{21}a_{13}r_{63}]E_1 = \frac{1}{2\sqrt{2}}r_{63}E_1 \quad 4.18$$

$$d = a_{11}a_{2m}a_{rn}r_{lmn}E_r = [a_{12}a_{23}a_{11}r_{41} + a_{13}a_{22}a_{11}r_{41} + a_{13}a_{21}a_{12}r_{41} + a_{11}a_{23}a_{12}r_{41} + a_{11}a_{22}a_{13}r_{63} + a_{12}a_{21}a_{13}r_{63}]E_1 = \frac{1}{2\sqrt{2}}r_{41}E_1 \quad 4.19$$

The next step is to calculate P, L, q and t which are given by:

$$P, L = \frac{(A+B)}{2} \pm \frac{1}{2} [(A-B)^2 + 4D^2]^{\frac{1}{2}} \quad 4.20$$

$$q, t = \frac{a+b}{2} \pm \frac{1}{2} \frac{(A-B)(a-b) + 4Dd}{[(A-B)^2 + 4D^2]^{\frac{1}{2}}} \quad 4.21$$

Substituting for A, B, D, a, b, d in the above gives:

$$P = S_{11} \quad 4.22$$

$$L = \frac{1}{2}(S_{11} + S_{33}) = \frac{1}{2} \left( \frac{1}{n_o^2} + \frac{1}{n_e^2} \right) = \frac{1}{n_{oe}^2} \quad 4.23$$

$$q = 0 \quad 4.24$$

$$t = -\frac{1}{\sqrt{2}}r_{41}E \quad 4.25$$

The electrically induced birefringence is given by:

$$\Delta n = \frac{1}{2} \left( \frac{Q}{P^{\frac{3}{2}}} - \frac{C}{L^{\frac{3}{2}}} \right) = -\frac{1}{2\sqrt{2}} n_{oe}^3 r_{41} E \quad 4.26$$

The electrically induced retardation is therefore given by:

$$\Gamma = \frac{2\pi}{\lambda} \Delta n = \frac{\pi}{\lambda} \frac{1}{\sqrt{2}} n_{oe}^3 r_{41} E \quad 4.27$$

and from the above the half wave voltage for unit aspect ratio is given by:

$$V_{\frac{\lambda}{2}} = \frac{\sqrt{2}\lambda}{n_{oe}^3 r_{41}} = 11.0KV \quad 4.28$$

This value is 29% greater than the corresponding half wave voltage of the 45° x cut.

4.6 Calculation of the effective permittivity for the (0° 45° 45°) cut crystal.

Another important parameter is the capacitance of the crystal. This is a very important figure of merit because it ultimately determines the frequency response of the modulator. The capacitance can be determined by the dielectric constant along the direction which the electric field is applied.

The dielectric matrix for the ADP is given by:

$$E = \begin{vmatrix} \epsilon_{11} & 0 & 0 \\ 0 & \epsilon_{22} & 0 \\ 0 & 0 & \epsilon_{33} \end{vmatrix} \quad 4.29$$

$$\text{where } \epsilon_{11} = \epsilon_{22} \cdot \epsilon_{33} \quad 4.30$$

Now from section 2.1 we have:

$$S_{k1} = a_{k1} a_{1j} S_{1j}$$

This transforms the dielectric matrix so that the dielectric constant along the required direction can be found. The dielectric constants along the three orthogonal edges  $X_1$ ,  $X_2$  and  $X_3$  are given by:

$$\epsilon'_{11} = a_{11} a_{11} \epsilon_{11} + a_{12} a_{12} \epsilon_{22} + a_{13} a_{13} \epsilon_{33} \quad 4.31$$

$$\epsilon'_{22} = a_{21} a_{21} \epsilon_{11} + a_{22} a_{22} \epsilon_{22} + a_{23} a_{23} \epsilon_{33} \quad 4.32$$

$$\epsilon'_{33} = a_{31} a_{31} \epsilon_{11} + a_{32} a_{32} \epsilon_{22} + a_{33} a_{33} \epsilon_{33} \quad 4.33$$

For the ADP material we have  $\epsilon_{11} = \epsilon_{22} = 56$ ,  $\epsilon_{33} = 15$  and in the  $(0^\circ, 45^\circ, 45^\circ)$  cut modulator the electric field is applied along  $X_1$ . Substituting gives:

$$\epsilon'_{11} = 45.75. \quad 4.34$$

#### 4.7 The composite modulator.

There are four possible ways that a  $(0^\circ, 45^\circ, 45^\circ)$  cut crystal can be placed on a plane and these are shown in fig. 4.4 and fig. 4.5. The polarisation directions and the two ray paths are also shown. From that it can be concluded that four crystals all differently orientated with respect to each other are required to eliminate both double refraction and natural birefringence. The four crystal composite

modulator is shown in fig. 4.6.a. The first crystal used in a composite modulator arrangement produces a displacement of the two beams that has to be compensated by a second crystal. Because an extraordinary ray continues to behave as an extraordinary ray in both crystals comprising a pair that splits and recombines the two beams it is necessary to use another crystal pair to interchange the role of the e-ray and o-ray. As a result compensation of birefringence occurs both for temperature changes and for changes in angle of incidence. Angular compensation is necessary because all the laser beams are bound to have a divergence that tends to limit the uniform illumination of the output aperture of the modulator resulting to poor extinction ratios. In the case of the  $(0^\circ, 45^\circ, 45^\circ)$  cut modulator, successful angular compensation is of prime importance because when light propagates at  $45^\circ$  to the optic axis, the change of birefringence for small deviations from this angle is at a maximum. An interchange of any of two or three crystals will not affect the operation of the modulator as long as each crystal stays in the same orientation and is driven by the appropriate electric field. This interchange of crystals gives another five possible arrangements for the composite modulator. These are shown in fig. 4.6 and fig. 4.8. Since all the six possible composite arrangements are equivalent, in theory they should give the same performance. From a practical point of view the composite schemes shown in fig. 4.7 present less engineering problems as it will be shown in 6.5.4.



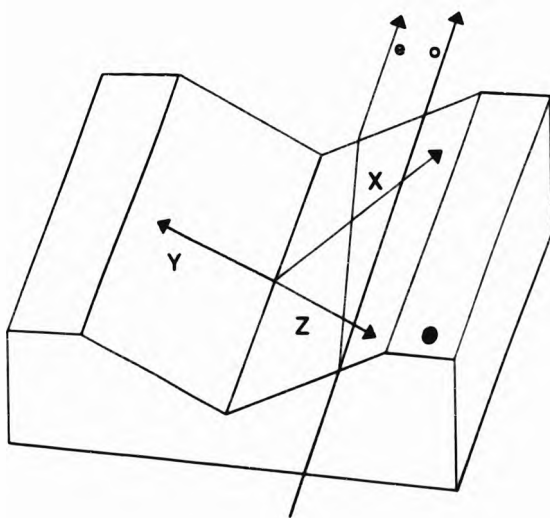
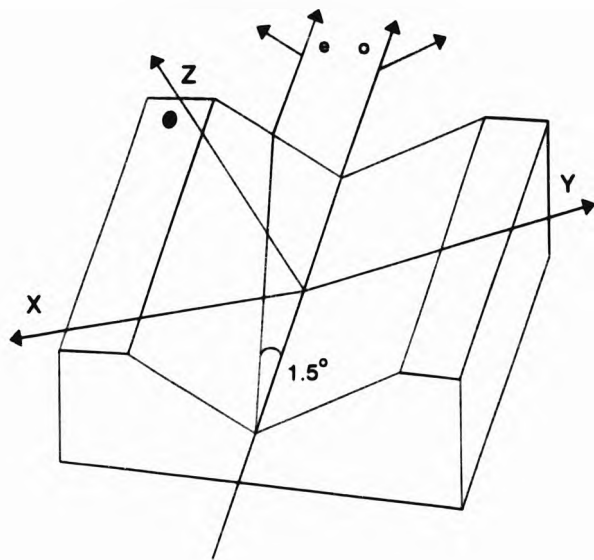


Fig. 4.4 Ray directions in the  $(0^\circ, 45^\circ, 45^\circ)$  cut crystal

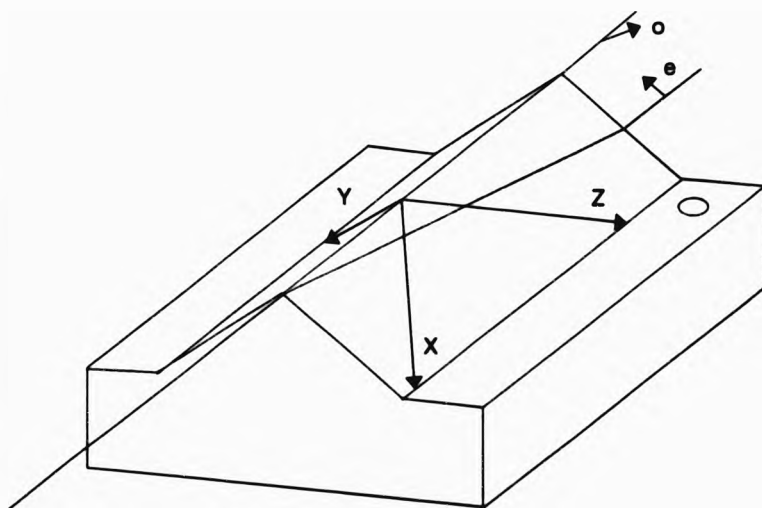
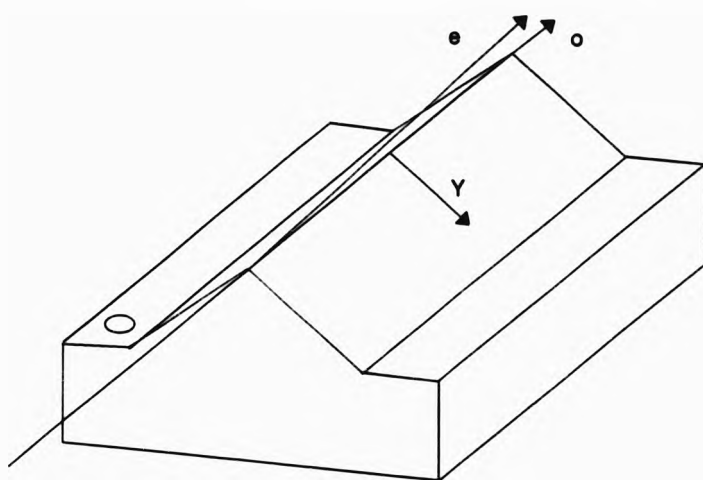


Fig. 4.5 Ray directions in the  $(0^\circ, 45^\circ, 45^\circ)$  cut crystal.

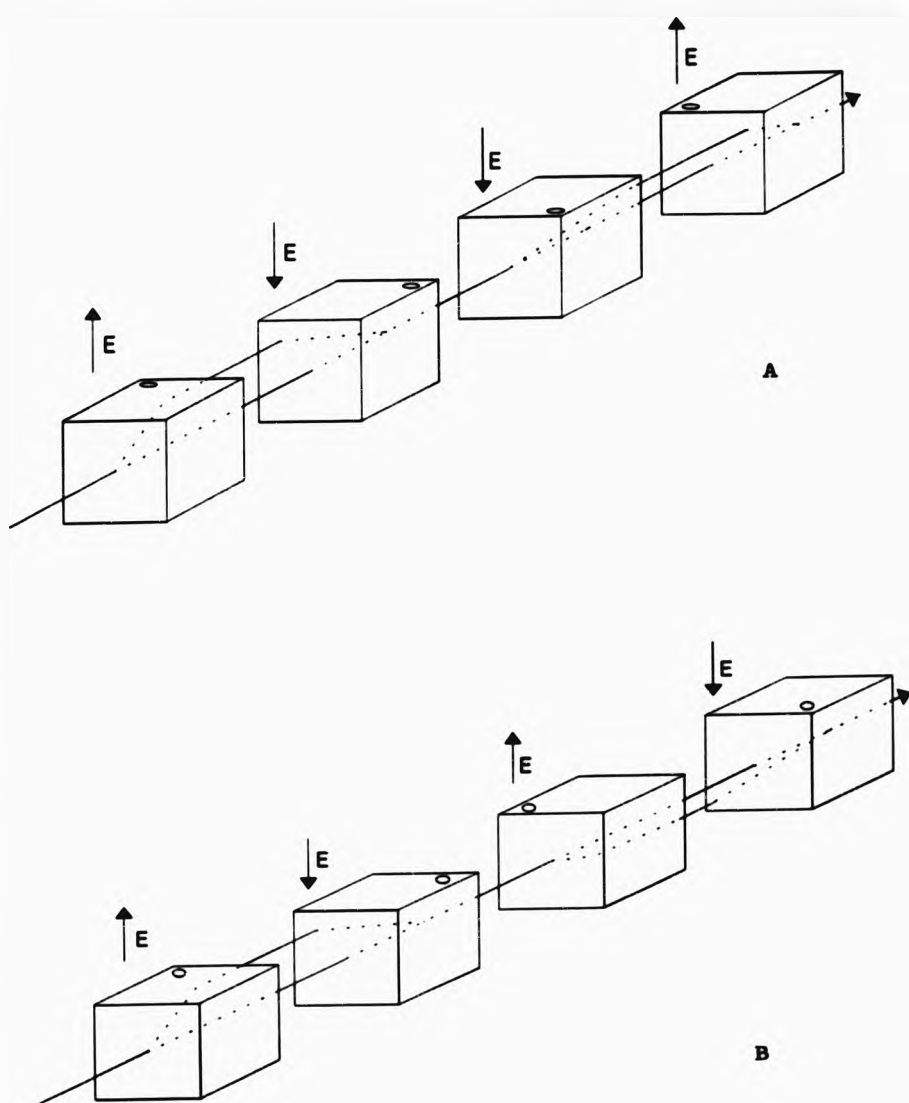


Fig. 4.6 Composite modulator schemes and ray directions.

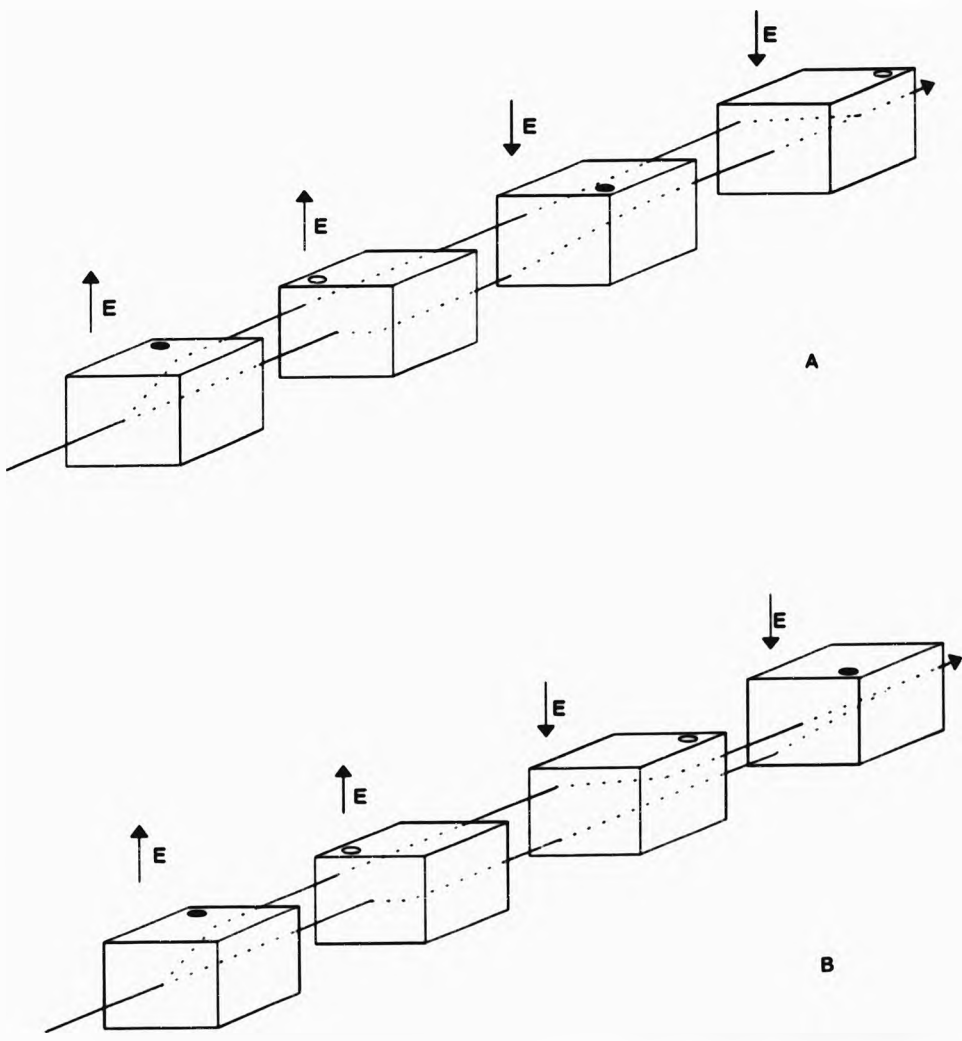


Fig. 4.7 Composite modulator schemes and ray directions.

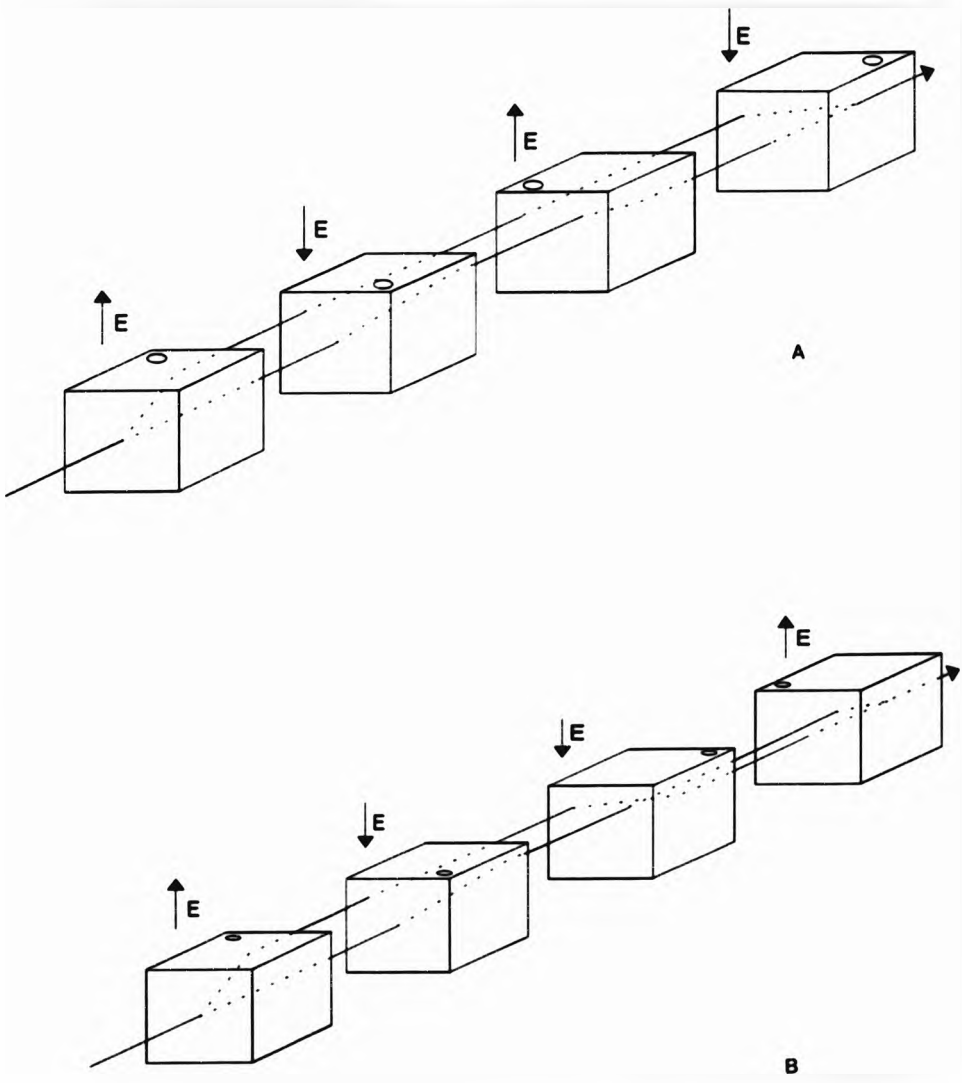


Fig. 4.8 Composite modulator schemes and ray directions.

## CHAPTER 5 THE DESIGN OF MULTIPATH MODULATORS

### 5.1 Basic considerations.

Considering the problems related to electro-optic multipath modulators, one of the most serious ones was to select the dimensions of the crystals to be used. The dimensions of the crystals and to a greater extent the width of them imposed the most severe limitations for the design. One would superficially assume that the bigger the width the better because more passes would be possibly accommodated through the crystals and this would lead to a further reduction of the half wave voltage. But as already stated in section 1.4 other parameters were equally important and in this case wider crystals would increase the total capacitance causing a reduction in the useful electrical bandwidth of the modulator.

Also because in every modulator the extinction ratio strongly depends on the quality of the polished crystal surfaces it was reasonable to expect an extinction ratio deterioration caused from the additional passes since perfect surfaces do not exist. Obviously one would expect that for more passes through the modulator the worse the extinction ratio. Another problem arose from the fact that the light beam had to have a longer path through the electro-optic material and any strain effects were more likely to further reduce the maximum available extinction ratio. An educated choice had to be made regarding the width of the crystals. A

rigorous theoretical analysis of the dependence of the extinction ratio on all the above parameters is a very difficult problem. To calculate or even predict a figure for the extinction ratio, given the number of passes, would be impossible because of the uncertainties related to the quality of the electro-optic material and optical finishing. But even if this was an easy task to perform, other phenomena discussed in a following chapter, would be the limiting factor of performance. In conclusion therefore such a theoretical investigation would not be very helpful from a design point of view. For these reasons such an analysis had not been attempted but instead the extinction ratio figures were experimentally obtained for electro-optic modulators whose crystal dimensions were chosen by considering other factors. The factor which determined the number of passes and consequently the crystal width was the percentage of reduction of the half wave voltage. Arbitrarily a length of 15mm and a height of 2.5mm were chosen for the crystals. The half wave voltage  $V_{HW}$  at 633nm for such a modulator is given by:

$$V_{HW} = \frac{A}{l} V_{\frac{1}{2}} = 452V \quad 5.1$$

where:

A is the aperture of the modulator

l is the length of the modulator

$V_{\frac{1}{2}}$  is the half wave voltage for a unit aspect ratio given from equation 4.28.

Two reflections would reduce it to 151V and another two

down to 90V. The transition from 452V to 151V corresponds to a 67% reduction but from 151V to 90V the reduction is now decreased to 40%. Adding more passes progressively makes this reduction become smaller. Table 5.1 gives the relation between the number of passes, the new half wave voltage and the improvement in terms of percentage relative to the previous one. Data on the power levels required for full modulation are also included.

n	V <sub>HW</sub> (V)	reduction (%)	P(W)	reduction (%)
1	452	-	673.0	-
3	151	67	75.0	89
5	90	40	27.0	64
7	65	28	14.0	49
9	50	23	8.0	41
11	41	18	5.6	32
13	35	17	3.8	32
15	30	14	3.0	21
17	27	13	2.3	23
19	24	11	1.8	21

TABLE 5.1 Voltage and power requirements for various number of passes. *(calculated data)*

The table shows that 9 passes is a critical point because increasing further the number of passes does not yield to a significant decrease of the driving requirements. So a good starting point was to design the modulator for 9 passes. Initially it was assumed <sup>that</sup> the beam <sup>would</sup> enter and leave the modulator through square apertures with dimensions of 2.5 mm x 2.5 mm. This aperture would easily accommodate a standard HeNe laser with a 1.0 mm beam diameter centrally through it.



Now referring to fig. 5.1 a distance S of 2.0 mm was assumed between any two successive spots. This gap was necessary for the beam to safely enter and leave the modulator. The necessary total width is given by:

$$W = \frac{A}{2} + 9 \left( \frac{d}{2} + \frac{S}{2} \right) + \frac{A}{2} = 16.0 \text{ mm} \quad 5.2$$

where :

A is the aperture

d is the beam diameter

S is the safety distance factor

The width was finally decided to be 16.5 mm. By varying the angle of incidence we can also vary the number of passes. Table 5.2 contains data on the relationship between n the number of passes,  $\theta_{INT}$  the internal angle of incidence and  $\theta_{EXT}$  the external angle of incidence assuming a refractive index for the modulator cavity of  $n_D=1.5$ .

n	$\theta_{INT}$ (Degrees)	$\theta_{EXT}$ (Degrees)
1	12.1	18.2
3	4.1	6.2
5	2.5	3.8
7	1.7	2.6
9	1.4	2.1

TABLE 5.2 Internal and external angles of incidence for various number of passes.

It seemed that differentiation between the small angles required to change the number of passes would be an easy task

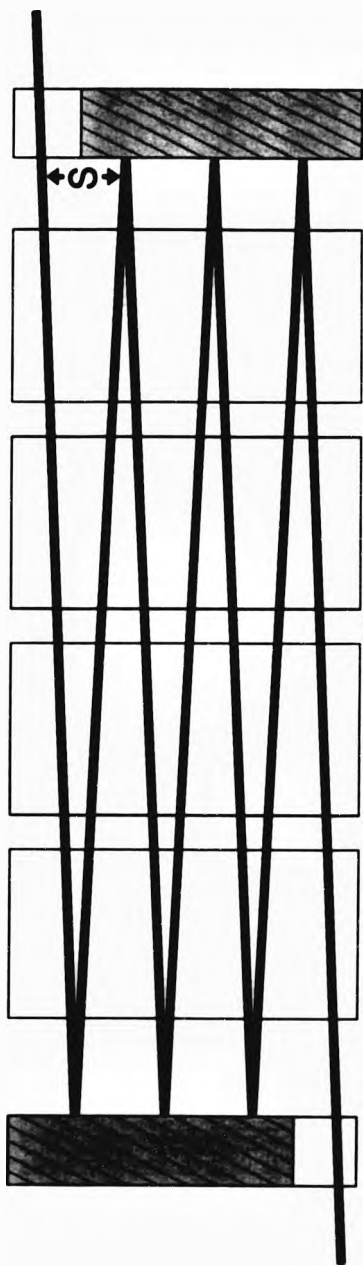


Fig. 5.1 The multipath reflection technique.

to perform. Such changes of the angle of incidence are well within the capabilities of the angular resolution of any rotation stage.

#### 5.2 Estimation of the modulator capacitance and bandwidth.

The capacitance of the modulator as seen from the driving generator output port is given by:

$$C_T = C_M + C_C = 4C_{CR} + C_P + C_C \quad 5.3$$

where :

$C_{CR}$  is the crystal capacitance

$C_P$  is the modulator parasitic/stray capacitance due to electrodes, modulator body connectors etc.

$C_C$  is the driving cable capacitance

The capacitance of the crystal is given by:

$$C = \epsilon \epsilon_0 \frac{A}{d} = \epsilon \epsilon_0 W \frac{l}{d} \quad 5.4$$

The dielectric constant is given by equation 4.34 as 45.75. Substituting in the above equation, one obtains 40pF per crystal. The inter-connecting cable between the modulator and the driving electronics adds a parasitic load as well and can easily equal the modulator capacitance for moderate lengths of cable. The modulator was driven using one meter of standard RG58 coaxial cable. The cable's capacitance is 100pF per meter and this results to 260pF total capacitance excluding  $C_P$ , the parasitic capacitance. Some stray capacitance is always present and special precautions were taken during design and assembly to keep it down to as a low

value as possible. Emphasis was given to the length of the electrodes and to produce a neat construction which would keep  $C_p$  down to a few picofarads. A bandwidth of up to 20 MHz would then be possible without having the modulator terminated to the characteristic impedance of the line.

### 5.3 Estimation of the transmission loss.

As a beam of light travels through the modulator a drop in the intensity is to be expected and this drop can be attributed to absorption and reflection losses. Absorption losses take place within the cavity of the modulator and the amount of it will depend on the wavelength of the laser light, the amount of the absorbing material in the total path of the beam and the absorptance of the material at that wavelength. The absorption of ADP is given<sup>(14)</sup> as 0.5 dB per meter over the entire visible range. If the modulator is air filled then any losses due to the air can be neglected but if instead, an index matching oil is used then these losses might be significant and should be taken into consideration. The oils used had a very good coefficient of transmission and the total path of the beam through the oil was kept to 5 mm per pass. Even in the case of 9 passes which was the maximum number achieved the total length did not exceed 45 mm so any losses due to the oil were not taken into account. Losses are due to Fresnel reflection at the following interfaces:

- (a) input port air-glass.
- (b) input port glass-air or oil.

- (c) ADP-air or oil.
- (d) mirror-air or oil.
- (e) output port glass-air.
- (f) output port glass-air or oil.

Table 5.3 contains transmission data for different number of passes and for different index matching conditions.

n	T <sub>AIR</sub>	T <sub>FREON</sub>	T <sub>FC43</sub>	T <sub>DC250</sub>	T <sub>DC550</sub>
1	72%	96%	97%	99%	100%
3	38%	88%	92%	97%	100%
5	20%	81%	88%	95%	100%
7	10%	75%	84%	94%	100%
9	5%	68%	79%	92%	100%

TABLE 5.3 Percentage of optical transmission for various number of passes. (calculated data)

#### 5.4 Index matching oil considerations.

The transmission figures given in table 5.3 dictate that high optical losses were to be expected in the case of the air filled modulator. The presence of an appropriate index matching liquid improves the overall performance of a modulator because of the following reasons:

- (a) The internal Fresnel reflective losses are reduced and the overall transmission is increased.
- (b) prevents the degradation of the crystal surfaces and protects the crystals. Although air filled electro-optic

cells are usually sealed a deterioration of the crystals surfaces is sometimes unavoidable and <sup>10e3</sup> should be refurbished from time to time to restore maximum performance.

(c) RF heating of the crystals through dielectric losses causes thermal gradients and mechanical strains. These effects result in deflection/or decollimation of the light beam and a shift of the operating point. The presence of the liquid minimises these effects by conducting the heat away from the crystals and keeping a more constant temperature operating point throughout the modulator cavity.

(d)\ Reduces the piezo-electric resonances that might be present by dampening the crystals piezoelectric movements. The electro-optic cell can turn on and off more cleanly with less ringing and this results into a flat frequency response.

(e) Unwanted diffraction patterns caused by imperfections of the surface quality of the crystals and scattering have a serious adverse effect on performance and in particular to the extinction ratio and output beam quality. The presence of the liquid reduces the scattering and the wavefront distortion of the emergent laser beam.

Ideal liquids for filling the modulator should be stable chemical compounds, non volatile, non toxic, should not contain or absorb water, transparent in the visible region with a low absorbtion coefficient, good insulators, with a good thermal conductivity and a low coefficient of thermal

expansion. In addition to all the above requirements, they should also ideally, have the same refractive index with the crystals.

Unfortunately, using a liquid inside the electro-optic cell can give problems with high pressure at elevated temperatures and vapour bubble formation at low temperatures. Usually volume compensating bellows are incorporated in the cell to remove the internal pressure changes which may cause crystal stress. Such extreme temperatures are unlikely to occur in a normal laboratory environment so the whole matter was not further pursued.

The following liquids were used at different stages of this work.

- (a) Freon,  $n_D=1.30$ .
- (b) Fluorocarbon FC 43,  $n_D=1.34$ .
- (c) Dow Corning silicon oil DC 250,  $n_D=1.40$ .
- (d) Dow Corning silicon oil DC 550,  $n_D=1.49$ .
- (e) Gargille siloxane,  $n_D=1.50$ .

#### 5.5 Basic description of the modulator.

All the modulators constructed during this research had a cylindrical type of shape. The electro-optic crystals were properly mounted on specially designed crystal cases and were safely kept inside the main cylindrical body of the modulator. The modulating voltage was applied using the connectors which were available on the main body. The crystal

cavity was sealed using the two glass-mirror windows. Mechanical parts aiming for the proper positioning and alignment of the mirrors were also incorporated in the design. Fig. 5.2 a and b shows the external view of the modulator and internal construction details.

#### 5.5.1 The modulator body.

Aluminium was chosen for its good thermal conductivity and ease of machining. Two holes were made on the top to support the four BNC connectors. The cylinder walls were quite thick (12mm) for rigidity and also to assist the conduction of heat and minimise thermal gradients within the cavity. Grooves were machined internally at both ends to locate a set of sealing o-rings.

#### 5.5.2 The crystal case and the mounting of crystals.

One serious problem associated with the use of electro-optic crystals as modulators is how to mount them on the crystal case. The crystals have to be safely kept in position otherwise changes in the transmission and deterioration of the extinction ratio is unavoidable. The worst case, of course, would be for the crystals to move freely or even completely come out. In such a catastrophic event it is possible for the crystals polished surfaces to touch and deterioration of the optical finish is more than certain. On the other hand too much pressure or heavy clamping can break the fragile crystals or photo-elastically bias the modulator. This effect



cavity was sealed using the two glass-mirror windows. Mechanical parts aiming for the proper positioning and alignment of the mirrors were also incorporated in the design. Fig. 5.2 a and b shows the external view of the modulator and internal construction details.

#### 5.5.1 The modulator body.

Aluminium was chosen for its good thermal conductivity and ease of machining. Two holes were made on the top to support the four BNC connectors. The cylinder walls were quite thick (12mm) for rigidity and also to assist the conduction of heat and minimise thermal gradients within the cavity. Grooves were machined internally at both ends to locate a set of sealing o-rings.

#### 5.5.2 The crystal case and the mounting of crystals.

One serious problem associated with the use of electro-optic crystals as modulators is how to mount them on the crystal case. The crystals have to be safely kept in position otherwise changes in the transmission and deterioration of the extinction ratio is unavoidable. The worst case, of course, would be for the crystals to move freely or even completely come out. In such a catastrophic event it is possible for the crystals polished surfaces to touch and deterioration of the optical finish is more than certain. On the other hand too much pressure or heavy clamping can break the fragile crystals or photo-elastically bias the modulator. This effect

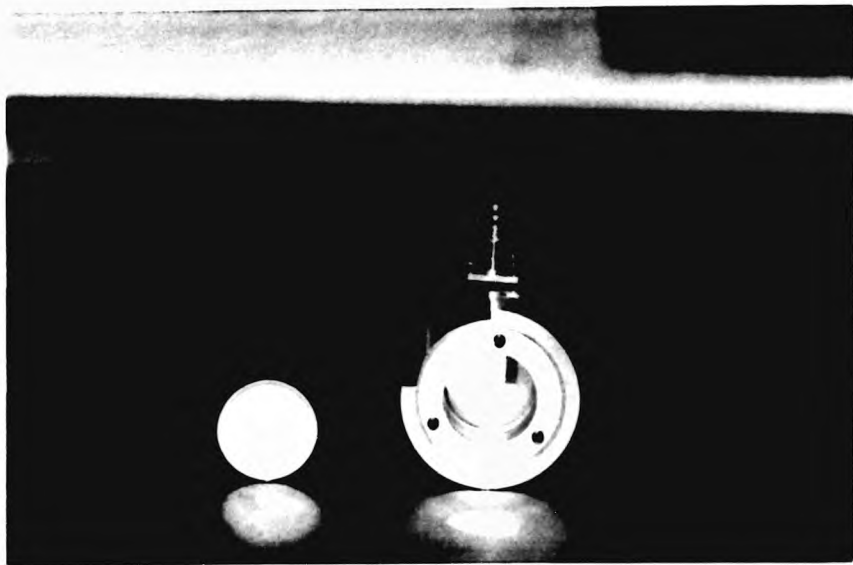


Fig. 5.2 External and Internal view of the modulators.

can be tens or hundreds of times bigger than the electro-optic effect and as a result electro-optic modulation will be rendered impossible. Also, if proper care is not taken in the mounting of crystals, unwanted strains may be introduced which will degrade the performance and in particular the extinction ratio of the modulator. Mechanical strains produce variations in the refractive index and in the birefringence throughout the crystal, distort the wavefront, diffuse the optical bias condition and reduce the degree of modulation<sup>(33)</sup>. It is clear from the above that the mechanism responsible for keeping the crystals in the right place was of prime importance.

Another problem was the electroding of the crystals. Although gold had been vacuum deposited on the two opposite sides of the crystals there was still the problem of how to make good and reliable contacts with the electrodes. Soldering methods widely used in electronics could not be used because the crystals would not survive such a thermal shock. Instead strip electrodes were cemented using an appropriate paste. Silver was preferred over the less expensive copper because of its marginally better conductivity. Extreme care was also taken to use the right type of silver paste and the minimum amount necessary to make proper contacts otherwise strain could have been introduced.

A number of modulators were constructed. The first prototype used the crystal case shown in fig. 5.3. Nylon was chosen for the material and a rod of it was machined down to



**Fig. 5.3 The crystal platform assembly.**

26mm, the internal diameter of the modulator body, and then accurately milled to its final shape. The milling process was of paramount importance because it created the two orthogonal reference planes used for proper positioning and alignment of the four crystals. Since it was a practical impossibility to achieve a true 90 degree shape from the milling-cutting process, a groove along the edge of the reference plane was machined to ensure an unobstructive (clear) edge. Four holes were drilled to enable the bottom electrodes to be pushed through and make contact with the crystal faces resting on the case. All four holes were opened from top to bottom otherwise uneven sections on the surface would be formed around the holes. A slow drilling speed was also used (300 revs per min) to avoid deformation of the crystal case because of heating up of the nylon material. V grooves were also machined on the outer surface for the electrodes to be pushed inside avoiding unwanted short circuits with the modulator body which for safety reasons was always at true earth potential. These grooves were located in such a way so that the minimum possible length of strip electrodes was required to interconnect all four crystals together and with the two BNC connectors. Keeping the length of the interconnecting strips to a minimum not only minimised the stray capacitance but also resulted to the lowest value for the parasitic inductance and ohmic losses. Flat silver strips were preferred over round silver wires because they have a greater surface to volume ratio thus ensuring a better behaviour of the conductors at frequencies where skin effects would be noticeable.

### 5.5.3 The mirror windows.

A very important element of the multipath modulator design was the necessity of <sup>having</sup> two mirrors and a mechanism of positioning and accurately aligning them. The mirrors required for such a modulator should meet stringent specifications. First because the beam had to be reflected several times within the cavity, reflection losses would limit the overall transmission, assuming no other losses, to

$$I_o = I_i r^{n-1} \quad 5.5$$

where:

$I_i$  is the intensity of the beam entering the modulator

$n$  is the number of passes

$r$  is the reflectivity of the mirrors

$I_o$  is the intensity of the beam leaving the modulator

A silver or aluminum mirror with an average reflectance of 0.94 typically, would account for a 40% loss in the total optical transmission after 9 passes. This was considered to be very high thus it was decided that high reflectivity multilayer dielectric mirrors should be used despite their relatively high cost of production.

In addition to the high reflectivity requirements, the mirrors had to also be broadband. Since one of the main features of the (0°, 45°, 45°) cut multipath modulator design is the elimination of the half wave plate and its wavelength dependence it would be very undesirable to limit the useful

optical bandwidth of the device because of the mirrors inability to perform accordingly over the visible range of wavelengths. Also because the operation of the (0°,45°,45°) cut modulator and every modulator is polarisation dependent the mirrors should not alter, shift or rotate the state of polarisation of the incident beam. Gold mirrors with a reflectance of 99% could also be a solution with the advantage of being cheaper compared to the dielectric ones. Two unsuccessful attempts were made to deposit pure gold on the two glass windows. It was soon found out that gold has not good adhesive properties on the glass substrate and the coatings produced were very soft. They were immediately destroyed after an attempt to clean them using a lens cleaning tissue. Chromium has to be deposited first which was not possible with the equipment used (Edwards Speedivac vacuum coating unit).

An aluminium jig capable of holding 16 BK7 glass windows was constructed and used to deposit the broadband dielectric coating in one run. The reflectivity specification for these mirrors was over 99% over the visible wavelengths and these were made commercially to our requirements.

#### 5.5.4 Mirror alignment mechanics and considerations.

The mechanics responsible for holding the mirrors in situ and aligning them are shown in fig 5.4. The inner set of o-rings was placed into the grooves machined on the modulator body at the points where the cavity ends. The bore<sup>in</sup> which the

two mirrors were kept was made 1 mm longer than the diameter of the glass substrates. This clearance gap provided a freedom of rotation of the mirrors inside the bore for alignment purposes. The mirrors were sandwiched between two sets of o-rings for protection and for sealing purposes. The outer set of o-rings were located in v-grooves machined on the two inner aluminium windows. Finally two aluminum windows with threaded external periphery were screwed in at both ends of the modulator which were internally threaded until they firmly touched with the inner windows. The applied pressure pushed the mirrors against the o-rings and effectively the cavity of the modulator was sealed at both ends.

The mechanics for the adjustments of the mirrors were designed to provide smooth and precise angular motion. A good degree of angular sensitivity was required to enable the mirrors to be accurately positioned parallel to each other and parallel with the crystals. This was necessary for the reflected beams inside the cavity to centrally re-enter the crystals at one end and come out again centrally at the other. Even misalignments of 5 minutes of an arc would cause the beam to deviate from the original path and strike either the top or bottom electroded surface of one of the crystals. The two external window rings were drilled and threaded at 3 points symmetrically placed at 120 degrees on the circumference of the ring. Control was provided by 3 grub screws. By forward screwing on the screws, excess pressure was applied at that point causing local compression of the o-ring. Backward screwing caused local expansion. These unequal



local deformations of the o-ring were thought to permit satisfactorily angular tilt of the mirrors in all directions.

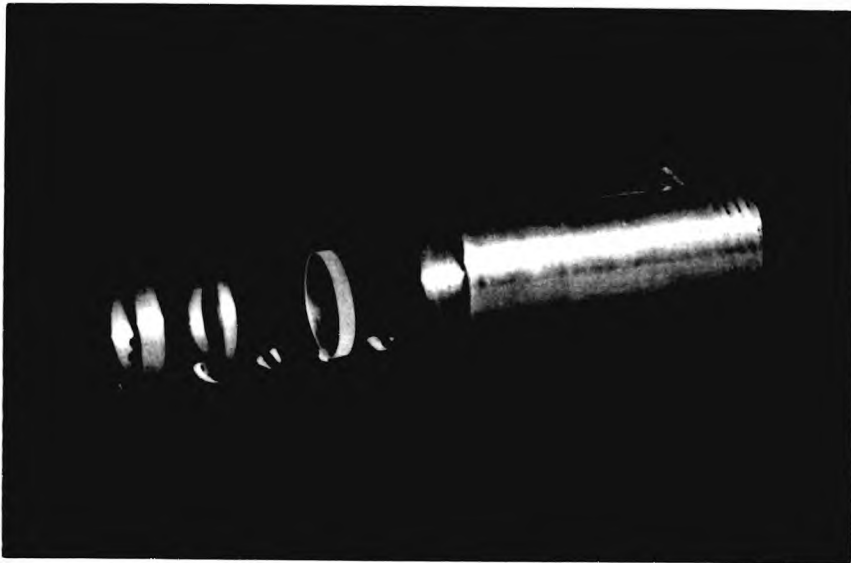


Fig. 5.4 The mirror alignment mechanics.

## CHAPTER 6 EXPERIMENTAL

### 6.1 Tests performed before the assembly of the modulator.

The crystals used for this research were obtained from Electro-optic Developments Ltd, Basildon, Essex, (who supported this work) and were polished flat to  $\lambda/10$  and with 30 arc seconds parallelism. Prior to assembly the following observations and measurements were made.

(a) All seven crystals available were visually checked for scratches and cloudy areas within the ADP material. Crystal number 7 was rejected because for not being of the same transparency standard compared to the other six crystals. The remaining 6 crystals were scanned throughout using the laser giving an interference free, clean spot on a white target 1 meter away. All the crystals were then assumed to be of the same high standard and four were randomly selected for the modulator.

(b) The capacitance of the crystals was measured and found 40pF per crystal. This value is in excellent agreement with the theoretical value predicted from equation 5.4.

(c) The angle between the ordinary ray and the extraordinary ray was experimentally found using the set up shown in Fig. 6.1. The lens focused the incident laser beam down to the diffraction limit giving a very small spot. The screen was a piece of graph paper placed at the focal point of the lens.

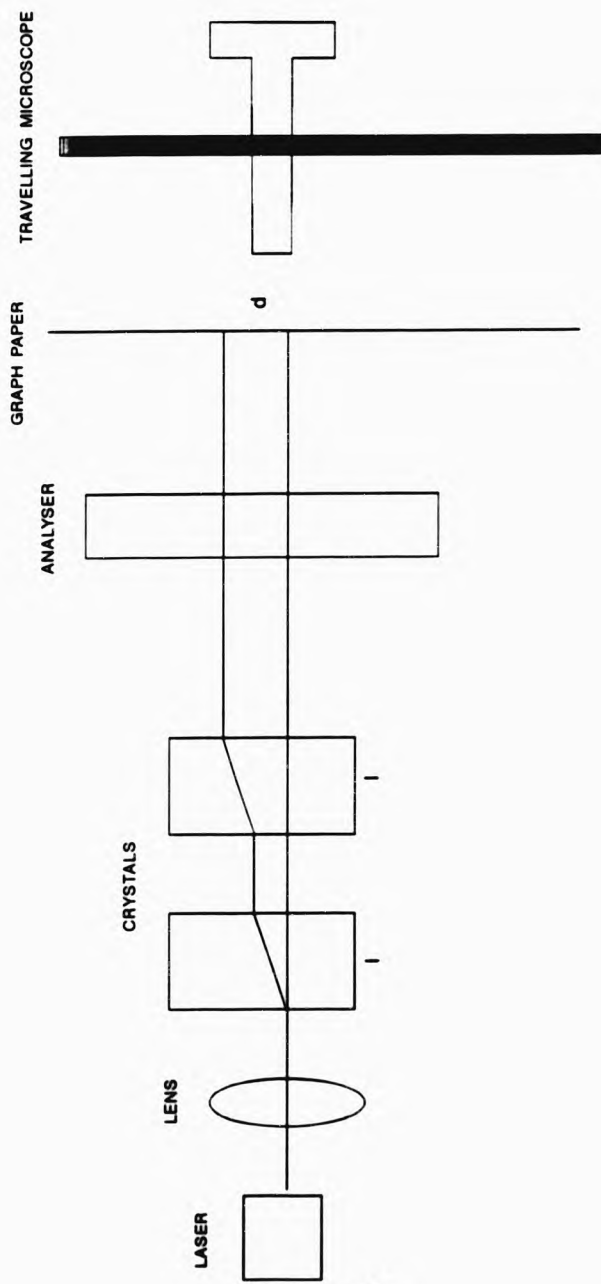


Fig. 6.1 Set up for the measurement of angle between the o-ray and the e-ray.

The travelling microscope was also focused on the other side of the graph paper screen. Two ADP crystals were placed on an appropriate glass test plate with the same orientation to reinforce the displacement of the two rays. Double refraction within the crystals caused the incident beam to split into two, therefore giving two distinct spots on the screen. The distance between them was easily measured using the travelling microscope. To verify that the two spots were actually created by the crystals double refraction properties an analyzer was introduced in the path of the beam after the crystals. Rotation of the analyzer caused extinction of one spot and a further 90 degrees rotation caused extinction of the other spot. The angle between the two rays was simply given by:

$$\alpha = \tan^{-1} \frac{d}{2} l = 1.52^\circ \quad 6.1$$

The value obtained is in close agreement with the theoretical value given by equation 4.2. The experimental values obtained for the angle between the two rays and the capacitance of the crystal was a good indication that the crystals were sliced out from the main crystal boule according to the required specifications. At this point it has to be mentioned that the above two conditions do not necessarily satisfy the criterion for the crystals to be of the (0°, 45°, 45°) cut because other cuts might also exhibit equal or very similar figures as the following table shows.

CRYSTAL CUT	$\theta$ (degrees)	$\epsilon$	$V_{\lambda/2}$ (KV)
45°Z	0	15	20.0
45°Y	1.52	56	7.8
45°Y	1.52	37	7.0
(45°, 45°, 45°)	1.52	-	9.9
(0°, 45°, 45°)	1.52	45.75	11.0

TABLE 6.1 Data for different ADP crystal cuts

Such an uncertainty could only be fully resolved from the measurement of the half wave voltage of the composite modulator.

#### 6.2 Assembly of the modulator.

Assembling the multipath modulator was in itself a lesson in assembly. Prior to assembly all parts to be used were left overnight in an isopropyl alcohol bath to remove dirt and grease. Forced hot air was used to completely dry them and the whole operation was done in front of a clean air booth. The most critical part was the mounting of the crystals. For simplicity two narrow strips of double sided adhesive tape were used. The two strips were placed along the crystal case 3mm and 13mm away from the reference edge. The four crystals were carefully positioned with the right orientation, against the vertical reference plane and then left lightly to slip down on the double sided strips. Proper positioning and alignment of the crystals at this stage was vital. The operation had to be done with extreme care, because in an unfortunate event of having to remove the crystals because of

bad alignment involved the danger of possible cracking and destroying them. After all four crystals were placed on the platform they were very softly pressed on the top to ensure a good and more reliable contact with the adhesive strips. The crystal case was turned upside down and silver strips with their ends previously dipped in silver paste were inserted in the holes to make contact with the bottom electroded surface of the crystals. The assembly was left overnight for the paste to set hard and then silver strips were cemented in the top surface of the crystals. All the connections made were checked by measuring the capacitance of the assembled crystal case which was found to be 162pF. Finally the whole assembly was gently pushed inside the modulator case and connections were made with BNC connectors. Because the length of the strip from the connector to the first electroded crystal was about 25 mm the soldering process was done at a low temperature and fast enough to prevent a possible thermal shattering of the crystals. Rubber gaskets were inserted between the body and the connectors for sealing purposes.

### 6.3 Initial set up and alignment procedures.

The modulator was set up on a 1.5 meter optical bench. Two cylindrical lasers at wavelengths of 633 nm and 560 nm having output powers of 1 mW and 0.2 mW respectively were used as light sources. The modulator was placed between two crossed polarisers mounted on vertical rotating tables. The set up is shown in fig. 6.2. Two detectors were used, a

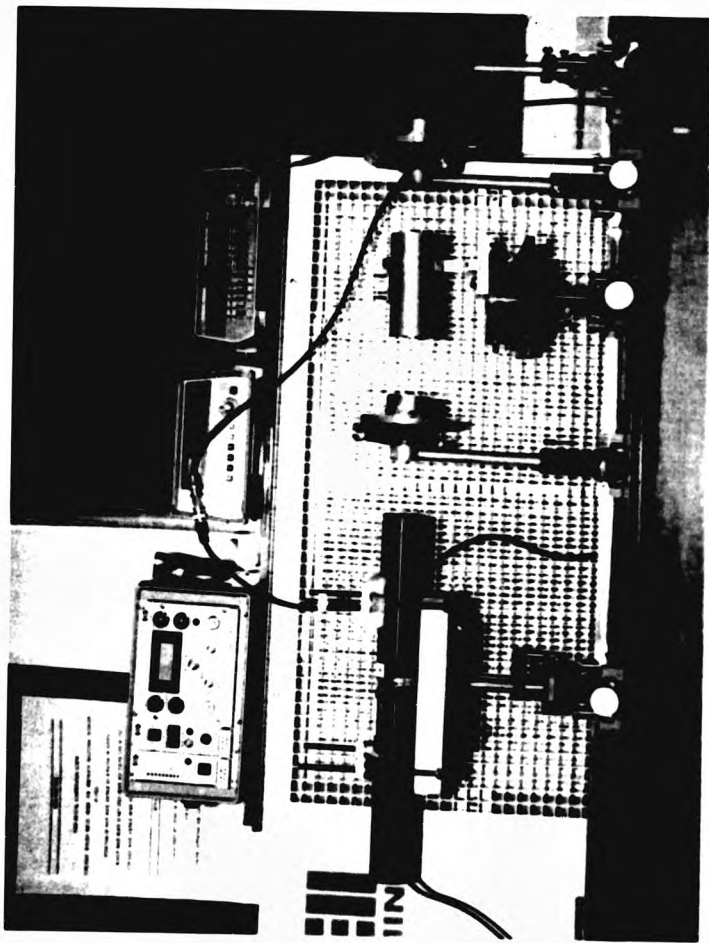


Fig. 6.2 The modulator set up.

Photodyne. Inc 11XE commercial power meter displaying in dBm and a home made optical receiver using a large area detector type obtained from Radio Spares, stock number 651-955. The detector was reverse biased at 15V with a 10K load resistor in series. The low value for the resistor load was selected to ensure high linearity of detection and wide dynamic range. For ease of alignment and rigidity the modulator was clamped using a suitable thick aluminum ring which was attached to a stand on the optical bench. Fine adjustments in horizontal and vertical translation were provided. Also elevation adjustments and rotation in the horizontal plane were possible. Passing the beam through the crystals proved to be an easy task. Fine adjustments were necessary to bring the four crystal reflections near to the beam exit point of the laser. The four reflections were scattered almost symmetrically around the laser output aperture and thus the modulator was assumed to be normal to the beam.

#### 6.4 Single pass operation, measurement of performance.

##### 6.4.1 Capacitance of the assembled modulator.

The capacitance of the modulator was measured and found to be 182pF as compared to the 4x40 pF value expected theoretically. This 22pF difference was attributed to the stray capacitance present inside the cavity.

##### 6.4.2 Measurement of the half wave voltage.



The half wave voltage was measured at two different wavelengths (633nm and 560nm). A unipolar driver was used to bias the modulator at a minimum and then the voltage was gradually increased until a second minimum was reached. The intensity versus applied voltage graph obtained is shown in figure 6.3. The difference between the two voltage values producing transmission minima corresponds to twice the half wave voltage. The following tables summarises results from several measurements.

$V_1(V)$	$V_2(V)$	$V_{min}(V)$	$V_{AVERAGE}(V)$	$V_{THEORY}(V)$	$\Delta V$
710	249	461	485	452	1.3%
810	357	453			
638	232	451			
796	331	465			

TABLE 6.2 Half wave voltage measurements at 633 nm

$V_1(V)$	$V_2(V)$	$V_{min}(V)$	$V_{AVERAGE}(V)$	$V_{THEORY}(V)$	$\Delta V$
125	521	396	395	405	2.5%
127	524	397			
136	529	393			
171	563	392			

TABLE 6.3 Half wave voltage measurements at 560 nm

From the above tables average values of 458V at 633nm and 395V at 560 nm were obtained. Although the difference between two maxima could have been selected to measure the half wave voltage, transmission minima tend to be more sharp and were located with a higher degree of confidence compared to the maxima, thus resulting to a more accurate half wave

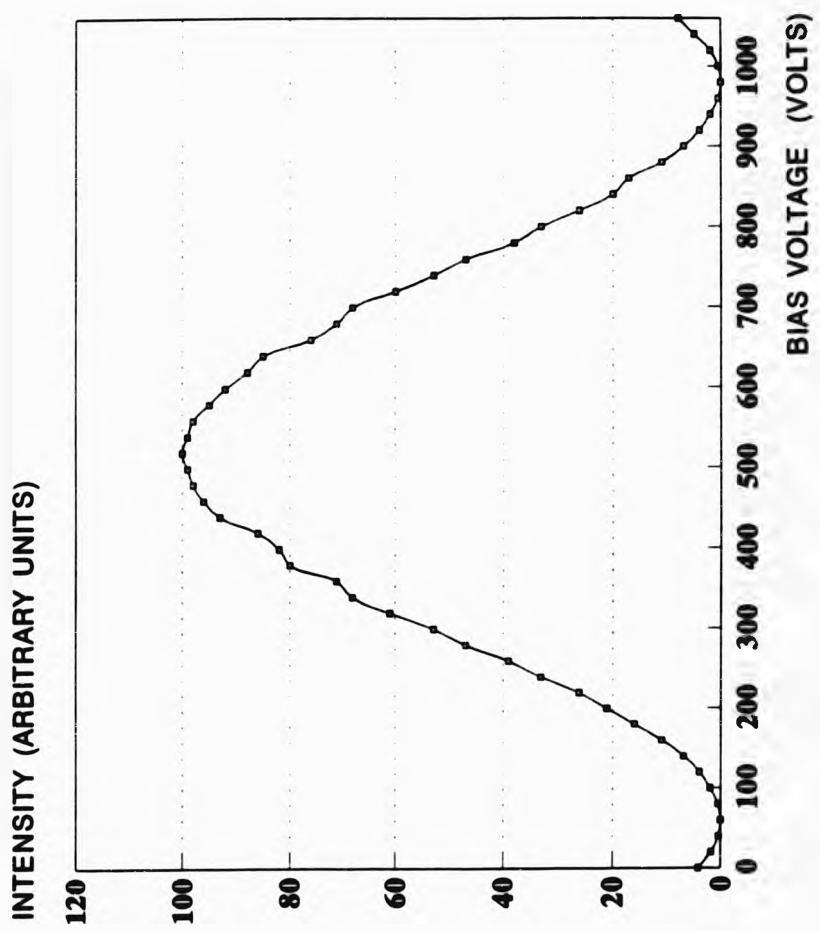


Fig. 6.3 Modulator transmission for one pass.

voltage measurement.

#### 6.4.3 Dielectric strength tests.

During the process of biasing the modulator to a second minimum, a potential difference of about 1.2KV was applied across the crystals which involved the danger of exceeding the safe limits of the crystals. Although a bipolar driver could have been used to locate two minima, one in the positive range and the other in the negative range of voltages, with the advantage of considerably reducing the maximum applied voltage across the modulator, such a high voltage test was performed to establish the neatness and the reliability of the electrode construction. Too close a gap between the strip electrodes and the body would possibly exceed the dielectric strength of the air. In such an unwanted event the electrical breakdown would certainly lead to a catastrophic short circuit. Voltages of up to 1.2KV were not normally required during operation of the modulator but when at a later stage the modulator had to be liquid filled, this would cause a reduction of the voltage breakdown limit because of the much lower dielectric strength of some of the liquids used compared to the air. The Gargille laser liquid used has an electric strength of only 350 volts per mm as compared to 2KV per mm for the air. Conducting paths formed in the liquid could occur at about 6 times lower voltage and although the application of 1.2KV was excessive for the air filled case it provided a degree of reassurance and confidence at lower voltages in the case of a liquid filled

cell.

6.4.4 Transmission measurements.

Without passing the beam through the modulator the intensity was measured and then the modulator was replaced in the light path and the new intensity reading was recorded. The Photodyne optical meter measured a 1.35dB insertion loss and from the RS large area detector an average total optical transmission of 73% was obtained. Both measurements are consistent and in excellent agreement with the estimated transmission value from section 5.3. The stability of the lasers used was quoted to be less than 1% so it was reasonably assumed that the above transmission figures were accurate to the same extent.

$I_{LASER}$ (Arb. Un.)	$I_{MOD}$ (Arb. Un.)	$I_{AVERAGE}$ (Arb. Un.)	T	$T_{PHOTODYNE}$	$\Delta T$
7.199	5.315	5.233	73%	72%	1%
	5.279				
	5.205				
	5.111				
	5.253				

Table 6.4 Transmission measurements at 633 nm.

$I_{LASER}$ (Arb. Un.)	$I_{MOD}$ (Arb. Un.)	$I_{AVERAGE}$ (Arb. Un.)	T	$T_{PHOTODYNE}$	$\Delta T$
2.972	2.245	2.155	72.5%	72%	0.5%
	2.060				
	2.143				
	2.173				

TABLE 6.5 Transmission measurements at 560 nm.

#### 6.4.5 Extinction ratio measurements.

The modulator was initially biased at a minimum and then at a maximum. The ratio of the two light intensities through the analyzer was measured to be 400 or 26dB. It is interesting that the measured extinction ratio varied significantly ( $\pm 3\text{dB}$ ) with the position of the light beam through the crystals. The modulator was translated horizontally at 1 mm steps and the new extinction ratios were obtained. The results are tabulated below.

Position	Extinction ratio	Average E.R
1	276:1	443:1
2	173:1	
3	520:1	
4	381:1	
5	373:1	
6	213:1	
7	850:1	
8	495:1	
9	630:1	
10	560:1	
11	425:1	
12	400:1	
13	460:1	

TABLE 6.6 Extinction ratio measurements at 633 nm.

Position	Extinction ratio	Average
1	221:1	317:1
2	310:1	
3	287:1	
4	388:1	

5	361:1
6	423:1
7	523:1
8	317:1
9	298:1
10	242:1
11	220:1
12	260:1
13	267:1

TABLE 6.7 Extinction ratio measurements at 560 nm.

This difference is believed to be due to the non-uniformity of the crystal material and to the degree of perfection and quality of the crystals polished surfaces. Local strains within the ADP material resulted in poor extinction figures while strain free portions permitted high contrast ratios to be achieved. Also the state of polish might not have been of the same standard throughout the total aperture of the modulator. The above observation verifies that the extinction ratio of the multipath modulator will critically depend on the effects described above, because the beam travels within most of the total crystal material.

#### 6.5 Multipath operation.

##### 6.5.1 Initial set up and mirror alignments.

After the two glass windows were replaced by the mirrors an alignment procedure <sup>was</sup> begun which aimed at achieving:

- (a) parallelism between the two mirrors.
- (b) parallelism between the crystals end faces and the mirrors.
- (c) positioning the crystals and the mirrors i.e. the modulator normal to the beam.
- (d) passing the beam several times centrally within the crystals.
- (e) obtaining a clean output beam.

The first step was to pass the beam through the input aperture and arrange for the four crystal reflections to be symmetrically scattered around the exit point of the laser. The crystals were then assumed to be normal to the beam. In fact none of the crystals was at a true 90 degrees angle with the input beam but an average misalignment with respect to the direction of the beam was assured this way. Then the three screws were adjusted so that the reflection from the first glass window went back into the laser. Similarly, the second mirror was also adjusted parallel to the crystals and the first window, all of them now being normal to the beam. Although the second window could have been aligned first its strong reflection from the mirror substrate would prevent a more accurate positioning of the weak reflection from the glass input window substrate. Superimposing a strong reflection on a weak one was found much easier. For best results the modulator and the laser head were kept as far away as the 1.5 meter optical bench permitted. The modulator was then rotated on the horizontal plane until the required number of passes was obtained. Fine adjustments on the

horizontal tilt of the modulator were necessary for the beam to enter and come out centrally. A white target located 0.5m after the modulator was used to visually inspect the beam and ascertain its quality. It was immediately noticed that a "clean" spot could not be obtained. Instead an interference pattern comprising of many secondary beams with the main beam hidden somewhere in the middle was observed. Application of an external voltage caused the intensity distribution of the pattern to change randomly but always giving a confused image. Many attempts to realign the system were made but it was soon found out that no amount of re-adjustment with the mirrors and the modulator adjustments would entirely solve the problem, and a distinct spot of acceptable quality could not be obtained.

The effect of light reflections from the successive crystal faces in the beam path was considered since it was an obvious explanation for the interference pattern observed. Optical reflections occurred when light passed from one media to another and in this case there were 8 x 7 ADP-air interfaces. The intensities of these 56 secondary beams present were proportional to

$$\left(\frac{n_0-1}{n_0+1}\right)^2 \quad 6.2$$

where  $n_0$  is the refractive index of the ADP material

It is of great consequence that these unwanted beams were moving along the same path towards the output of the modulator. The emergent modulated beam contained a number of



these beams which continued almost parallel to the main beam but displaced laterally. To prevent interference of these beams with the main beam could only be done by either deflecting or suppressing them. Deflection of these beams was impossible because of geometrical considerations. An improvement was achieved by using an index matching technique. The modulator cavity was filled with freon and this reduced the reflection losses from 4% in the ADP-air interface to 0.5% in the ADP-freon one. Although the quality of the output beam improved dramatically, diffraction patterns were present. These were attributed to silver paste particles or dust particles possibly, inside the cavity which were swept away by the liquid and ended up on the crystals polished surfaces. The modulator was thoroughly rinsed a few times using freon to remove the particles present and finally a beam of acceptable quality was obtained.

#### 6.5.2 Measurement of performance.

##### 6.5.2.1 Half wave voltage.

The modulator was rotated so that 3, 5, 7 and 9 passes were successively obtained. For every number of passes a biasing voltage was applied and the transmission was recorded. Typical results are shown in Fig.6.4. a-b from which the halfwave voltage for each number of passes was obtained.

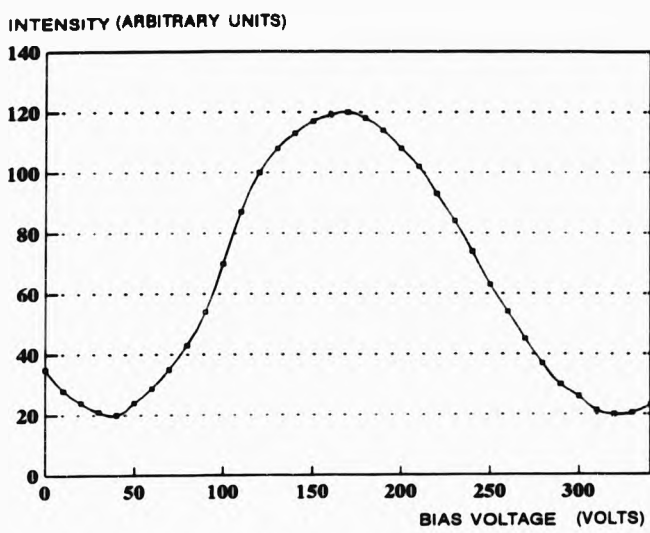


Fig. 6.4a Modulator transmission for three passes.

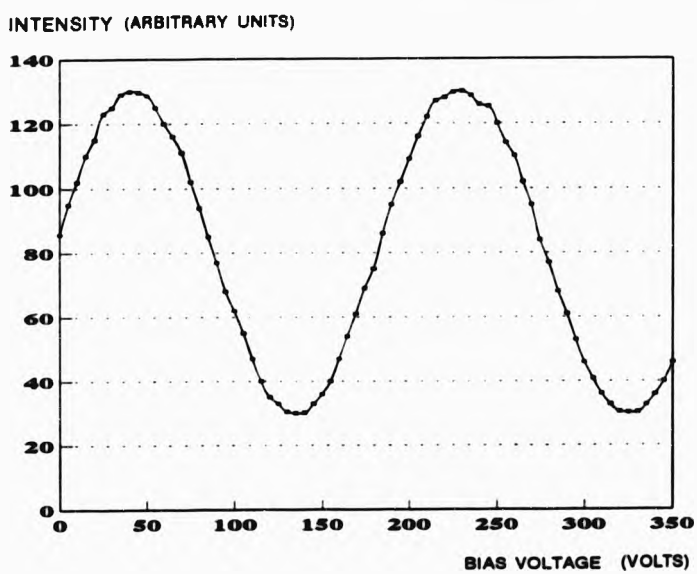


Fig. 6.4.b Modulator transmission for five passes.

n	V <sub>1</sub> (V)	V <sub>2</sub> (V)	V <sub>HW</sub> (V)	V <sub>THEORY</sub> (V)	ΔV%
3	35	340	153	151	1.3
5	45	227	91	90	1.1
7	103	223	65	65	0.0
9	21	123	51	50	2.0

Table 6.8 Half wave voltage measurements for various number of passes.

The small differences between the theoretical and the experimental values are not only due to the experimental error but also because the halfwave voltage was calculated at normal incidence and not at an oblique angle. At oblique incidence the angle between the direction of the beam and the optic axis changes and this results in a different halfwave voltage. The new halfwave voltage can be found by plotting the electrically induced birefringence as a function of the angle between the beam and the optic axis for the (0°,45°,45°) cut. From similar graphs for other known crystal cuts the difference between the two half wave voltages for angles of incidence differing by 1 to 2 degrees is only marginal<sup>(7)</sup>. Therefore a correction was not made for these effects.

#### 6.5.2.2 Transmission measurements.

The overall optical transmission was also measured for different number of passes. The results are tabulated below.

n	I <sub>IN</sub> (Arb. Un.)	I <sub>OUT</sub> (Arb. Un.)	T
3	7.3	5.8	80%
5	7.3	5.2	71%

7	7.3	4.8	66%
9	7.3	4.0	60%

TABLE 6.9 Transmission measurements for various number of passes.

The reflectivity of the mirrors was assumed fairly constant for small changes of the angle of incidence and for the freon interface so the above theoretical results are accurate to this extent.

6.5.2.3 Extinction ratio measurements.

To determine the extinction of the multipath modulator a similar procedure as with the single pass modulator was followed. The modulator was adjusted at the beginning for 3 passes and biased to a minimum, then at a maximum. The ratio of the two light intensities determined the extinction ratio. The procedure was repeated for all number of passes and the results are tabulated below.

n	$I_{MAX}$ (Arb. Un.)	$I_{MIN}$ (Arb. Un.)	Extinction ratio
3	5.70	0.95	6
5	5.30	1.30	4
7	4.80	0.81	6
9	4.30	0.86	5

TABLE 6.10 Extinction ratio measurements for various number of passes.

Irrespective of the number of passes the modulator

suffered from an extremely poor extinction ratio. The mirrors were replaced again by glass windows and the new extinction ratio on a single pass was measured at normal incidence. A value of about 800:1 was obtained.

#### 6.5.3 Discussions.

As a result of the tests performed on the first modulator for single pass and multipass operation considerable experience was gained. The conclusions drawn so far from the initial measurements were:

1. The theory of the multipath reflection technique had been verified. The half wave voltage is reduced by the same factor as the number of passes.
2. Very good overall performance was obtained on a single pass and the predicted optical transmission behaviour for multipass operation was also established.
3. The extinction ratio from the multipath set up was very poor. No firm physical explanation of this behaviour is offered at this stage. Clearly an investigation is to be attempted at a latter stage.
4. The mirror adjustments were not smooth and precise, they also lacked of dynamic range. Firstly the lead of the screws used was too big giving abrupt changes of the mirror position and secondly the three screw adjustments were not

independent. Finally the grooves for the o-rings proved to be small. A tight groove allows no space for the rubber to deform. The compression of the rubber is normally 10 per cent which proved to be insufficient.

5. There was significant leakage of fluid. The pressure around the o-ring was not uniform causing unequal compressions. At the points where the elastic deformations did not exceed the fluid pressure the seal was impossible.

#### 6.5.4 An improved composite crystal scheme.

There are six possible crystal modulator schemes which are shown in figures 4.6, 4.7 and 4.8. As already mentioned, all these should be equivalent, in theory at least, in terms of performance because all of them fulfil the composite modulator requirements which are:

- (a) the electro-optic effect to be additive in all four crystals.
- (b) recombination of the two beams at the output of the modulator.
- (c) cancellation of the natural birefringence and its temperature dependence by ensuring equal path lengths as an e-ray and an o-ray for the two refracted beams inside the crystals.

For the first prototype modulator the composite scheme shown in fig. 4.7.b was chosen purely because of engineering

considerations. These were:

1. Common electrodes for the two pairs of crystals hence simplification of the assembly and less engineering problems related with the application of the fields.
2. Shorter silver strip conductors thus minimisation of the parasitic inductance, capacitance and ohmic losses.
3. The feature of a common electrode also allowed the bottom electrode to assist with the thermal equilibrium and minimise any temperature gradients and differences between the crystals.

The way the crystals were arranged in this composite scheme caused the e-ray in the first crystal to deviate towards the top electrode and the e-ray in the second crystal towards the bottom electrode. At the exit of the second crystal the two beams came out parallel with the maximum possible vertical displacement.

This lateral displacement was given by :

$$d = \frac{l}{\sqrt{2}} \tan \phi = 0.6 \text{ mm} \quad 6.3$$

where:

$l$  is the length of the crystal

$\phi$  is the angle between the ordinary ray and the extraordinary ray.

This corresponds to 24 per cent of the total aperture of the modulator so the 2.5 mm aperture might not had been enough to safely accommodate the beams through. To allow for alignment tolerances, beam divergence due to diffraction effects and beam scattering in the crystal the working aperture to total available aperture ratio or most commonly known as the safety factor should be as high as possible. In particular the beam can be passed through a rod with little difficulty<sup>(34)</sup> with a safety factor of 3, but others<sup>(35)</sup> have also reported a modulator with a safety factor of 2 only. It is interesting that the above safety factors apply for single pass modulators but in the multipath modulator one would expect a larger safety factor requirement to allow for the growth of the beam diameter after the longer total path. Nevertheless the 1mm beam has been passed through the modulator with some difficulty but with little added loss with a safety factor of 1.6 only. At this point it seemed reasonable to assume that the tight aperture limited the performance and accounted for the poor extinction ratio obtained. Portions of the beam were probably striking the top and bottom electroded surfaces, and effectively spoiling the coherence of the output beam throughout the aperture. This could explain in a way the non uniform illumination of the output aperture and the interference line or isobar observed. By choosing any of the schemes shown in fig. 4.6.a and fig. 4.8 the lateral vertical displacement of the two beams is reduced by a factor of 2 and as a result the safety factor is increased to about 2. The interference of two beams for producing intensity modulator strongly depends on the wavefront distortion. Clearly a



larger aperture is advantageous. The schemes shown in fig. 4.8 produce the same lateral displacement of the two beams as before but in the horizontal direction, while scheme fig. 4.6.a recombines the two beams after the first pair of crystals. Because of this feature of keeping the beams as close as possible in any direction the composite scheme fig.4.6.a was selected this time. This scheme also offers the advantage of having the maximum number of common entrance and exit points on the crystal surfaces in the direction of the beams. Thus any crystal surface polishing imperfections are more likely to equally affect the two beams, keeping the relative wavefront distortion to a minimum. Such a balanced operation it was anticipated that it should yield to a higher extinction ratio.

#### 6.5.5 Performance comparison of the six composite modulator schemes.

To verify the above analysis the extinction ratio performance of all the composite crystal schemes was experimentally obtained. The crystals were mounted on a glass test plate and non permanent electrodes were used to apply the electric field. Measurements have been carried out not only at normal incidence but at oblique angles as well. The glass plate was mounted on a horizontal rotational stage and the dependence of the extinction ratio on the angle of incidence was obtained for changes from -10 degrees to +10 degrees. All the measurements were repeated for two different positions of the modulator relative to the laser head, 0.6m

and 0.1m respectively. Typical performance graphs are shown in fig. 6.5 and fig. 6.6. From the comparison of the graphs the following points were concluded.

(a) The schemes in fig. 4.7 that produced maximum displacement in the vertical position also gave the lowest overall extinctions as compared to the other schemes that keep the ray lateral displacement to a half.

(b) Comparison of the graphs for the far and near laser position showed that the same two schemes were affected more by the beam growth.

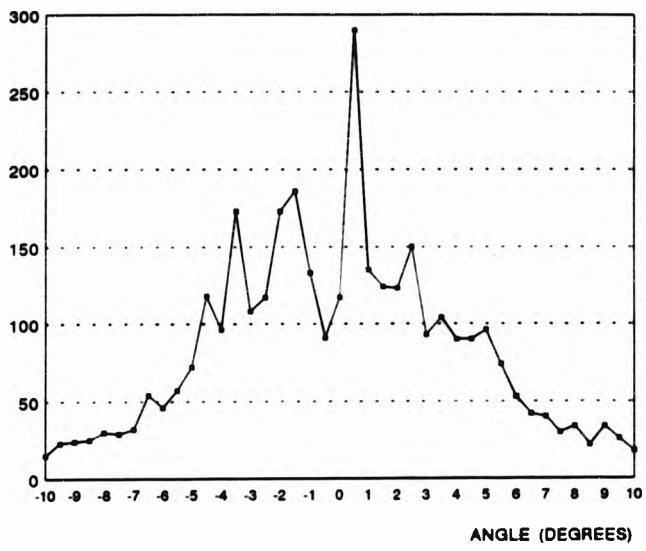
(c) all graphs show a rapid degradation of the extinction ratio at oblique incidence. Even small angles of about 1 degree caused the extinction ratio to drop by a factor of five.

Points a and b above were expected for the reasons given already in section 6.5.4. No explanation is given for the moment for the poor behaviour of the extinction ratio at oblique angles of incidence.

#### 6.5.6 Second prototype, an improved modulator design.

On the basis of the conclusions of sections 6.5.3, 6.5.4, and 6.5.5 a second modulator prototype was constructed. Several modifications were made to boost the performance of the device. The new design used the composite crystal arrangement shown in fig. 4.6 a. Modifications of the mechanics were also made. To provide a good degree of

EXTINCTION RATIO FOR COMPOSITE SCHEME Fig. 4.8 a



EXTINCTION RATIO FOR COMPOSITE SCHEME Fig. 4.8 b

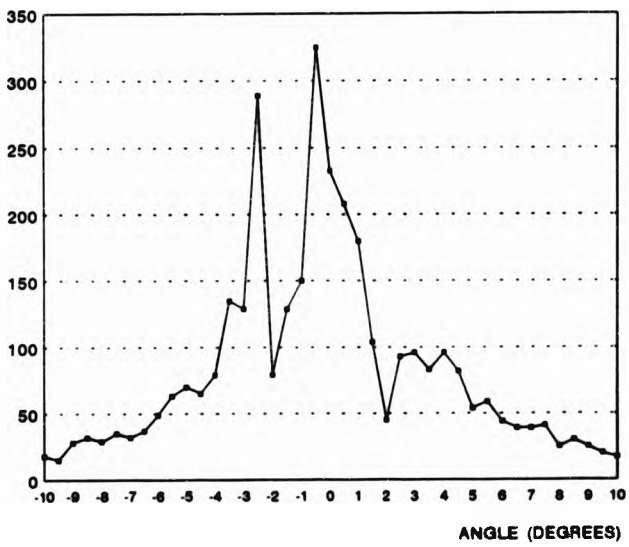
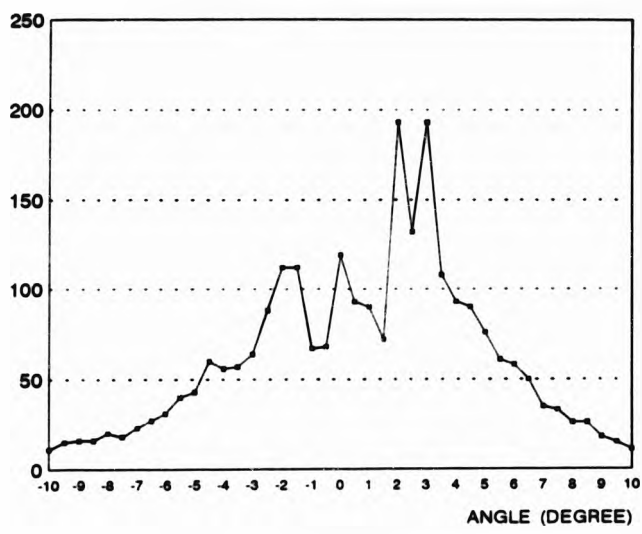


Fig. 6.5 Extinction ratio versus angle of incidence.

EXTINCTION RATIO FOR COMPOSITE SCHEME Fig. 4.7 a



EXTINCTION RATIO FOR COMPOSITE SCHEME Fig. 4.7 b

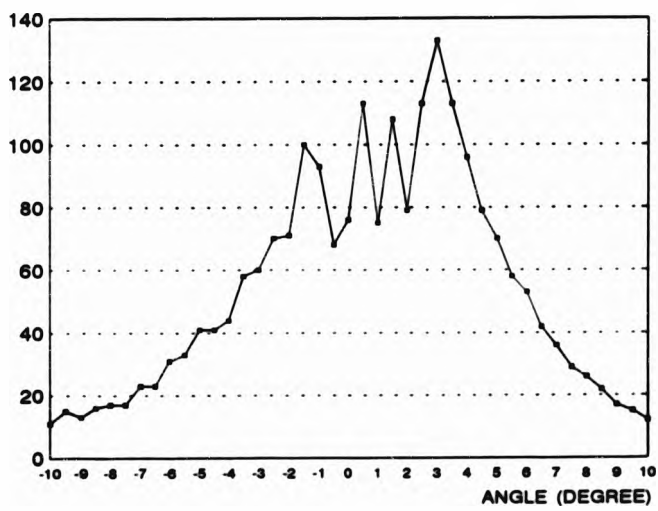


Fig. 6.6 Extinction ratio versus angle of incidence.

isolation between horizontal and vertical adjustment, four screws were used now to align the mirrors. Two of them lie in the vertical direction and the other two in the horizontal. Also thicker rubber o-rings were selected and allowance was made for changes of the rubber deformation by machining bigger grooves this time. Finally double sided tape was again used for the mounting of crystals.

#### 6.5.7 Measurement of performance of the second prototype.

A similar set up to the one shown in fig. 6.1 was used and the mirrors were aligned using the method described in section 6.5.1. This time the adjustments proved to be very smooth and precise. Also the leakage of the freon liquid was effectively prevented. The expected results were obtained for the halfwave voltage and the transmission, but the new composite crystal arrangement gave a marginal improvement for the extinction ratio which was about 10:1 as opposed to 5:1 before.

#### 6.5.8 The extinction ratio of an electro-optic modulator.

Because of the poor extinction performance of the first and second ( $0^\circ, 45^\circ, 45^\circ$ ) multipath prototypes a study of the extinction ratio and in particular of the factors which affect it was undertaken. Emphasis will not be given on deriving mathematical expressions and relationships but instead the physical mechanism of these factors will be discussed. The study will reveal what is possible and what

is not from a practical point of view to improve the extinction ratio. In general the extinction ratio of an electro-optic cell depends on:

1. The characteristics of the laser light
2. The crystals
3. The engineering of the modulator
4. The correct set up, alignment and use

#### 6.5.8.1 The characteristics of the laser light

1. The linewidth of the laser. Because all laser wavelengths are not truly monochromatic, interference of the two beams will be affected by the degree of coherence. The degree of coherence imposes limitations to the maximum and minimum interference intensities that can be obtained from light consisting of spectral components that cover a frequency range

2. The beam divergence. Angular spread of the laser beam as it passes through the crystals causes each portion of the light beam to have a different path length, experience a different refractive index and induced electrical birefringence. It is of great importance since it determines the spatial coherence of the two interfering beams at the output of the modulator.

3. The radiant power. Although the light absorption of ADP and most of the electro-optic materials is very low, high

laser power levels can heat up the material and introduce strains in the path of the beam.

4. The beam diameter. The quality of the surface polishing is of greater concern with large diameter beams. This is because wavefront distortion effects are more likely to be present and the resulting interference will be subject to some of the limitations normally associated with them.

5. The peak wavelength of the laser. Because the extinction ratio is related to the imperfections of the polished crystal surfaces it is reasonable to expect a degradation at shorter wavelengths.

#### 6.5.8.2 The crystals.

1. Strain within the crystal material tends to distort the wavefront and as a result to reduce the extinction ratio.

2. The accuracy of orientation of the crystallographic axes during the alignment and cutting process of the crystal boule. Misalignments from the required angles reduces the effectiveness of the compensation mechanism.

3. Strain introduced during the cutting and polishing process. Similar considerations to 1 apply here as well.

4. The quality of surface polish. The degree of surface perfection affects the wavefront of the beam and causes

deformation of the intended shape.

5. The degree of non parallelism between the end surfaces of the electro-optic crystals causes each portion of the light beam to have a different path length in the crystal.

6. The difference between the lengths of the crystals. Differences in length cause a separation between the centres of the two rays. A complete superposition of the two rays is not possible at the output of the modulator and the extinction ratio suffers because only the overlapping parts contribute to the modulation.

#### 6.5.8.3 The engineering of the modulator.

The proper engineering of the modulator can be a key factor not only for the extinction ratio but for the overall performance as well. Particular emphasis should be given on the mounting of crystals. Consideration of every detail is essential to achieve best results. There are two dangers in mounting the crystals on the crystal case, introducing strain and not positioning the crystals correctly. Both dangers require care and some strategy.

1. The application of mechanical stress to the crystals has the effect of rotating and changing the form and shape of the index ellipsoid. This is equivalent to changing the cut of the crystals and in general compensation and electro-optic modulation are significantly reduced. The modulator is biased



at a constant level and complete cancellation of the two beams is not possible.

2. The extinction ratio and the angular aperture of the modulator is affected to a large extent by the accuracy with which the crystals are aligned with each other. For best results all crystals should be accurately in line as possible.

3. The presence of a suitable index matching oil improves the extinction ratio for the reasons stated in section 5.4. Care must be taken to use a low absorption oil especially with medium and high power applications to avoid heating of the oil which causes lensing effects that destroy the wavefront of the beam. The resulting mode distortion or blooming can seriously degrade the extinction ratio. A low absorption fluid combined with a short fluid path length ensures a higher optical throughput capability.

4. The very stringent thermostatic requirements necessary for large dynamic extinction ratios can be relaxed if the cavity where the crystals are kept is of high thermal conduction. Also any external temperature transients should be buffered effectively by the modulator walls.

5. Low voltage designs also tend to minimise the heating of the crystals due to dielectric losses within the electro-optic material itself, thus less strain is introduced.

#### 6.5.8.4 The correct alignment and use.

With careful alignment of the device in the light beam and proper orientation of the polarisation and analyzer with respect to the crystals the highest possible extinction ratios available from the modulator can be achieved. The electro-optic devices should ideally placed normal to the beam and good quality polarisers able <sup>to obtain</sup> a reasonable polarisation ratio should be used.

#### 6.5.9 The quest for better extinction ratio.

The first thing to do when considering how to gain higher extinction ratios is to understand the conditions for maximum interference and the factors which affect them on a practical device. All these factors have been briefly discussed in the previous paragraph and at a first glance it seems that there is a wide choice of things that can be altered or modified to boost the extinction ratio performance. But in reality not much can be done. The electro-optic material used was of the same standard and quality <sup>of</sup> the materials used in the electro-optics industry and the degree of surface polishing and inclination between the crystal end faces was within the limits of the present technology. A typical good quality laser from a reputable manufacturer was used and all the necessary precautions during the assembly were taken. To support all the above, the two prototypes constructed and tested so far, resulted in excellent performance on single pass operation. The high extinction ratios obtained, 400:1

and 800:1 with air and freon filled cells respectively, proved that the crystals and crystal polishing were of high quality and no strain had been introduced during the crystal mounting process. These were extinction ratios corresponding to the highest quality of commercial low voltage modulators. Numerous attempts of aligning the mirrors and proper setting up of the modulator resulted in the same poor extinction ratio for the multipath modulator. An improvement was obtained by using a better index match. Silicon oil DC250 with a refractive index of 1.4 reduced the optical reflection loss to 0.1% per interface and resulted in an extinction ratio of about 20:1.

Mansell<sup>(36)</sup> has discussed the problems associated with the misalignment of the crystals with respect to each other and in particular the dependence on the extinction ratio and angular aperture. He concluded that large angular apertures can be achieved provided all crystals are correctly aligned. The misalignment of the crystals used for the first two prototypes was easily measured from the relative positions of the crystal reflections back on a target situated around the laser output aperture. An average distance of 10mm between the four reflections and the laser output was measured when the modulator was 0.8 meters away from the laser head. These figures suggested an average misalignment of 25 minutes of an arc between the crystals which was thought to be very high and a possible explanation for the low extinction ratios at an oblique angle. The graphs in fig. 6.5 and 6.6 show a rapid, almost abrupt deterioration for angles of incidence <sup>changes of</sup> incidence

greater than about 1 degree. If this effect was due to the misalignment of the crystals, better crystal positioning would result in a more broad extinction ratio curve. Deviations from the absolute flatness for the crystal platform were caused by the double sided tape strips used. Variations in the thickness of the strips of, say, only 40  $\mu\text{m}$  could have given rise to errors of 30 arc minutes in the vertical direction. Even when the crystals were placed directly on the nylon crystal platform, misalignments of 20 arc minutes were measured. More careful observations showed that the case was not absolutely flat but a bow existed in the middle. This bow although extremely small was responsible for the misalignments present. Without too much trouble a flat surface can be made by suitably clamping and milling a nylon rod in the workshop within so small a deviation from its true shape that it can be considered as perfect. But immediately after the finished piece is released internal stresses within the material are generated and deform the surface from the ideal. Ways of improving on these mechanical engineering problems *was not practicable for the purposes of this thesis.* Instead the crystals were placed on a thick glass test plate which by all means can be considered almost flat. Surprisingly the crystals were again misaligned by about 10 to 15 arc minutes. Such misalignments could have easily been created by dust particles or by variations in thickness of the deposited gold electrode layer on the crystals. Dust particles that can easily have a diameter of 20 $\mu\text{m}$  could have given rise to an error of 5 arc minutes. Therefore it was desirable to look out for other methods, capable of better

accuracy and providing the means of a more precise alignment of the crystals.

6.5.10 Third prototype, a modulator with a better crystal alignment.

In the arrangement shown in fig. 6.7 an accurate positioning of the crystals was possible. Individual crystal control was provided in both the horizontal and normal directions. Four individual aluminium crystal cases were used to hold the crystals. The crystal was placed against a thin strip of a soft rubber material located in one side of the crystal case, pushed slightly to compress the strip so the crystal can slip down on the aluminium base. An extremely light clamping was ensured by appropriate selection for the material and the width of the strip.

The four aluminum crystal cases were not completely flat at the bottom but they were machined so that a small step was created at one end. The shape and the slope of the step was such so that when the individual crystal case was placed on a flat surface there was an initial inclination of 30 arc minutes. Screws were used from underneath in the nylon main crystal case to screw on the aluminum, and clamp each piece separately against the surface which ideally should be flat. Another screw was used from underneath to adjust the vertical tilt. By turning the screw clockwise the crystal was pushed upwards and by turning anticlockwise the clamping action of the holding screw tended to bring it back to the original

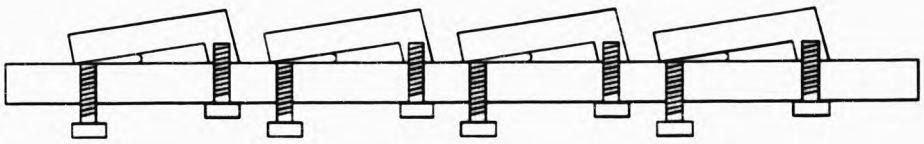
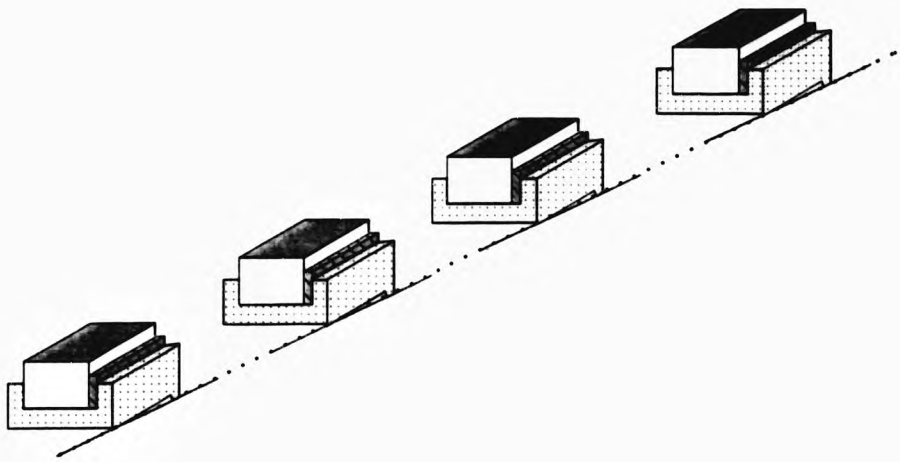


Fig. 6.7 Mechanics for individual crystal adjustment.

position. It is perhaps surprising that the tolerances between the clamping screw and the nylon material are so small, indeed a few tens of microns, but this was just the elasticity tolerance wanted for our purpose. Control in the horizontal plane was achieved by a similar mechanism. The position where the clamp screws were located was 0.5mm offset from the centre lines so that an initial angle of 30 arc minutes was provided for the crystals on the horizontal. Holes in the centre of the aluminium base were also made for the bottom strip electrodes to go through and make contact with the crystal. A piece of rubber was used to tightly keep the strip in the hole while a length of about 2mm protruded from the top side. A 1mm clearance was provided for the crystal to push the strip in and lie flat on the aluminum base and a thin sheet of mica was sandwiched between the crystal and the base for electrical isolation. Finally all strips coming out from each crystal were soldered on separate BNC connectors at the bottom of the modulator body. The top electrodes take a different form. The whole purpose of it was to completely eliminate the use of silver paste needed to electrode the crystals. The reasons being that it was a messy operation involving the danger of using large amounts of it and accidentally ending up in places where it should not. Also if for any experimental reasons, which occurred very often during the time of this research, the silver paste had to be removed it proved to be a very difficult task, most of the times not being successful. Another technique was devised which used the electrode structure shown in fig. 6.8. A copper screw was soldered on a BNC connector along the



Fig. 6.8 Top electrode construction.

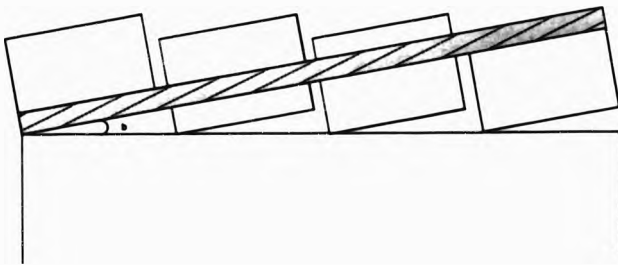


Fig. 6.9 Reduction of the modulator usefull aperture as a result of non parallellism between the crystals and the platform.



direction of the centre contact pin. A copper leaf was soldered on a nut and the whole assembly was screwed on the main body. Another nut was also used to lock the copper leaf in the proper position. Electrical contact with the crystal was achieved by bending the copper leaf and allowing it to touch the top electroded surface. The spring back action arising from the elastic recovery property of the copper material provided the contact mechanism. Limitations such as a general lack of spring back strength, overbending, application of excessive stress and others had to be balanced against desirable characteristics such as reliable contact, highly conductive, long life etc. Several trials were necessary to obtain the desired results.

Prior to inserting the crystal case inside the modulator body all crystals were aligned. The crystal case was mounted on an appropriate base and the laser beam was used to obtain four reflections from the crystal surfaces on a white target located 4 meters behind the laser. Although the alignment should be straight forward there was a danger of not setting correctly the position of the first reflection. This was the position that made all crystals acquire a position parallel to the crystal case. Parallelism of the crystals with the case was a critical part of the alignment because it affected the useful aperture of the modulator. By referring to fig. 6.9 errors from the ideal position could have resulted in an aperture reduction which was easily calculated from :

$$d_N = d_o - \frac{3}{4} l \tan \phi$$

6.4

where:

$d_N$  is the new aperture

$d_o$  is the crystal height

$l$  is the length of the crystal case

An angle of 30 arc minutes reduces the aperture of the device from 2.5 mm to 2.09 mm. The first step was to set the first crystal case parallel to the main crystal case. This was going to be the reference direction for the alignment. To verify the correct positioning a 0.1 mm feeler gauge blade was used to approximately measure the gap which should be equal to the height of the step machined on the bottom of the aluminum base. Then each crystal was separately adjusted in both the horizontal and normal directions so all reflections were gathered together as close as possible, the ideal being of course all of them to overlap. The positions of all spots on the white target were adjusted so that their centres were within about 2 mm. Better positioning proved to be impossible because of the beams growth due to the finite divergence of the laser and interference between the four beams. But even that resulted to an alignment of all crystals better than 2 arc minutes which was a tremendous improvement compared to the 30 arc minutes before. The mechanics easily provided the required smoothness and degree of resolution making the alignment quite easy and quick. Changes of the position of the spot in steps of about 1mm could be obtained with some care which corresponded to an angular resolution of something less than 1 arc minute. The crystal platform was then

inserted in the modulator case and the standard assembly procedure was followed. Finally the modulator was filled with DC550 Dow Corning Silicon Oil . This was a much better index match as compared to the DC250 silicon oil used before. Its refractive index of 1.49 is close to the mean refractive index value of the extraordinary and the ordinary ray for the ADP material.

6.5.11 Third prototype, measurement of performance and conclusions.

The extinction ratio was again measured for angles of incidence ranging from -10 degrees to +10 degrees in 0.5 degree steps, for a single pass. Typical graphs are shown in fig. 6.10 and fig. 6.11. From these graphs the following points were concluded.

1. There is a dramatic improvement of the extinction ratio at normal incidence and at small angles of incidence as well. Values of at least 2500:1 have regularly been achieved. The maximum value obtained was about 7000:1.
2. There was no significant improvement of the extinction ratio at large angles of incidence even for the single pass.
3. The central region of the extinction ratio graphs was affected a lot more from the crystals better positioning as compared to the regions on the left and right. This unequal distribution of improvement suggested that there must be at

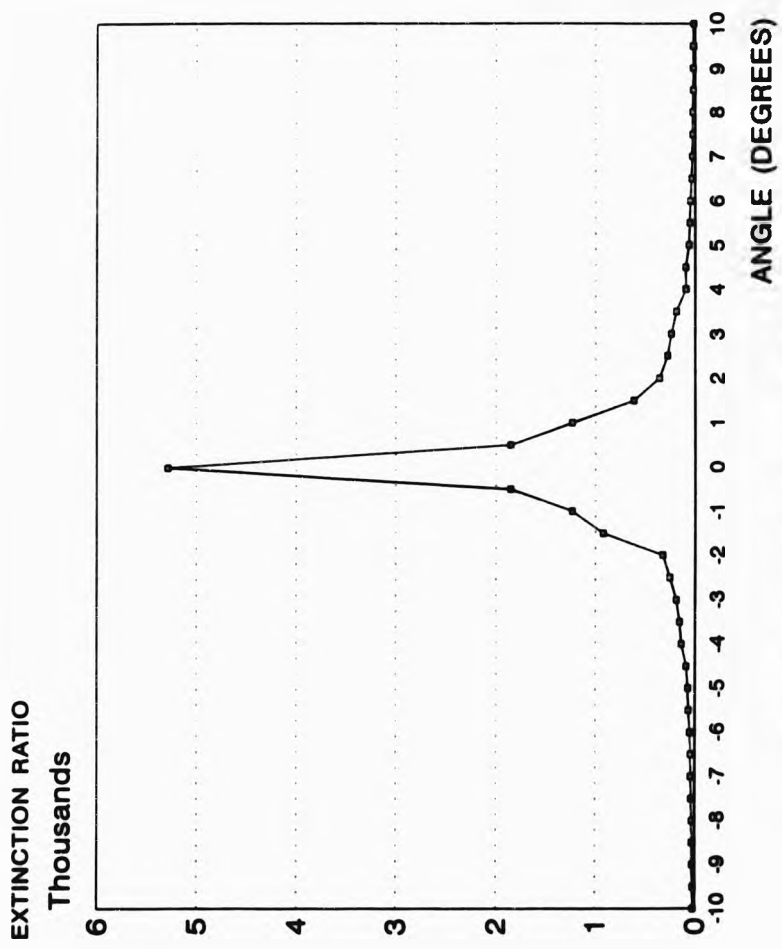


Fig. 6.10 Extinction ratio versus angle of incidence.

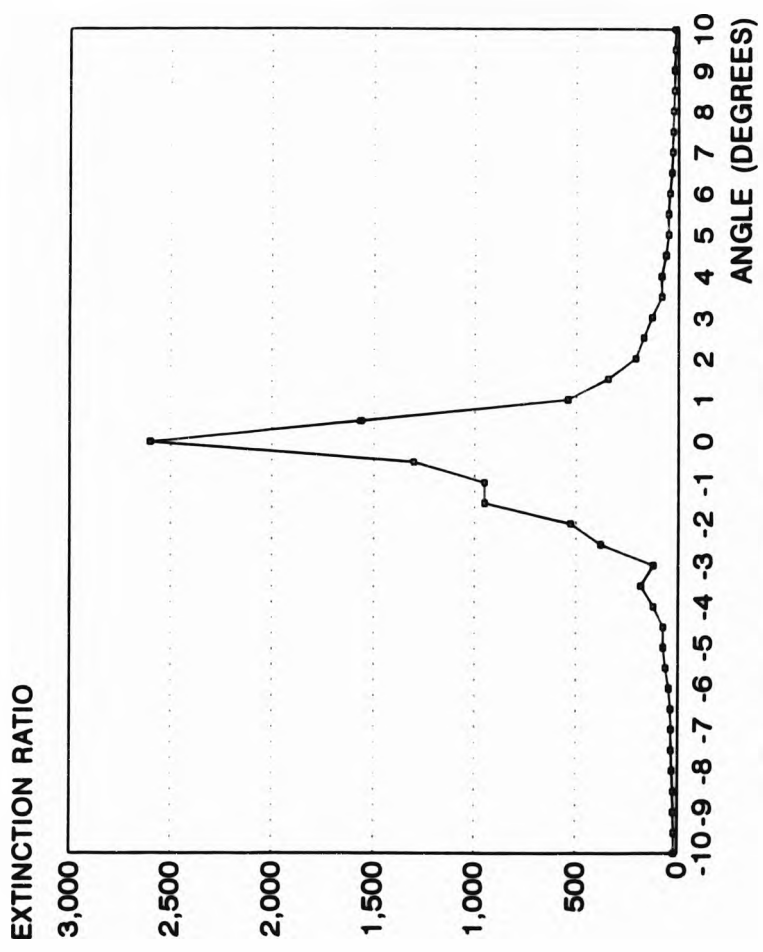


Fig. 6.11 Extinction ratio curve versus angle of incidence. Modulator as in fig. 6.10 but for a different light path through the crystals.

least two significant factors which affect the extinction ratio. The first factor, that of the crystal alignment, was not critical at large angles of incidence, while an other parameter yet 'unknown' seemed to be totally responsible for the poor behaviour at these angles.

4. Point 3 above further suggests that a significant extinction ratio improvement for the multipath modulator is more likely not to be achieved because the unknown parameter will again dominate the extinction performance. This was experimentally verified by measuring the extinction ratio of the device. Values between 15:1 to 25:1 were obtained for different number of passes. Inspection of the beam spot on a white target clearly showed an isobar arising from interference effects. The presence of the isobar did not permit uniform extinction of the whole beam aperture.

It is interesting to note that varying the applied voltage also changed the position of the isobar so that initially the top of the beam spot was totally extinguished and then gradually the isobar was moving downwards causing extinction of new regions of the beam.

#### 6.5.12 Performance with a reduced angle of incidence.

Once the need for critical evaluation of the problems had been established from the points just discussed and the careful observations made, then it only remained to investigate the behaviour of the modulator with a reduced

angle of incidence needed to achieve the required number of passes. It would probably be found that a reduction of angle of incidence could raise the extinction ratio. In such a case this would be supporting evidence to establish the existence of a physical phenomenon which if fully investigated and understood could provide answers and explain the reasons of the poor extinction behaviour. For convenience one of the mirrors was removed and replaced by a glass window. The mirror was placed externally and was translated horizontally to change the number of passes through the modulator while keeping the angle of propagation constant. A series of extinction ratio measurements was obtained for two different mirror positions i.e. two different angles of propagation  $\varphi_1$  and  $\varphi_2$ , and for different number of passes. The results are shown below.

n	$\varphi_1^0$	ER <sub>1</sub>	$\varphi_2^0$	ER <sub>2</sub>
3	0.5	250:1	0.4	367:1
5	0.5	114:1	0.4	163:1
7	0.5	63:1	0.4	70:1
9	0.5	22:1	0.4	NA

TABLE 6.11 Extinction ratio for various passes and for two different angles of propagation.

From the above it is obvious that the extinction ratio of the multipass modulator can be substantially improved by reducing the angle of incidence.

6.5.13 An optimisation study for the angle of propagation of the laser beam.

This section discusses from a geometrical point of view the angle of propagation of the light beam through the modulator and its dependence on other parameters such as the length of the modulator, the number of passes, the beam divergence etc. Figure 6.12 shows a typical situation for a beam entering the modulator at one end and after  $n$  reflections inside the cavity comes out from the other end. Unfortunately there is a lower limit for the angle of propagation which arises from the necessity to separate the last two beams at the output window so that only the last pass can exit the cavity. By bringing the two beams very close together it is bound to clip the last pass at the mirror edge thus destroying the ideal Gaussian profile, reducing the overall optical transmission and extinction ratio. The above considerations suggest that a safety distance is required between the edges of the last two successive spots. This distance will mainly depend on :

1. The degree of transition between the mirror and the glass substrate which ideally should be abrupt. This is a limitation set by the vacuum deposition production method used and the engineering of the jig used to hold the glass windows.

2. The Gaussian irradiance profile. The commonly adopted definition of the laser beam diameter is the diameter at which the irradiance has fallen to a function  $1/e^2$  of its peak axial value. Even though a significant amount of energy extends beyond these points and if allowance is not made for



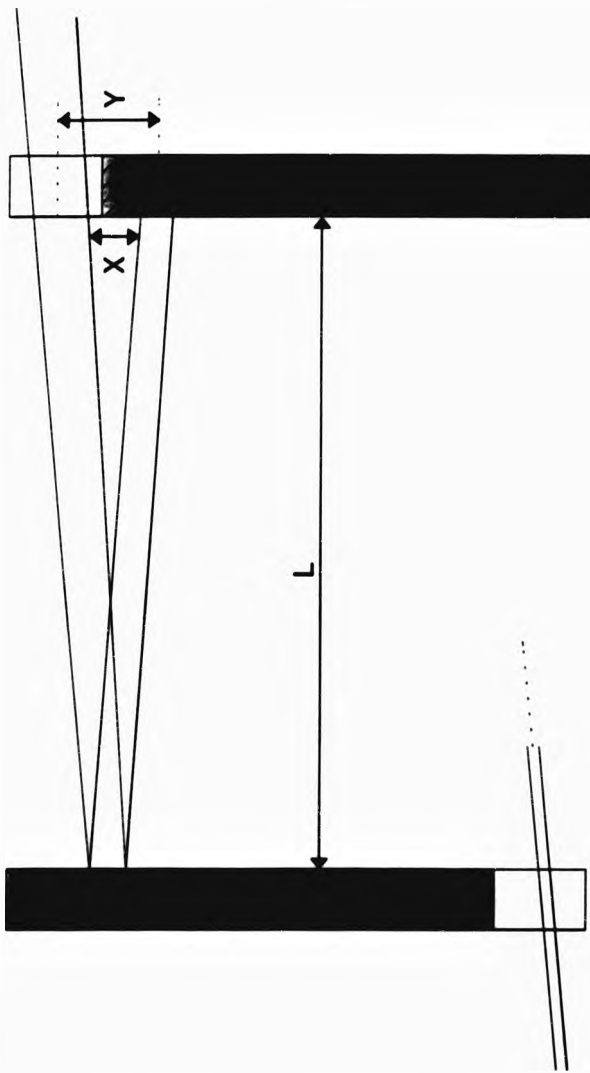


Fig. 6.12 Beam propagation through the modulator.

most of the light to exit the cavity then transmission loss and interference is unavoidable.

By referring back to Fig 6.11 the following assumptions are made.

$l$  is the distance between the modulator mirrors in mm

$d$  is the beam divergence in mrad

$n$  is the number of passes

$s$  is a safety distance between two successive beam spots in mm

$w_0$  is the beam waist at the input of the modulator in mm

$w_n$  is the beam waist after the  $n$  pass

$n_c$  is the refractive index of the modulator cavity

The beam divergence inside the cavity is given by :

$$d_c = \frac{d}{n_c} \quad 6.5$$

The diameter of the beam after travelling  $n$  passes is given by:

$$w_n = w_0 + n l d_c 10^{-3} \quad 6.6$$

Similarly the diameter of the beam at the end of the  $(n-2)^{\text{th}}$  pass is given by :

$$w_{n-2} = w_0 + (n-2) l d_c 10^{-3} \quad 6.7$$

By referring to the figure the distance between the two centres is  $y$  which can be found by:

$$y = \frac{w_n}{2} + s + \frac{w_{n-2}}{2} \quad 6.8$$

Assuming the angle of propagation to be  $\varphi$  we have:

$$\tan\phi = \frac{Y}{l} = \frac{w_n + w_{n-2} + 2S}{4} \frac{1}{l} \quad 6.9$$

Some simple algebraic manipulation yields to :

$$\tan\phi = \frac{w_o + S}{2l} + \frac{(n-1)d_c 10^{-3}}{2} \quad 6.10$$

For small angles we can write to a good approximation

$$\phi = \tan\phi, \quad \phi \text{ in radians} \quad 6.11$$

therefore:

$$\phi = \frac{w_o + S}{2l} + \frac{(n-1)d_c 10^{-3}}{2} = \phi_1 + \phi_2 \quad 6.12$$

#### 6.5.14 Discussion of the optimisation analysis results.

1. The first parameter relates the angle of propagation to the length of the cavity. Obviously the longer the length the smaller the angle. If the laser was perfectly collimated then this angle would be independent of the number of passes ie  $\phi = \phi_1$ .

2. On the other hand the term  $(n-1)$  implies length and this results to a beam growth. This has to be compensated in the design of a practical device. Assuming the angle  $\phi_1$  to be zero then a starting angle  $\phi_2$  is required to compensate for the beam divergence effects after a certain length of propagation.

3. Since it is a practical impossibility to have a perfectly

collimated light beam then the total angle of propagation will depend on both  $\varphi_1$  and  $\varphi_2$  and since  $\varphi_2$  is fixed for a given number of passes and laser divergence then the only control we have is to change the length of the modulator.

4. Practical considerations impose severe limitations on what can be done. Very long units are not very desirable and there is also the possibility of  $\varphi_2$  to be the main contribution to the total angle. So considering a longer modulator is not a good choice. If on the other hand  $\varphi_2$  is as small as possible compared to  $\varphi_1$ , then a change of length will result to a drastic reduction in the angle of propagation and therefore a corresponding improvement of the extinction ratio. The angles  $\varphi_1$  and  $\varphi_2$  have been computed for different number of passes, modulator lengths and for the typical HeNe laser divergence. To compute these angles, a value for the safety factor was needed and this was found experimentally to be about 2mm. The following table summarises data for  $\varphi_1$  and  $\varphi_2$ .

n	$l_{mm}$	$\varphi_1^0$	$\varphi_2^0$	$\varphi^0$
3	60	1.43	0.06	1.49
3	100	0.86	0.06	0.92
3	120	0.72	0.06	0.78
3	140	0.61	0.06	0.67
3	180	0.48	0.06	0.54
5	60	1.43	0.11	1.54
5	100	0.86	0.11	0.97
5	120	0.72	0.11	0.83
5	140	0.61	0.11	0.72
5	180	0.48	0.11	0.59
7	60	1.43	0.17	1.60

7	100	0.86	0.17	1.03
7	120	0.72	0.17	0.89
7	140	0.61	0.17	0.78
7	180	0.48	0.17	0.65

TABLE 6.12 Optimised angles of propagation for various number of passes and modulator lengths.

These are the optimised values for  $\varphi$  ie the smallest angle of propagation so that the last pass just manages to come out from the modulator. To verify the above theoretical figures the set up shown in Fig 6.13 was used. Two mirrors were placed parallel on a rotation table with the provision of changing the distance between them and translating horizontally the exit mirror. Rotation of the whole unit caused multipath reflection between the mirrors. The determination of the minimum angle to achieve the required number of passes was done by gradually rotating the table to reduce the angle and adjusting horizontally the exit mirror so that the beam leaves unclipped. The same procedure was repeated for 3, 5 and 7 passes and for various lengths between the mirrors. The distance Z was recorded each time and from this value the angle of incidence  $\varphi_{EXP}$  was calculated. Results are shown below :

$l_{mod}$	n	$z_{min}$	$\varphi_{EXP}^{\circ}$	$\varphi_{THEORY}^{\circ}$	$\Delta\varphi$ (arc mins)
60	3	12	1.43	1.37	3.6
60	5	13	1.49	1.54	3.0
60	7	14	1.60	1.60	0.0
100	3	17	0.97	0.91	3.6
100	5	19	1.08	0.91	5.4

100	7	21	1.20	1.14	3.6
120	3	15	0.86	0.77	5.4
120	5	17	0.97	0.91	3.6
120	7	19	1.08	0.99	5.1
140	3	12	0.69	0.72	1.8
140	5	14	0.80	0.80	0.0
140	7	16	0.92	0.93	0.6

TABLE 6.13 Experimental results for the angle of propagation for different number of passes.

In conclusion:

The table below summarises data for the modulators tested so far.

n	$l_{mod}$	$\theta^{\circ}$	E.R.
3	65	4.10	20.:1
5	65	2.50	20:1
7	65	1.70	20:1
9	65	1.40	20:1
5	180	0.65	100:1
7	180	0.65	80:1
3	220	0.5	367:1
5	220	0.5	163:1
7	220	0.5	45:1

TABLE 6.14 Extinction ratio measurements for various number of passes and angles of propagation.

The experimental results from table 6.14 indicate that longer modulators result to higher extinction ratios.

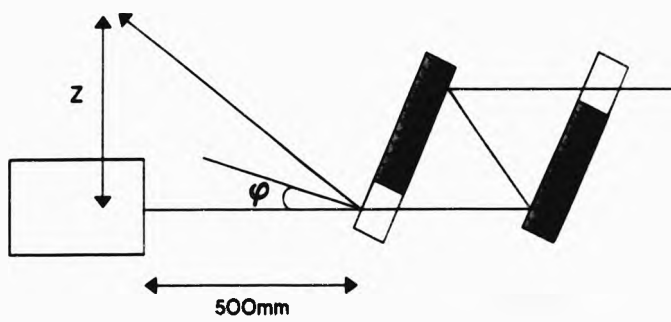
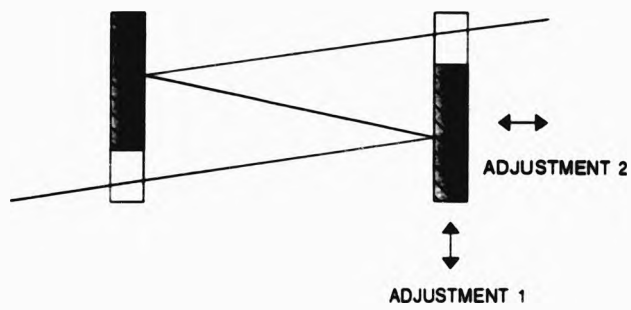


Fig. 6.13 Experimental set up for the measurement of the minimum angle of incidence

#### 6.5.15 The optimised modulator and its performance.

A modulator case in which the mirrors were kept 180mm apart was constructed. This modulator was identical to the previous prototypes in all respects except of the much longer cavity. The cavity was filled with DC550 index matching oil. The setting up of the modulator and the mirror adjustments were carried out the same way as before except that this time a lens cleaning tissue was used as diffusing target to assist a more accurate alignment of the beam through the crystals. A piece of the tissue was held between the laser and the modulator so that some scattering of the beam was created. Back reflection of the scattered light from the crystal's surface onto the tissue created an image of the input aperture with the location of the beam within the aperture clearly identified. Similarly by observing the light coming out from the modulator on a white target accurate location of the main beam within the aperture was also possible. It was then a matter of tilting and translating the modulator in the vertical plane, to pass the beam centrally through the crystals. Results for the extinction ratio obtained for various passes and different lasers are tabulated in the following table.

Laser type	n	E.R.
Spectra physics HeNe 0.2 mW at 633 nm	3	150:1
	5	160:1
	7	120:1



Melles Griot HeNe 1 mW at 633 nm	3	100:1
	5	80:1-120:1
	7	60:1-80:1
Melles Griot HeNe at EOD, 1mW at 633 nm	3	75:1
	5	105:1
Argon ion at EOD		
1mW	5	80:1
2mW	5	50:1
5mW	5	25:1
10mW	5	NA

TABLE 6.16 Extinction ratio measurements for the optimised modulator.

**CHAPTER 7 A STUDY OF DOUBLE REFRACTION AND ASSOCIATED EFFECTS ON THE EXTINCTION RATIO OF (0°,45°,45°) MODULATORS.**

7.1 The problem of double refraction.

The study of the extinction ratio was carried out after all tests had been completed and all four modulator prototypes had been fully tested for single pass and multipass operation. It will be shown that the poor extinction ratios observed at oblique incidence can be explained by a detailed analysis of double refraction. This will be supported with further experimental results. Double refraction besides being of interest in itself, is important in that it might prevent the use of (0°,45°,45°) cut modulators for high extinction switching of light. Lame in 1852 was the first to recognise that double refraction presents a mathematical problem which is by no means simple. To the best of the writer's knowledge double refraction is treated in the literature either in a very elementary way or in a very complex and highly mathematical manner.

1. Huygens construction illustrates well the origin of double refraction and it is therefore widely used in the undergraduate literature (Longhurst<sup>(27)</sup>, Jenkins and White<sup>(28)</sup>, etc). In this construction the surface of propagation of the light in the crystal is not a sphere but a certain combination of a sphere and an oblate ellipsoid of rotation. Thus two envelopes and thereby two wavefronts are obtained, one associated with the system of spheres and another for the

system of ellipsoids. However it gives an incomplete description because :

(a) it presupposes that a diverging bundle of rays which originates from a point source within the crystal behaves in the same way as a system of mutually independent plane waves.

(b) it gives no information about the polarisation of ordinary or the extraordinary wave.

(d) the construction leaves the question of the amplitude ratios between the two waves unanswered.

2. In the advanced treatments<sup>(39)</sup> a complete and quantitative theory of double refraction is obtained by considering the boundary conditions of refraction and reflection for isotropic and anisotropic materials. Light is treated as infinitely extended plane waves and not as rays. However, such an analysis is very mathematical and deals mostly with matters of theoretical interest.

The analysis attempted here is concerned only with essential conclusions and is not intended of course as a complete survey of the subject. The general ideas developed and the results given are in relation to the present practical application.

## 7.2 Double refraction in uniaxial crystals.

Let us consider a plane wave incident from an isotropic medium, (air), onto a plane surface of an anisotropic medium at an oblique angle, fig. 7.1. Solutions of the boundary conditions lead to Fresnel's equation and Snell's law of reflection and refraction. Snell's laws and Fresnel's equations together determine unambiguously the direction, intensity and polarisation of the reflected and refracted waves as a function of the properties of the incident wave and the dielectric characteristics of two interfacing media. The most important result is that in general each incident wave will give rise to two refracted waves polarised at right angles to each other. To each of these waves there corresponds a ray direction and a ray velocity describing the propagation of energy within the crystal. The two waves are progressing at different angles of refraction and each of the directions satisfies the law of refraction therefore we have for the ordinary wave,

$$\frac{\sin a}{\sin b} = n_o \quad 7.1$$

and similarly for the extraordinary wave,

$$\frac{\sin a}{\sin c} = n_e \quad 7.2$$

Also the two refracted waves lie in the plane of incidence. Expressions for the amplitude ratios that can be determined from the Fresnel formulae is not necessary to be discussed.

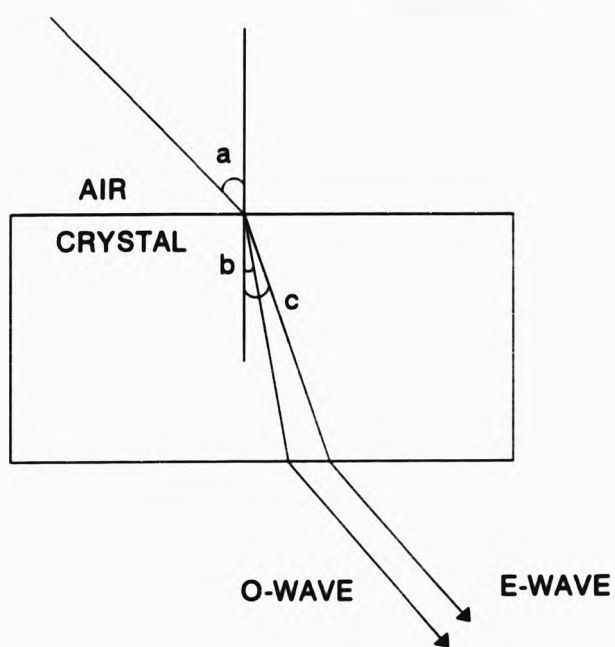


Fig. 7.1 Double refraction in uniaxial crystal.

### 7.3 Double refraction in $(0^\circ, 45^\circ, 45^\circ)$ cut crystals.

We can apply the above results to our problem of a light beam incident at oblique angle on a  $(0^\circ, 45^\circ, 45^\circ)$  cut crystal. By referring to fig. 7.2 the incident wave splits into two refracted waves. These waves lie in the plane of incidence which is the horizontal plane. It is well known that the structure of an anisotropic medium permits two monochromatic plane waves with two different linear polarisations at right angles and two different velocities of propagation, (ordinary and extraordinary wave), in any given direction. It is also true that the two distinct wave directions inside the  $(0^\circ, 45^\circ, 45^\circ)$  cut crystal which arise as a result of the double refraction properties of the crystal are also plane polarised with their directions of polarisation perpendicular to each other. These are the results obtained from the solutions of the boundary conditions which state that any monochromatic light incident on a anisotropic medium is resolved into two waves only, polarised at right angles. This is of course quite understandable, the fact that only two distinguishable oscillations are permitted gives crystals their importance as principal components of polarisation apparatus.

To determine the directions of polarisation we can use another crystal optics important result which simply states that the directions of polarisation are determined by the crystalline structure and that the ordinary wave vibrates normal to the principal section and the extraordinary wave

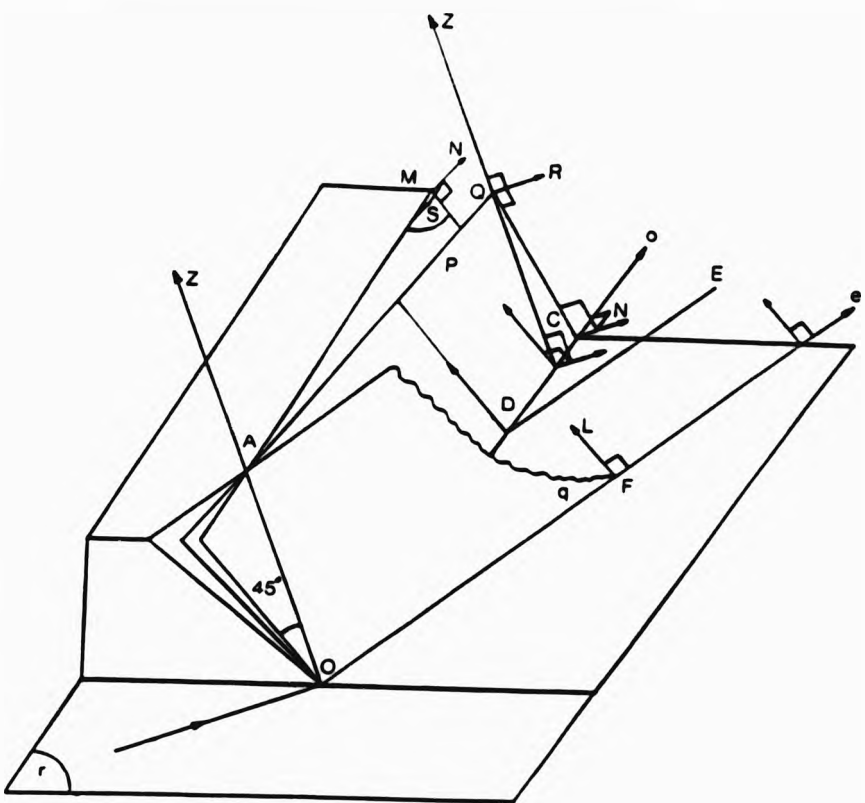


Fig. 7.2 Double refraction at oblique angle of incidence in a  $(0^\circ, 45^\circ, 45^\circ)$ -cut crystal.

vibrates in the principal section. Although many definitions for the principal plane exist in the literature, the correct and most comprehensive one is that the principal plane is the plane containing the optic axis and the normal to the wavefront i.e. the direction of the wave inside the crystal. Therefore, because two wave directions exist then surprisingly two principal planes must also be present. These planes are shown in fig 7.2. ADP material belongs to the negative uniaxial family of crystals so the angle that the ordinary wave makes with the normal to the crystal surface is smaller than the corresponding extraordinary wave angle. Therefore plane p is the ordinary principal section which contains the ordinary wave vibrating normal to this plane and plane q is the extraordinary principal section which contains the extraordinary wave. How does this result compare with the known optical behaviour of the anisotropic media? Let us assume the two vibration vectors CN and FL for the ordinary and extraordinary wave respectively. To make a valid comparison we must recall the important property of these vectors i.e. that they should vibrate at right angles to each other. By referring to fig. 7.2 the following assumptions are made.

p is the principal plane for the o-wave,  
q is the principal plane for the e-wave,  
r is the plane of incidence,  
s is the principal plane at normal incidence.

Let vector CN to be the o-wave vibration. Then CN is



normal to the  $z$  optic axis, the wave direction and hence normal to the  $p$  principal plane. Because  $CN$  is normal to the  $p$  plane then  $CN$  is normal to all the lines contained in this plane. Let  $FL$  to be the vibration for the  $e$ -wave. The two vibration directions are normal to each other therefore  $FL$  is also contained in plane  $p$ .

Alternatively we can draw the parallel  $DE$  to the  $e$ -wave direction which intersects plane  $p$  at  $D$ . We can always find a direction in this plane which makes an angle of  $90^\circ$  with the parallel  $DE$  and hence with the  $e$ -wave direction. Now since this direction is contained in plane  $p$  it is normal to  $CN$ . As a result of the above the  $e$ -wave vibrates in the  $o$ -wave principal plane and because plane  $p$  and  $q$  are not parallel, (intersect along  $z$ ), therefore  $FL$  does not lie in its principal plane  $q$ . The most important result so far is that:

(a) At normal incidence there is one principal plane because the two wave principal planes coincide. The  $o$ -wave vibrates normal to the plane and the  $e$ -wave in a direction contained in the plane.

(b) At oblique incidence there are two principal planes. The  $o$ -wave direction is in the  $o$ -wave principal plane and vibrates normal to the plane. The  $e$ -wave direction is in the  $e$ -wave principal plane but its vibration vector lies in the  $o$ -wave principal plane.

At normal incidence the o-wave vibration is MN, therefore MN is normal to plane s. At oblique angle of incidence the o-wave vibrates along QR, normal to p. The planes p and s are not parallel, because they intersect at z, thus QR is not parallel to MN. So the second important result is that there is a rotation of the polarisation directions

The rotation of the polarisation directions was also verified experimentally. The input polarizer was rotated by  $45^\circ$  therefore it was placed in parallel with one of the modulator's polarisation directions. At normal incidence complete extinction was obtained by rotating the analyzer by  $45^\circ$ . This is understandable because only one plane polarised wave was allowed to propagate through the modulator. Any rotation of the modulator polarisation axes could then be detected by examining the state of polarisation of the light coming out at an oblique angle. The rotation present resolved the input light into two components giving rise to elliptically polarised light and hence a lower extinction ratio. Results for various angles of incidence are tabulated below.

$\varphi$ in degrees	$I_{MAX}$ (V)	$I_{MIN}$ (mV)	E.R.
0	2	0.1	20000:1
1	2	1.4	1429:1
2	2	3.5	571:1
3	2	9.0	222:1

4	2	35.0	57:1
5	2	125.0	16:1

Table 7.1 Extinction ratio for different angles of incidence.

The concept of the two wave normals and the corresponding two distinct principal planes has been discussed. It has been proved that directions exist so that the two waves can vibrate at right angles. All it remains is to find the directions of these new electrical excitations.

7.4 The angle between the new and the old directions of polarisation.

These directions can be more easily found with the aid of three dimensional geometry. Fig. 7.3 shows a cut of the crystal for two different cases. OA corresponds to the wave direction at normal incidence and plane q is the associated principal plane. OB is the direction of the ordinary wave propagating at an angle because the incident beam entered the crystal at an oblique angle. The plane q contains the z optic axis and the new direction of propagation hence it is a principal section for the o-wave. At normal incidence the principal plane makes an angle of  $45^\circ$  with the horizontal plane which is also the plane of incidence. Also at normal incidence the o-wave vibrates normal to plane p ie at  $45^\circ$  to the horizontal. An important theorem of stereometry<sup>(40)</sup> states that if we draw the normal to a plane from a point B and from the intersection point another normal to a line contained in

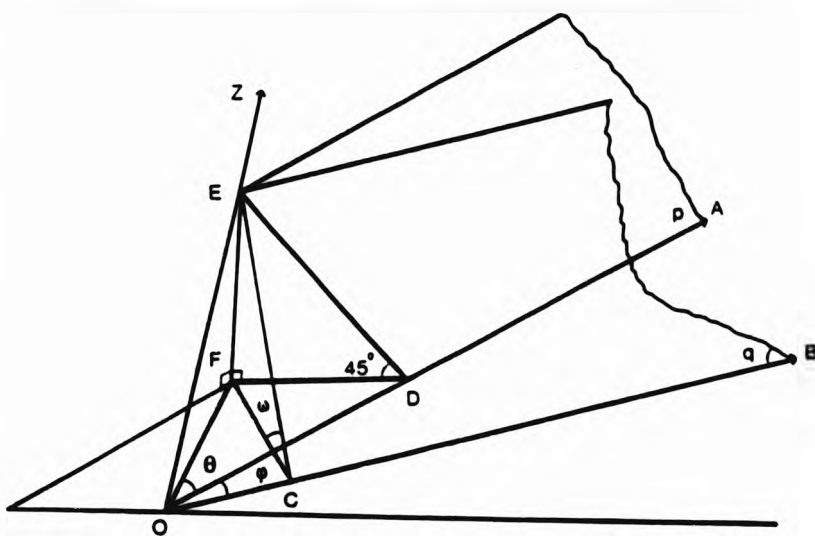


Fig. 7.3 The angle between the new and the old polarisation directions.

the plane at C then the line joining the points C and E is normal to the line contained in the plane. So by referring back to the figure we have:

EF normal to the horizontal plane,  
 FC normal to the direction of the refracted wave,  
 Hence the line EC is normal to OB.

The o-wave vibrates normal to its principal plane and normal to OA thus EC is the direction normal to the vibration. EC makes an angle  $\omega$  with the horizontal which can be very easily found as follows:

Let DE = a then it can be easily proved using Pythagoras theorem that:

$$OE = \sqrt{2}a \quad 7.3$$

$$DF = \frac{a}{\sqrt{2}} \quad 7.4$$

$$EF = \frac{a}{\sqrt{2}} \quad 7.5$$

$$OF = \sqrt{\frac{3}{2}}a \quad 7.6$$

using the sine rule for the triangle ECF we have:

$$\frac{CE}{\sin EFC} = \frac{EF}{\sin \omega} \quad 7.7$$

$$\sin \omega = \frac{EF}{EC} \sin EFC = \frac{a}{\sqrt{2}EC} \quad 7.8$$

using the sine rule for the triangle OFD we have:

$$\frac{FD}{\sin \theta} = \frac{OF}{\sin FDO} \quad 7.9$$

$$\sin \theta = \frac{FD}{OF} = \frac{1}{\sqrt{3}} \quad \text{ie } \theta = 35.26^\circ \quad 7.10$$

Using the sine rule for the triangle OFC we have:

$$\frac{FC}{\sin(\theta + \phi)} = \frac{OF}{\sin OCF} \quad 7.11$$

$$FC = OF \sin(\theta + \phi) = \sqrt{\frac{3}{2}} a \sin(\theta + \phi) \quad 7.12$$

Using the Pythagoras theorem for the triangle EFC we have:

$$EC^2 = EF^2 + FC^2 \quad 7.13$$

$$EC^2 = \frac{a^2}{2} + \frac{3}{2} a^2 \sin^2(\theta + \phi) \quad 7.14$$

$$EC = a \left( \frac{1 + 3 \sin^2(\theta + \phi)}{2} \right)^{\frac{1}{2}} \quad 7.15$$

Substituting the above value for EC into 7.8 yields to:

$$\sin\omega = \frac{a}{\sqrt{2}EC} = [1 + 3\sin^2(\theta + \phi)]^{-\frac{1}{2}} \quad 7.16$$

According to this result the angle of the vibration of the extraordinary vector with the horizontal is not constant but changes as a function of the angle of incidence. Therefore a beam of light vertically polarised entering the crystal at an angle will not be resolved any more in two components at 45° to the normal (or horizontal). Instead it will be resolved along two new directions which make an angle with the previous direction given by:

$$z = \omega - 45^\circ \quad 7.17$$

7.5 The effect of the rotation of axes in the modulator operation.

So an important conclusion is derived from this analysis which simply says that a change of the angle of incidence causes a rotation of the crystals polarisation directions. It is a rather unexpected result and at a first glance it seems that we can compensate for this effect by rotating the input polariser by the same angle  $z$  so that the incident beam will again equally be resolved in two components at 45° along the new induced directions. In practice this has not resulted to an improvement of the extinction ratio. If we more carefully examine the composite modulator and in particular the polarisation directions for each crystal it is easily understood that the rotation of the axes is not of the same sense in all crystals. To be more specific there is a

clockwise rotation in the first pair of crystals but an anticlockwise one in the second pair. Fixed directions of polarisation throughout the modulator is essential for proper compensation. The effects of these two opposite polarisation rotations on the modulator performance can be found as follows:

Assuming that an angle of incidence  $\varphi$  causes a rotation of angle  $z$  and that the input polarisation direction makes an angle  $\theta$  with one of the crystals polarisation axes, fig. 7.4.a, then the two light components along the new directions are given by

$$E_A = \cos\theta \cos\omega t \quad 7.18$$

$$E_B = \sin\theta \cos\omega t \quad 7.19$$

The two beams exit the first crystal with a phase difference caused from the crystals natural birefringence and the modulating field so that:

$$E_A = \cos\theta \cos(\omega t + \varphi_o + \varphi_E) \quad 7.20$$

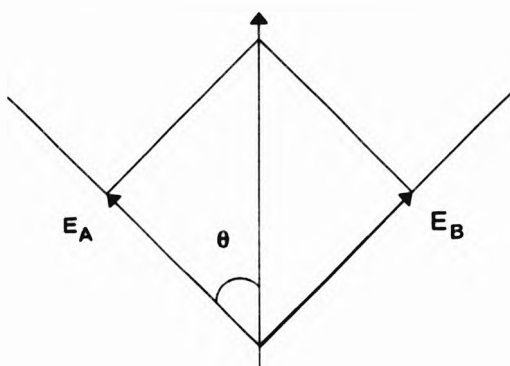
$$E_B = \sin\theta \cos(\omega t + \varphi_o - \varphi_E) \quad 7.21$$

where:

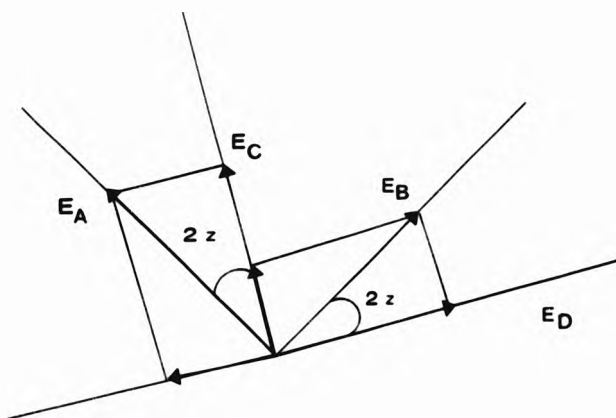
$$\varphi_o = \frac{2\pi}{\lambda} n_o l_o \quad 7.22$$

$$\varphi_E = \frac{2\pi}{\lambda} n_e l_e \quad 7.23$$

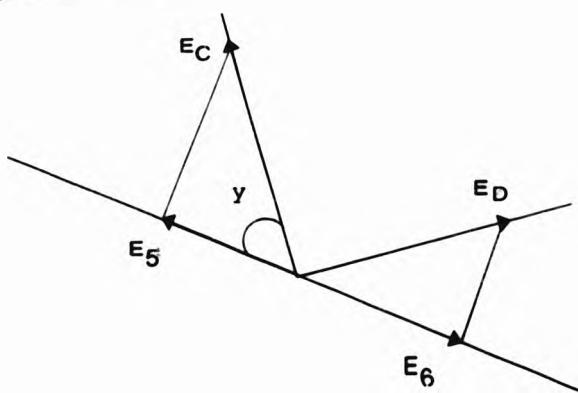




(A)



(B)



(C)

Fig7.4 Polarisation directions.

$$\varphi_E = \frac{\pi}{\lambda} \frac{1}{\sqrt{2}} n_{os}^3 r_{41} \frac{dE}{I} \quad 7.24$$

The two waves enter the second crystal with their polarisation unaltered and because the electro optic effect is additive we can write for the waves coming out from the first pair of crystals:

$$E_A = \cos\theta \cos(\omega t + 2\varphi_o + 2\varphi_E) \quad 7.25$$

$$E_B = \sin\theta \cos(\omega t + 2\varphi_o - 2\varphi_E) \quad 7.26$$

The directions of polarisation of the second pair of crystals are not parallel to the first pair's so the waves entering the third crystal are resolved in four components along the new directions, fig. 7.4.b. If  $z$  is the rotation of the axes with respect to the normal then the two set of axes are at an angle of  $2z$ . Therefore the components along the new directions are given by:

$$E_C = E_1 \cos 2z + E_2 \sin 2z \quad 7.27$$

$$E_D = E_2 \cos 2z - E_1 \sin 2z \quad 7.28$$

At the exit of the third crystal we can write for the light components:

$$E_C = \cos 2z \cos\theta \cos(\omega t + 2\varphi_o + \varphi_o + 3\varphi_E) + \sin 2z \sin\theta \cos(\omega t + 3\varphi_o - \varphi_E) \quad 7.29$$

$$E_D = \cos 2z \sin \theta \cos (\omega t + 2\phi_o + \phi_o - 3\phi_E) - \sin 2z \cos \theta \cos (\omega t + 3\phi_o + \phi_o) \quad 7.30$$

Similar considerations apply also here as the waves enter the fourth crystal, so finally the components coming out from the modulator are given by:

$$E_C = \cos 2z \cos \theta \cos (\omega t + 2\phi_o + 2\phi_o + 4\phi_E) + \sin 2z \sin \theta \cos (\omega t + 4\phi_E) \quad 7.31$$

$$E_D = \cos 2z \sin \theta \cos (\omega t + 2\phi_o + 2\phi_o - 4\phi_E) - \sin 2z \cos \theta \cos (\omega t + 4\phi_E) \quad 7.32$$

We can now assume that the analyzer at the output of the modulator makes an angle  $\gamma$ , fig. 7.4 c with one the vibration directions therefore the components leaving the analyzer are:

$$E_s = E_C \cos \gamma \quad 7.33$$

$$E_e = E_D \sin \gamma \quad 7.34$$

The total transmitting field is:

$$E_T = E_s - E_e = E_C \cos \gamma - E_D \sin \gamma \quad 7.35$$

So the resulting amplitude depends on the superposition of four waves. In general the sum of  $N$  such waves is given<sup>(41)</sup> by:

$$E = E_o \cos (\omega t \pm \alpha) \quad 7.36$$

$$\text{where } E_o^2 = \sum_{i=1}^N E_{oi}^2 + 2 \sum_{j>1}^N \sum_{i=1}^N E_{oi} E_{oj} \cos (\alpha_i - \alpha_j) \quad 7.37$$

$$\text{and } \tan \alpha = \frac{\sum_{i=1}^N E_{oi} \sin \alpha_i}{\sum_{i=1}^N E_{oi} \cos \alpha_i} \quad 7.38$$

The four waves are :

$$E_1 = \cos 2z \cos \theta \cos y \cos (\omega t + 2\varphi_o + 2\varphi_e + 4\varphi_g) \quad 7.39$$

$$E_2 = \sin 2z \sin \theta \cos y \cos (\omega t + 4\varphi_o) \quad 7.40$$

$$E_3 = \cos 2z \sin \theta \sin y \cos (\omega t + 2\varphi_o + 2\varphi_e - 4\varphi_g) \quad 7.41$$

$$\begin{matrix} (-) \\ E_4 = \sin 2z \cos \theta \sin y \cos (\omega t + 4\varphi_o) \end{matrix} \quad 7.42$$

We can simplify the above by assuming a common phase of  $2(\varphi_o + \varphi_e)$ , therefore the waves can be written now as:

$$E_1 = \cos 2z \cos \theta \cos y \cos (\omega t + E_T) \quad 7.43$$

$$E_2 = \sin 2z \sin \theta \cos y \cos (\omega t + 2\varphi_N) \quad 7.44$$

$$E_3 = \cos 2z \sin \theta \sin y \cos (\omega t - E_T) \quad 7.45$$

$$\begin{matrix} (-) \\ E_4 = \sin 2z \cos \theta \sin y \cos (\omega t - 2\varphi_N) \end{matrix} \quad 7.46$$

Where  $E_T = 4\varphi_e$  is the electrically induced birefringence and  $\varphi_N = (\varphi_o + \varphi_e)$  is the natural birefringence contribution to the total phase difference.

Furthermore the expression of the resultant amplitude contains the two unmodulated terms  $E_2$  and  $E_4$ . These components arise from the fact that a portion of the ordinary wave in the first pair of crystals continues to behave as an ordinary wave in the second pair. The same applies also for the extraordinary wave so the phase of these components is not sensitive to the applied electric field. The general solution of the expression for the resultant amplitude is a very lengthy calculation. To simplify matters summation of the four waves can be also represented graphically as an addition of vectors in the complex plane. The four phasors are shown in fig. 7.5 a.

Since it is a practical impossibility to accurately determine a value for  $\varphi_N$ , the vectors  $E_2$  and  $E_4$  can lie anywhere in the complex plane. So in general complete cancelation of the main waves  $E_1$  and  $E_3$  will not necessarily result to zero overall transmission. Some light will be present because of  $E_2+E_4$ , fig. 7.5 b, so the best we can do is a matter of finding conditions to minimise the resultant vector  $E_1+E_3$ . Obviously the vector  $E_1+E_3$  is reduced to zero when the vectors  $E_1$  and  $E_3$  have equal amplitudes and be  $180^\circ$  out of phase. Therefore,

$$\cos\theta\cos\gamma = \sin\theta\sin\gamma \quad 7.47$$

$$\text{or } \cot\theta = \tan\gamma \quad 7.48$$

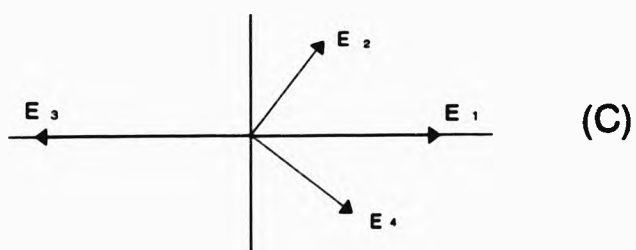
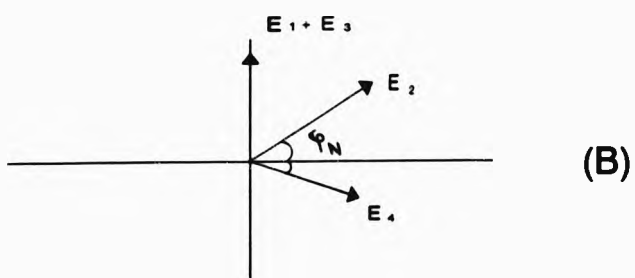
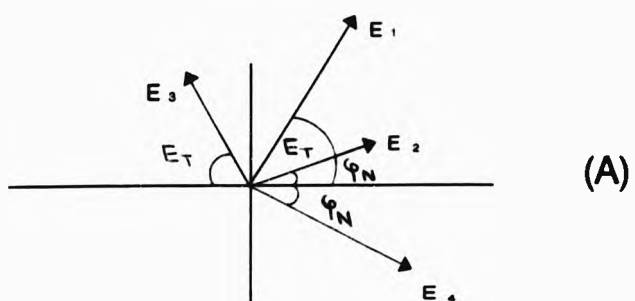


Fig. 7.5 Polarisation directions.

or  $\theta=45^\circ$  and  $\gamma=45^\circ$

7.49

An important result arises here that minimum transmission occurs not for a crossed polariser and analyzer but when the input polariser is at  $45^\circ$  to the fast and slow axes of the first pair of crystals and vice versa for the output analyzer and the second pair of crystals. In practice at zero incidence minimum transmission occurs with the polarisers crossed as expected and at oblique angles of incidence with the polarisers rotated in opposite sense to each other by the same angle. This angle was also found experimentally to be very close to the value predicted by equation 7.17. The presence of  $E_2$  and  $E_4$  imposes a limitation to the maximum extinction ratio available from the modulator.

The four vectors now become:

$$E_1 = 0.5 \cos 2z \cos(\omega t + E_T) \quad 7.50$$

$$E_2 = 0.5 \sin 2z \cos(\omega t + 2\phi_H) \quad 7.51$$

$$E_3 = 0.5 \cos 2z \cos(\omega t - E_T) \quad 7.52$$

$$E_4 = 0.5 \sin 2z \cos(\omega t - 2\phi_H) \quad 7.53$$

The extinction ratio of the modulator can be found as follows:

$$I_1 = (E_1 + E_3)^2 = E_1^2 + E_3^2 + 2E_1E_3 \cos 2E_T = \cos^2 2z \quad 7.54$$

$$I_2 = (E_2 + E_4)^2 = E_2^2 + E_4^2 + 2E_2E_4 \cos 4\phi_N = \sin^2 2z \cos^2 2\phi_N \quad 7.55$$

The vectors,  $E_1 + E_3$  and  $E_2 + E_4$  are always at right angles so the magnitude of the resultant vector sum is:

$$I_{MAX} = I_1 + I_2 = \cos^2 2z + \sin^2 2z \cos^2 2\phi_N \quad 7.56$$

The minimum intensity is :

$$I_{MIN} = I_2 = \sin^2 2z \cos^2 2\phi_N \quad 7.57$$

The extinction ratio is given by:

$$ER = \frac{I_{MAX}}{I_{MIN}} = \frac{I_1 + I_2}{I_2} = \frac{\cot^2 2z}{\cos^2 \phi_N} + 1 \quad 7.58$$

Further points :

1. At zero incidence  $z=0$  therefore complete cancellation of the wave components is possible, at least in theory thus resulting to an infinite extinction ratio. In practice of course this can never be achieved for a number of obvious reasons.

2. The minimum extinction ratio is 1 and occurs for  $I_{MAX} = I_{MIN}$ . The number one contained in the above expression for the extinction ratio, sets this limit even at an angle  $90^\circ$  where  $\cot^2 2z$  is 0.

3. As the angle of incidence is increased more, then more of the incident beam energy is contained in the unmodulated components  $E_1$  and  $E_4$ , and this results to poor extinctions. It



is rather interesting that even at large angles of incidence equation 7.57 allows for even an infinite extinction ratio to be obtained assuming the vectors  $E_1$  and  $E_2$  have the correct phase i.e.  $\phi_N=90^\circ$ . In practice a high extinction ratio was never observed at wide angles of incidence. This will be explained in the analysis following.

#### 7.6 The effect of spatial coherence in the modulator performance.

By referring to figure 7.5.c it can be easily seen that for any position of the vectors  $E_1$  and  $E_2$ , some light leakage through the analyzer is unavoidable since the sum of the four wave vectors can never be zero. One would expect the angular aperture of the modulator to be uniformly illuminated and the amount of illumination when the modulator is biased at a minimum to be set by the term

$$I_{MIN} = \sin^2 2z \cos^2 2\phi_N \quad 7.59$$

As already mentioned, in practice an interference pattern was observed. Complete extinction of portions within the aperture was possible, giving rise to an isobar. The result of a change in the biasing voltage was that the retardation altered across the aperture thus the position of the isobar also changed. Also as the angle of incidence was progressively increased the width of the isobar was accordingly reduced and larger voltage variations were needed to move the isobar from the top of the aperture to the bottom. Clearly the effects observed were created by interference caused by variations of the beam's spatial

coherence at the output of the modulator. Assuming a laser beam with a divergence of  $1mR$  or  $0.064^\circ$  then inside the crystals, fig 7.6 a, the divergence becomes

$$d_c = \frac{d}{n_D} = 0.037^\circ \quad 7.60$$

The phase difference between the points A and B is given by:

$$\varphi_A - \varphi_B = \frac{360^\circ}{\lambda} n (l_2 - l_1) \quad 7.61$$

For the unmodulated components  $E_2$  and  $E_4$  which behave as an ordinary ray and extraordinary ray respectively throughout the modulator and by taking  $n_o = n_e = n$  the phase difference is given by:

$$\varphi_A - \varphi_B = \frac{360}{0.633 \times 10^{-6}} 1.49 \times 0.06 \left( \frac{1}{\cos 0.018^\circ} - 1 \right) \quad 7.63$$

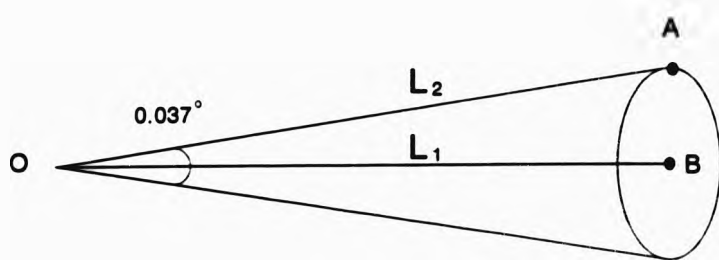
$= 2.5^\circ$

Therefore the spatial coherence of the beam is reasonably good and the vectors  $E_2$  and  $E_4$  have to be replaced by a small sector of vectors with an angular spread of  $2.5^\circ$  only, fig 7.7 a. When the beam enters the modulator at an angle of say  $10^\circ$ , fig. 7.6 b, then the situation is a lot different. The phase difference between the points O and A becomes now:

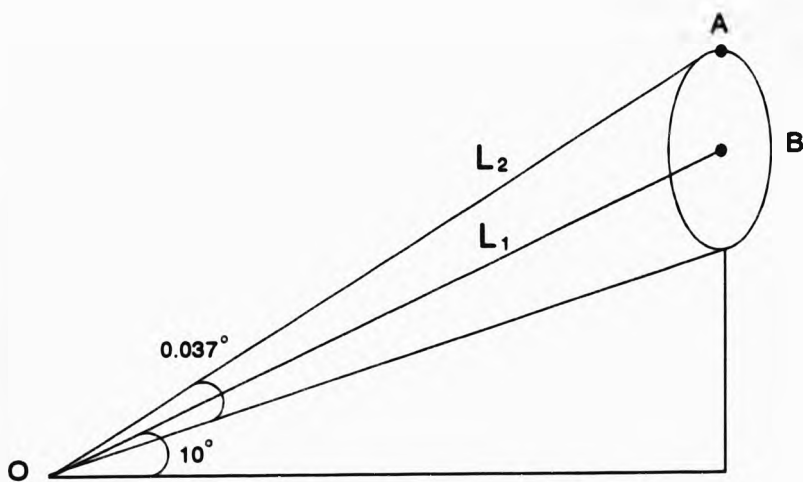
$$\varphi_A - \varphi_B = \frac{360}{0.633 \times 10^{-6}} 1.49 \times 0.06 \left( \frac{1}{\cos 10.028^\circ} - \frac{1}{\cos 10^\circ} \right) \quad 7.64$$

$= 4455^\circ$

The vectors  $E_2$  and  $E_4$  have now to be replaced by sectors of vectors  $4455^\circ$  wide, fig. 7.7 b. For every particular position of the main vectors  $E_1$  and  $E_3$  extinction of only a small sector of vectors is achieved so only the corresponding portions of the output aperture are at zero illumination. The



(A)



(B)

Fig. 7.6 Beam divergence and spatial coherence.

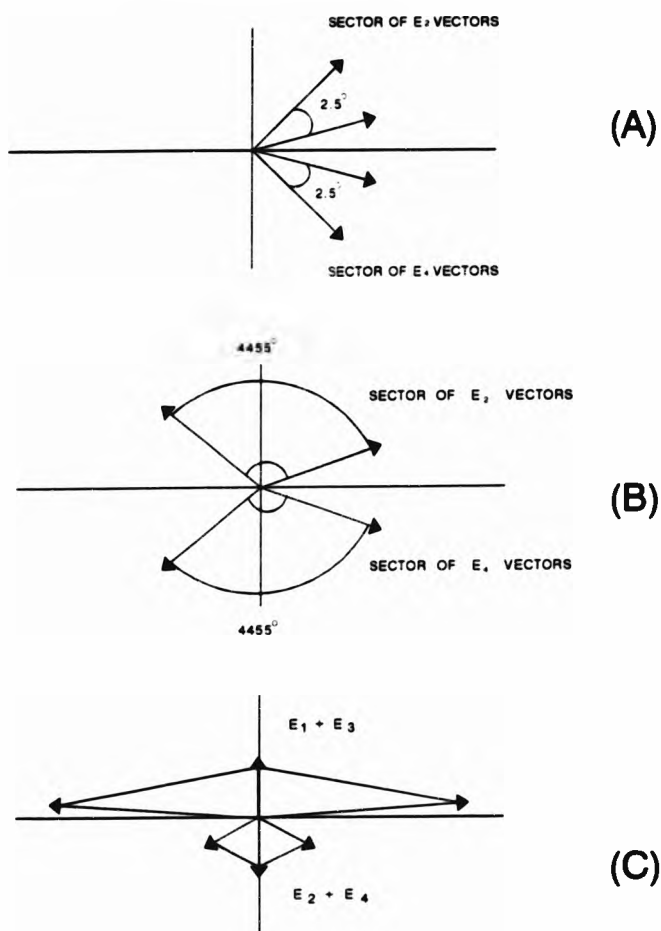


Fig. 7.7 Polarisation directions.

geometric loci of these points gives rise to the isobar observed. Rotation of the vectors  $E_1$  and  $E_2$ , which is achieved by changing the biasing voltage, causes extinction of another sector of vectors and the intensity of another portion of the output aperture to be reduced to a minimum. Therefore, the isobar moves and changes position. Good extinctions at normal incidence are possible because of a limited angular spread of the unwanted vectors  $E_1$  and  $E_2$ , which also have a very small amplitude because of the  $\sin^2 z$  factor contained in their amplitude expression. Poor extinctions at oblique incidence are caused because of the wide spread of the vectors which also have now a rather significant amplitude. The degree of variation of the relative phase of these components across the beam aperture is rapid, therefore giving rise to progressively thinner isobars at larger angles of incidence and consequently wide voltage changes to move the isobar from one end of the illuminated aperture to the other. As a final test a lens was used to increase the divergence of the beam so that  $\varphi_A - \varphi_B \gg 360^\circ$ . This had the effect of making many different portions of the aperture to experience the same relative phases and as a result of a number of very thin isobars were observed moving parallel and equally spaced within the aperture as expected.

#### 7.7 The 45° y-cut and 45° z-cut modulators at oblique angle of incidence.

In section 7.3 it was shown that double refraction at oblique angles of incidence in (0°, 45°, 45°) cut crystals causes a

geometric loci of these points gives rise to the isobar observed. Rotation of the vectors  $E_1$  and  $E_2$ , which is achieved by changing the biasing voltage, causes extinction of another sector of vectors and the intensity of another portion of the output aperture to be reduced to a minimum. Therefore, the isobar moves and changes position. Good extinctions at normal incidence are possible because of a limited angular spread of the unwanted vectors  $E_2$  and  $E_1$ , which also have a very small amplitude because of the  $\sin 2z$  factor contained in their amplitude expression. Poor extinctions at oblique incidence are caused because of the wide spread of the vectors which also have now a rather significant amplitude. The degree of variation of the relative phase of these components across the beam aperture is rapid, therefore giving rise to progressively thinner isobars at larger angles of incidence and consequently wide voltage changes to move the isobar from one end of the illuminated aperture to the other. As a final test a lens was used to increase the divergence of the beam so that  $\varphi_A - \varphi_B \gg 360^\circ$ . This had the effect of making many different portions of the aperture to experience the same relative phases and as a result of a number of very thin isobars were observed moving parallel and equally spaced within the aperture as expected.

#### 7.7 The 45° y-cut and 45° z-cut modulators at oblique angle of incidence.

In section 7.3 it was shown that double refraction at oblique angles of incidence in (0°,45°,45°) cut crystals causes a

rotation of the crystal's polarisations direction and as a result the generation of uncompensated and unmodulated terms in the final expression for the resultant wave leaving the modulator. The interference pattern associated with these effects limits the uniform extinction of the beam, and therefore degrades the maximum extinction ratio available from the device. Mansell<sup>(36)</sup> has reported that wide angular apertures are possible with the 45° y-cut and 45° z-cut compensated modulators. Uniform illumination and extinction of a beam with angular spread as high as 50° can be achieved. This can be also explained by examination of double refraction at oblique angles for these modulators. A beam entering the modulator at an angle is refracted in two waves, both of them contained in the horizontal plane or plane of incidence. Again two principal planes are defined but because the optical axis z is either normal or contained in the plane of incidence the waves continue to be polarised as before i.e. normal and parallel to the incident horizontal plane. The directions of polarisation remain unaltered throughout the modulator so that only two waves are allowed to propagate. Unwanted terms similar to the ones discussed in the previous paragraph are not present therefore high extinctions can be obtained even at wide angles of incidence.

#### 7.8 Estimation of the extinction ratio of the (0°, 45°, 45°) cut modulator.

The expression for the extinction ratio as given by equation 7.58 is:

$$ER = \frac{\cot^2 2z}{\cos^2 2\phi_N} + 1$$

It has been shown that because of their wide angular spread only a small portion of the components contained in the sector of vectors  $E_2$  and  $E_4$  can be combined with the main vectors  $E_1$  and  $E_3$  to result into zero intensity. In general the remaining vectors correspond to different positions of the output aperture, cancellation of them is not possible therefore to a good approximation we can assume that the minimum intensity through the analyzer is the sum of all these intensities, therefore,

$$I_2 + I_4 = 1 - (I_1 + I_3) = 1 - \cos^2 2z = \sin^2 2z \quad 7.65$$

This is the case when  $\cos^2 2\phi_N = 1$  so the extinction ratio now becomes:

$$ER = 1 + \cot^2 2z \quad 7.66$$

Substituting the values of  $z$  obtained from 7.16 and 7.17 into 7.65 and plotting the E.R. versus  $\phi$  gives the graph shown in fig. 7.8. Comparison of the curves obtained experimentally, figs 6.10 and 6.11 and the theoretical curve clearly shows that they are in very close agreement. *(in terms of profile)*

### 7.9 Conclusions.

In a properly compensated system the ordinary and the extra-ordinary rays are interchanged so that the total optical path length of the two waves is equal not only for normal incidence but for oblique incidence as well. The two birefringent systems must be so orientated that the splitting



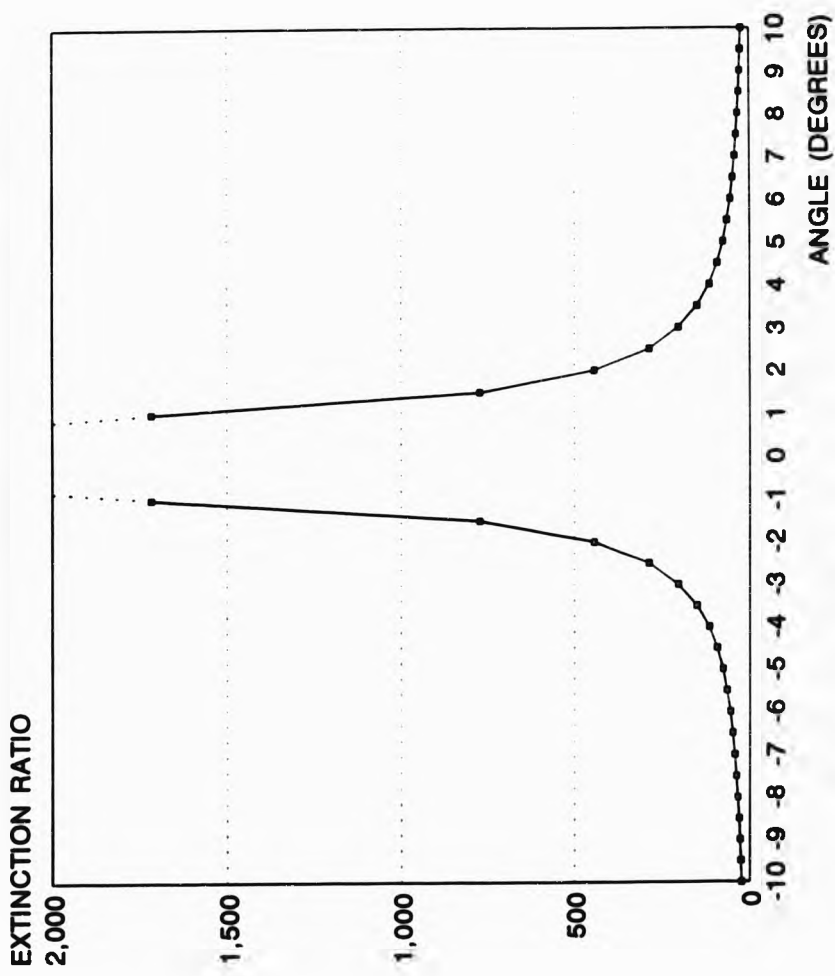


Fig. 7.8 Theoretical extinction ratio versus angle of incidence.

and path difference produced by one are exactly cancelled by the other. In the case of a beam entering normal in a  $(0^\circ, 45^\circ, 45^\circ)$  cut modulator the above condition is complied with. At an oblique angle the optical path length of the rays are no longer equal. It is this lack of compensation which causes a phase distortion of the emergent wavefront. These variations of birefringence tend to produce the same effects as variations of birefringence caused from local strains within the electro-optic material, strains due to non uniform heating, non parallelism of the crystal's end faces etc. These effects result to diffusion of the optical bias condition and reduction of the degree of modulation.

For comparison reasons the magnitude of these effects were estimated using simple models. Results for the linewidth, strain, non-parallelism between the crystal's end faces and flatness convincingly show that they are insignificant compared to the phase changes resulting from the oblique angle of propagation. Further evidence in support of this argument is the fact that at normal incidence the extinction ratios obtained were high and even better than the corresponding extinction ratios from commercial modulators. Therefore these effects are not responsible for the poor extinctions at oblique angles of incidence.

The combined effect of adding the electrically controlled phase changes of the two compensated components  $E_1$  and  $E_2$  and the random ones produced from the uncompensated and unmodulated waves  $E_3$  and  $E_4$  forms an interference pattern, the

observed isobar. The lack of uniform illumination and extinction degrades the maximum extinction ratio available from the modulator.

## CHAPTER 8 BEAM PROFILE AND TEMPERATURE STABILITY PERFORMANCE

### 8.1 Beam profile performance.

#### 8.1.1 Introduction.

The profile of the laser beam leaving the modulator has been studied. The printing industries have seen the development of the laser printer in the last few years. In reprographics where dots are exposed directly on film a helium neon laser is frequently used as a writing device. In the printing process the beam is turned on and off at a high frequency by a modulator. Beam quality affects these applications so beam analysis was essential to determine the spatial properties and in particular the shape of the beam coming out of the modulator. Beam quality also influences other performance parameters in applications where an electrooptic modulator is used. Scanning reliability, coupling efficiency, optical recording density are some of these parameters.

A beam profile can be defined as the irradiance, the power per unit area, along an axis perpendicular to the propagation axis. This irradiance is often considered to have a perfect Gaussian shape but in practice real lasers never have a perfect Gaussian profile. Even though to a good approximation a laser is assumed to have a cylindrical Gaussian irradiance distribution by assuming that only the lowest order transverse electromagnetic mode  $TEM_{00}$  is present. This mode

experiences the minimum possible diffraction loss, has minimum divergence and can be focused to the smallest possible spot. For these reasons it is often imperative that the modulator should not distort the profile of the beam by exciting higher order modes. In addition to the beam distortion higher order modes also have a larger spread and suffer higher diffraction losses.

In practice the excitation of higher order modes is unavoidable. Deviations from perfect flatness in the surfaces of the modulator windows, crystals and mirrors, inhomogeneities of the refractive index of the windows, crystals and index matching fluid, lensing effects created by non uniform heating of the crystals and matching fluid are all sources of wavefront distortion which deforms the ideal Gaussian profile of the beam entering the modulator. Unwanted diffraction patterns caused by scratches on the mirror, window and crystal surfaces, dust particles present inside the cavity or even molecular diffraction inside the crystal and fluid material can lead to problems. The finite size of the modulator crystal aperture blocks some of the propagating power also resulting in diffraction of the beam. Because of constructive and destructive interference between the waves geometrically transmitted through the aperture and the spherical waves produced at the edges of the aperture the profile of the transmitted beam changes as it propagates beyond the diffracting element.

#### 8.1.2 Measurement method and results.

The pinhole method was used to measure the profile of the beam leaving the modulator. A commercial beam profiler instrument with a 25  $\mu\text{m}$  hole, much smaller than the beam itself, measured the irradiance (the power/area of the aperture). Although to acquire complete information the hole must be scanned through the entire two dimensional beam profile, in practice scanning in the horizontal and then in the vertical direction was found adequate. Measurements at a transmission maximum and minimum were taken. During the measurements the beam profiler pinhole head was held 0.3m away from the modulator. Then it was moved 0.3m further away and results from this new position were identical with the results acquired from the initial position. This suggested that the beam profile had been recorded in the far field where the beam had assumed a constant shape. The results are shown in fig. 8.1 and fig. 8.2. Also the profile of the beam was recorded for a single pass, at a transmission minimum for normal and  $5^\circ$  angle of incidence, fig. 8.3.

#### 8.1.3 Analysis of results and conclusions.

Figures 8.1 a and b show that the shape of the beam is close to the Gaussian and indicate that the modulator did not affect significantly the profile of the beam. Figure 8.1 c shows that uniform extinction in the vertical direction was not possible but some light leakage was always present. The deep in the middle shows the presence of the horizontal isobar regularly observed during the extinction ratio measurements. On the other hand from figure 8.1 d uniform

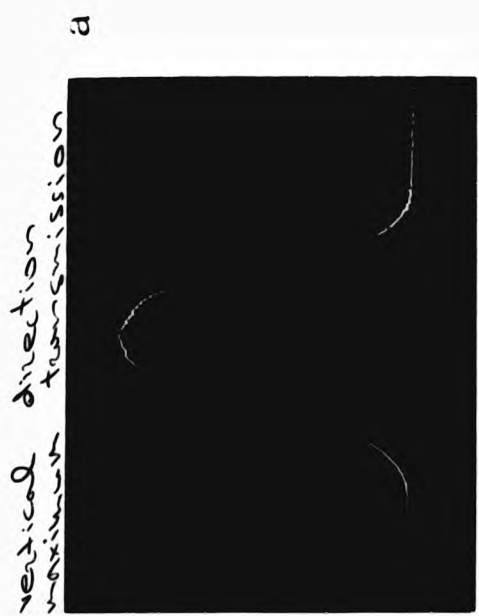
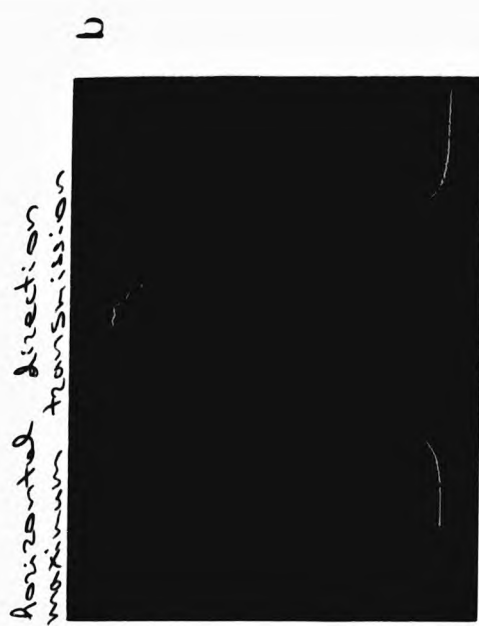


Fig. 8.1 Beam profiles for three passes.

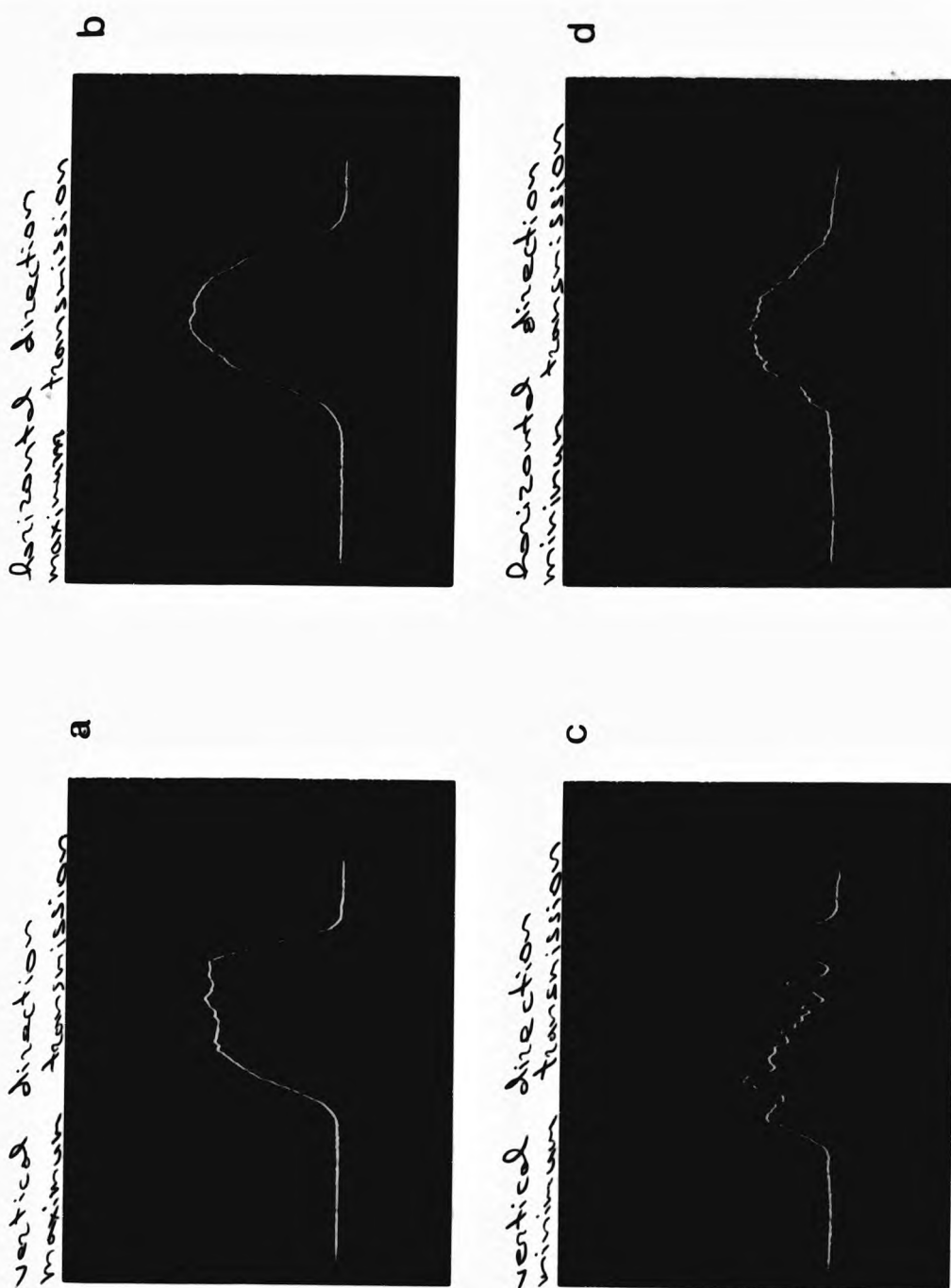


Fig. 8.2 Beam profiles for five passes.



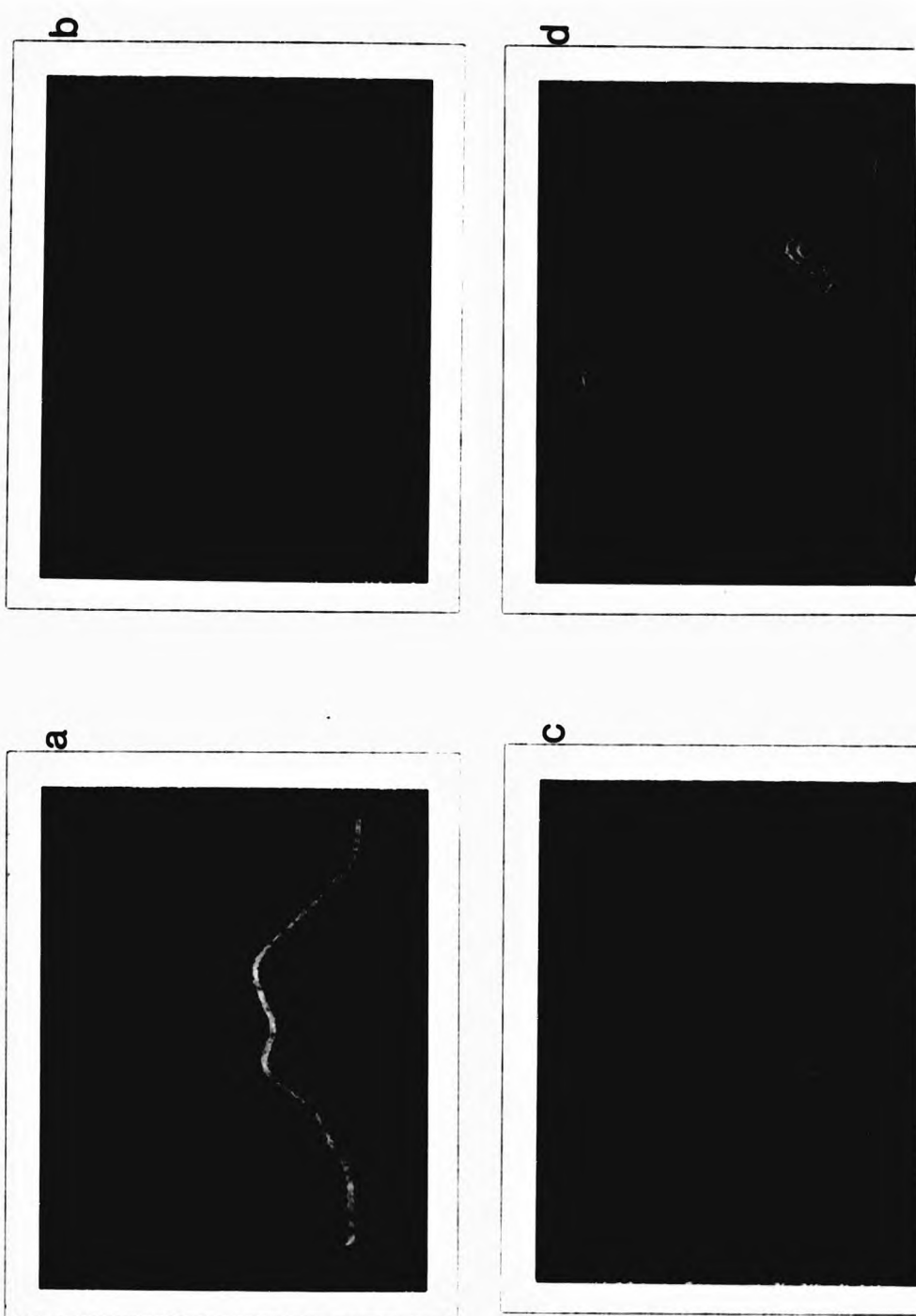


Fig. 8.3 Beam profiles for single pass.

extinction in the horizontal direction was possible. Figure 8.1 d shows some light present at a transmission minimum. This was done intentionally by not applying the full half wave voltage. It was then possible to distinguish the shape of the beam from the zero baseline of the instrument and verify its Gaussian shape. Increasing the biasing voltage by a few volts caused the beam to disappear completely. Figure 8.2 a shows clipping of the beam and severe distortion of its ideal shape. this can be easily explained from the fact that after five passes the beam had travelled more than a meter so that the crystal aperture was not big enough to compensate for the growth of the beam. Scanning in the horizontal direction, figure 8.2 b, indicates that there was not any clipping present, as expected, in this direction. Similar observations made for figures 8.1 c,d apply also for figures 8.2 c,d respectively. Figure 8.2 c shows the combined effect of the isobar present indicated by the dip on the right and the clipping effect which resulted in the irregular pattern in the middle and left side. Clipping of the beam can be overcome either by using larger aperture crystals and/or by reducing the modulator cavity length and hence the laser beam path length.

It is interesting also that by repeating the beam profile measurements with a less powerful beam (0.2mW as opposed to 1mW before) the beam growth was kept smaller and even after seven passes the shape of the beam was reasonably Gaussian. It is believed that lensing effects associated with the heating of the relatively viscous and thick index matching

fluid used, combined with an excessive fluid path length of almost 800mm increased the growth of the beam which resulted to the clipping even at such low power levels. A low absorption fluid combined with a much shorter fluid path length can ensure a higher optical power throughput capability with no mode distortion or blooming. Figure 8.3 a shows a good extinction which was possible because the beam propagated at normal incidence. The deviation from the true Gaussian shape is because the beam has a finite divergence which produces phase shifts as explained in section 7.6. These phase shifts although small result to a very weak isobar which was not possible to observe visually. At an oblique angle of incidence the situation is a lot different. Figure 8.3 b shows the presence of a well defined isobar which did not allow uniform extinction of the output aperture. The phase shifts at an oblique angle of incidence are much bigger as predicted by equation 7.64. These variations were rather significant and caused a rapid variation of the intensity pattern as compared to figure 8.3 a. The theory developed and presented in chapter 7 also suggested that complete extinction at any point of the output aperture would be possible under the application of a different biasing voltage. To verify this argument, the biasing voltage was gradually increased and then decreased so that complete extinction of different portions of the beam throughout the whole aperture were possible for different voltage settings. Results for a change of +10V and -10V caused the displacement of the isobar shown in figures 8.3 c and d accordingly.

#### 8.1.4 Conclusions.

In conclusion, intensity modulation depends on interference of beams which in turn demands good spatial coherence for uniform illumination and good degree of modulation. This is something that can not be achieved with the oblique angle multipath modulators. The most obvious solution would be a means of achieving many passes at normal incidence. Such a modulator will not suffer from a low extinction and provided that the crystal aperture is adequate, good Gaussian beam profiles should be achievable.

#### 8.2 Modulator temperature stability performance.

##### 8.2.1 Introduction.

One serious problem associated with the use of electrooptic crystals is the change in birefringence as a function of temperature. This is because transverse electrooptic modulators are path length dependent devices. The change in birefringence with temperature is due to two factors. One factor is associated with the changes happening in the environment surrounding the modulator and the other factor is because of heat generated inside the modulator. Dielectric losses occurring due to the electrical and optical field cause power dissipation not only within the crystal material but on the electrodes and electroded crystal surfaces and within the index matching fluid as well. The

result is that the operating point of the modulator drifts not only because the difference in refractive indexes ( $n_o - n_e$ ) is temperature dependent but also because of the crystal's thermal expansion. Assuming that the power losses cause a uniform heating inside the crystals then variations of the refractive indexes although small are sufficiently large to cause a deflection of the beam and hence a change in birefringence. In practice because heat is generated within the crystal material but cooling occurs only on the surfaces and to a greater extent on the electroded surfaces there is a parabolic (non-uniform) temperature distribution. This causes each ray of the beam to suffer a different angular deflection which more simply means that the beam is decollimated. These effects are more pronounced at high modulating frequencies since the power dissipated in the crystal is larger at higher frequencies for a given degree of intensity modulation. All the effects described above reduce the extinction ratio and the degree of modulation, diffract the beam inside the modulator, change and diffuse the optical bias condition<sup>(33)</sup>.

Obviously these are effects that should be avoided and Peters<sup>(20)</sup> was the first to overcome these problems by constructing the first compensated, thermally stable modulator. As a result of the various composite schemes reported compensation of birefringence and stability is achieved both for temperature changes and for changes in angles of incidence as well. An essential requirement of this technique is that the temperature changes should be equal in

each crystal, which is difficult to achieve in practice. Other stability problems also exist associated with long composite schemes and the half wave plate, sometimes present inside the modulator.

The need for stability has led to a demand for devices which perform automatic optical bias control. Many different types of auto bias control have been reported but they all rely on some form of a negative feedback closed loop control system to generate a voltage, which in turn changes the modulator bias in a direction necessary to minimise the drift and restore the operating point. Even though a well compensated composite crystal scheme without an auto bias control results to a stability of a few tens of mrad per degree as opposed to changes of many rads per degree for an uncompensated crystal scheme.

#### 8.2.2 Method of measurement and results.

The modulator was filled with a high thermal conductivity index matching fluid (silicon oil DC550) to achieve rapid heat transfer and ensure fast thermal equilibrium within the modulator cavity. The modulator was placed inside a temperature controlled chamber but unfortunately accurate stabilisation of the temperature was not possible. A stability of about  $\pm 1^\circ$  was obtained with a thermostat. The modulator was placed between crossed polarisers. The polarising elements, laser and detector were placed outside the chamber in order to avoid possible birefringence changes

not related with the modulator stability. A chart recorder and a thermocouple were used to record the detector voltage versus the temperature change. Results were obtained for different number of passes. For comparison purposes the temperature stability of a commercial 45° y-cut air filled crystal modulator was also obtained. The results are presented in figures 8.4 and 8.5. The intensity variation of the liquid filled (0°,45°,45°) cut and air filled 45° cut modulators was also plotted for an abrupt temperature change, fig. 8.6. Comparison of the two graphs clearly shows that the index matching liquid assists to a rapid heat transfer and as a result the modulator stabilises faster to the new operating point.

	V <sub>MIN</sub> (mV)	V <sub>MAX</sub> (V)	ΔV (mV)	ΔΓ	drift	
One pass at 0°	6	6.0	1.0	1.5°	0.8%	A
One pass at 5°	120	6.0	25.0	7.4°	4.1%	B
45°x cut at 0°	6	4.0	3.5	3.4°	1.9%	C
3 passes	90	5.0	35.0	9.6°	5.3%	D
5 passes at 1mW	45	4.5	45.0	11.4°	6.3%	E
5 passes at 5mW	10	1.0	75.0	32.0°	18.0%	F
7 passes	90	4.0	25.0	9.0°	5.0%	G
9 passes	80	3.5	50.0	13.7°	7.6%	H

Table 8.1 Temperature stability results.

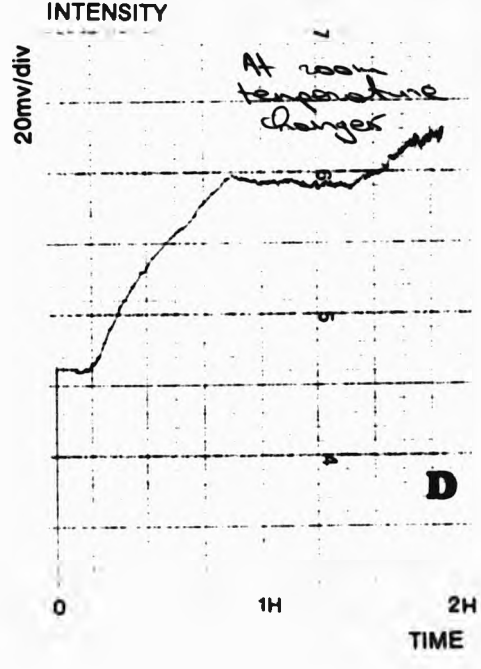
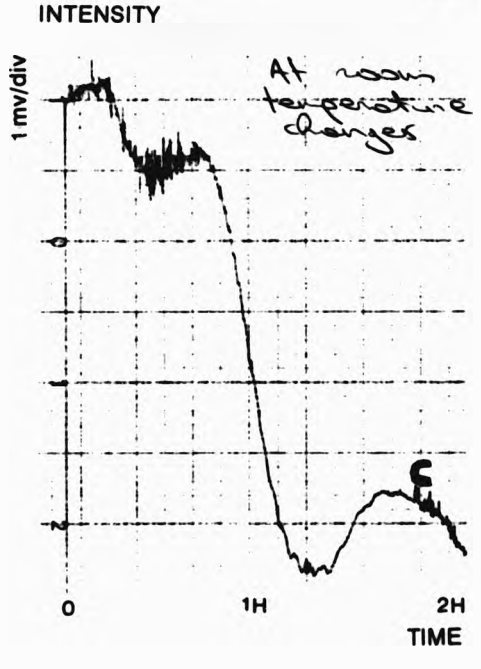
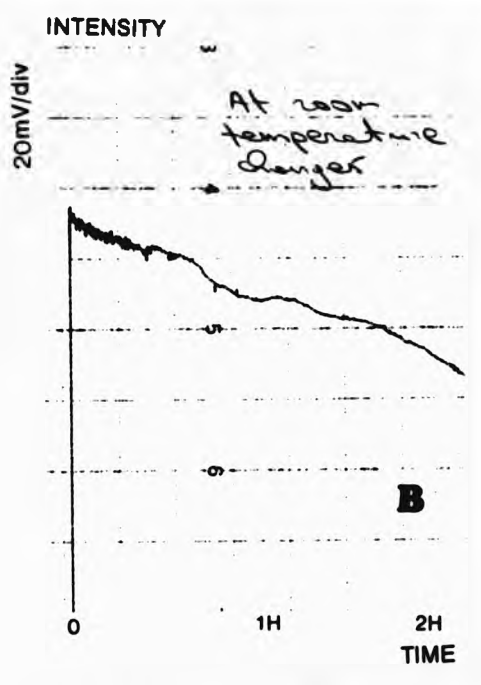
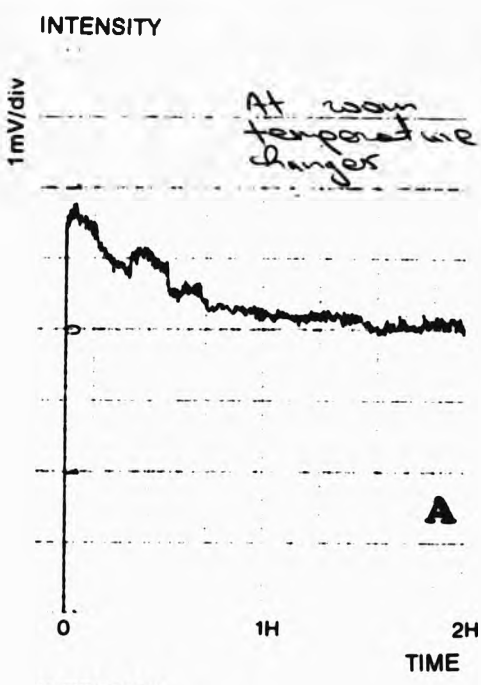


Fig. 8.4 Temperature stability results.



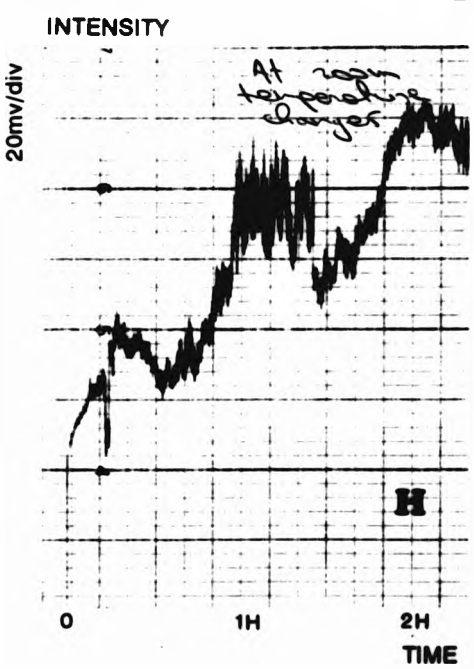
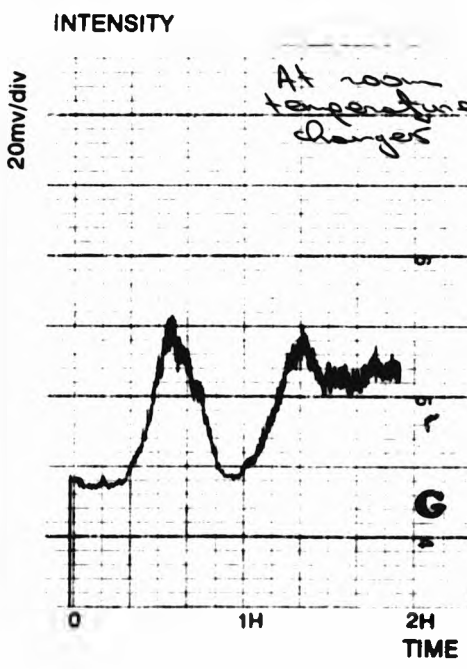
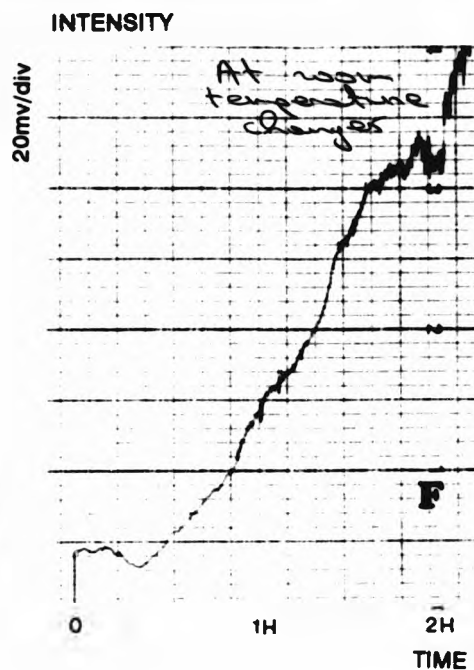
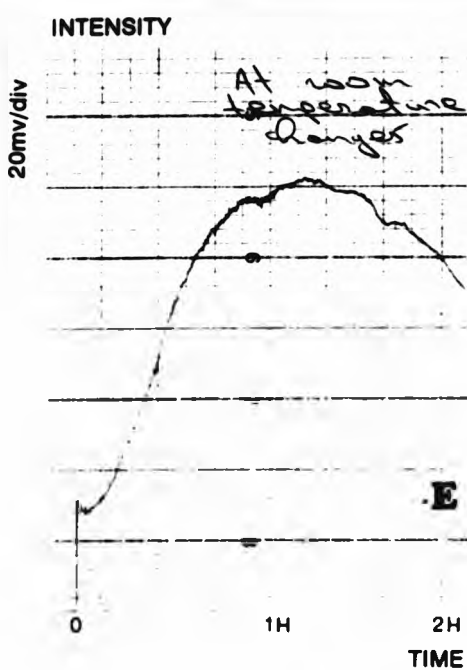


Fig. 8.5 Temperature stability results.

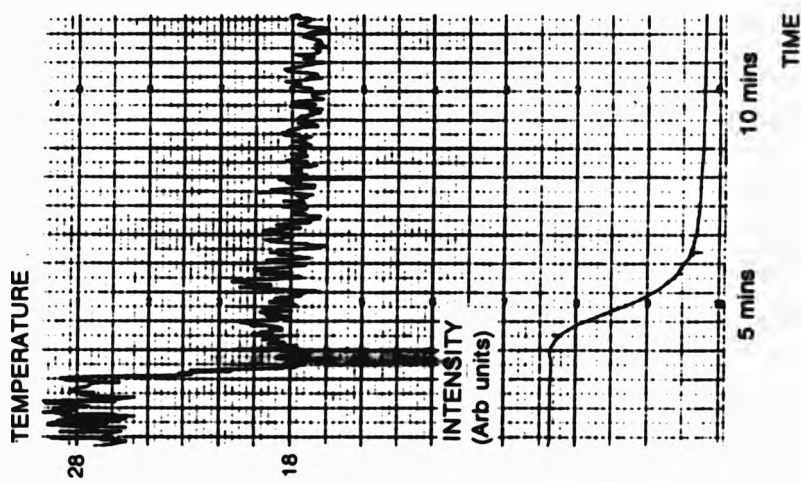
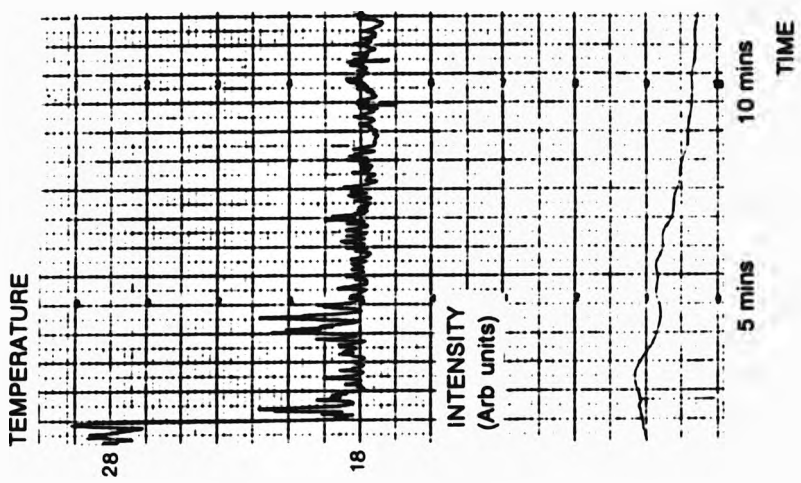


Fig. 8.6 Temperature stability results.

## CHAPTER 9 FREQUENCY RESPONSE OF AN ELECTRO-OPTIC MODULATOR

### 9.1 Introduction.

When considering the problems associated with electro-optic modulators one severe limitation is their bandwidth. The purpose of this chapter is to consider some of the basic factors limiting the highest usable modulation frequency. It is also intended to discuss and present methods of overcoming these limitations to some extent and as a result utilise a wider bandwidth for a given modulator. As the state of the art in laser beam recorders advances and optical media with large storage density capability and rapid access time become available the need for broader modulation bandwidths increases. This demand has marked the design of modulators in the last few years. Viewing an electro-optic modulator as a dielectric then its simplest equivalent is that of a real capacitor. The dielectric material corresponds in its electrical behaviour to an ideal condenser and a resistor in parallel. The representation of an electro-optic crystal by lumped circuit equivalents is done so that the storage and dissipation of electric and magnetic energy in the medium can be determined and hence its frequency behaviour. The parallel resistance represents the dielectric loss ie the energy dissipated in the crystal in unit time when an electric field acts on it, which in turn causes heating of the dielectric. In the case where a number of electro-optic crystals are connected in parallel, then they can be regarded as a capacitor loading the modulating amplifier. For most

practical purposes a certain length of transmission line is also used to connect the modulator with the driving electronics. The lumped circuit can be easily analyzed but it should be noted however that as the modulation frequency increases the transit time of light across the modulator becomes significant compared to the period of the modulating voltage. This not only decreases the efficiency of modulation but it also makes the lumped circuit equivalent inadequate to describe the behaviour of the circuit. Similar considerations dictate that the modulator length should be much shorter than the electrical wavelength at the frequencies of interest. The above conditions more simply mean that the electric field in the modulator should be constant during the transit time for the light through the crystals and uniform over the length of the modulator, ie:

$$\begin{aligned} \tau_m > \frac{nl}{c} \quad \text{and} \quad \lambda_m > L \\ \text{or} \quad L < \frac{c}{f_m n} \quad \text{and} \quad L < \frac{c}{f_m \sqrt{\epsilon}} \end{aligned} \quad 9.1$$

where:

$f_m$  is the highest modulating frequency

$\sqrt{\epsilon}$  is the dielectric constant of the crystal in the direction of the applied field

$L$  is the total length of interaction between the electrical and optical waves.

$n$  is the refractive index associated with the light wave propagating through the crystal

It has to be mentioned that in the case of the multipath modulator the first condition in 9.1 becomes even tighter

because the total time for the light to pass through the modulator is a multiple of the number of passes  $d$  ie,

$$L \ll \frac{c}{df_m n} \quad 9.2$$

Since usually  $\sqrt{\epsilon} \gg n$  the first restriction is dominant for a single pass modulator but in a multipath modulator the two values can be comparable in magnitude. In such a case both values for  $L$  have to be computed and the smaller has to be the dominant restriction for the design. Considering now the situation illustrated in fig. 9.1 a, where:

$R_0$  is the generator impedance (usually  $50\Omega$ )

$TL$  is a length of a transmission line

$C_T$  is the modulator total capacitance including the parasitic capacitance which is in the order of a few tens of picofarads

$G$  is the lossy component of the crystal given by

$$G = 2\pi f C \tan \delta \quad 9.3$$

where  $\tan \delta$  is the loss tangent of the electro-optic material. The magnitude of  $G$  is usually very large and can be ignored<sup>(42)</sup> for most practical purposes. The input impedance  $Z_{IN}$  loading the generator is

$$Z_{IN} = Z_c \frac{Z + jZ_c \tan \beta l}{Z_c + jZ \tan \beta l} \quad 9.4$$

where  $Z_c$  is the characteristic impedance of the line and  $\beta$  is the phase factor. If the interconnecting cable between the modulator and the driver has a physical length much smaller than the wavelength of the modulating field inside the cable at the maximum modulation frequency ie  $l/\lambda_m \approx 0$  then,

$$\tan \beta l = \tan 2\pi \frac{l}{\lambda_m} = 0 \quad 9.5$$

The capacitance of the cable can be ignored and as a result  $Z_{IN}$  can be written as,

$$Z_{IN} = Z = \frac{1}{j2\pi f C_T} \quad 9.6$$

From the transfer function

$$T(j\omega) = \frac{V_M}{V_S} = \frac{V_M}{V_S + V_M} = \frac{1}{R_0 + \frac{1}{j\omega C}} \quad 9.7$$

the -3dB bandwidth is found to be

$$f_{-3dB} = \frac{1}{2\pi R_0 C_T} \quad 9.8$$

For typical modulator capacitances (180pF) and a 50Ω driver output impedance bandwidths of up to about 20MHz can be achieved this way, at a reasonable halfwave voltage. Increasing the bandwidth can be achieved in a number of ways. In fig 9.1 b an inductance is provided in series with the modulator and if the inductance value is correctly chosen then the resulting inductive peaking increases the bandwidth by a factor of  $\sqrt{2}$  over the value given by 9.8. The correct value of inductance can be calculated from

$$L = \frac{CR^2}{\sqrt{2}} \quad 9.9$$

In fig 9.1 c the modulator is terminated with a load resistor  $R_L$  that is matched to the generator impedance  $R_0$ . From the transfer function

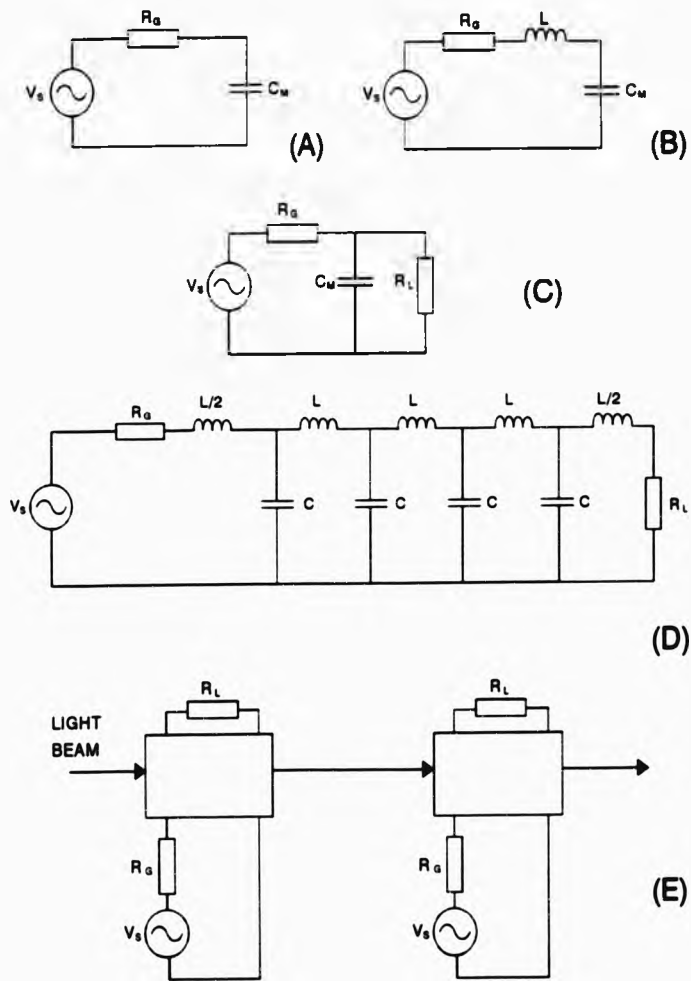


Fig. 9.1 Modulator driving configurations.

$$T(j\omega) = \frac{V_M}{V_S} = \frac{R_L}{R_G + R_L + j\omega C_T R_L R_G} \quad 9.10$$

the -3dB bandwidth is

$$f_{-3dB} = \frac{1}{\pi R_G C_T} \quad 9.11$$

Although this results in a bandwidth improvement factor of 2, half of the modulating voltage drop is across  $R_G$  and is thus wasted since it does not contribute to the modulation. This can be only remedied by doubling the modulating signal level. If bandwidth requirements exceed the limits of the modulator configurations discussed so far, the most efficient method of obtaining a broader bandwidth is to configure the modulator as a transmission line. An artificial delay line is constructed in which the crystals and their electrodes are incorporated as lumped elements, fig. 9.1 d. Effectively this is a constant  $k$  delay line or filter<sup>(43,44)</sup> with a cut off frequency  $f_c$  given by:

$$f_c = \frac{1}{\pi\sqrt{LC}} \quad 9.12$$

For frequencies much lower than the cut off frequency  $f_c$  the characteristic impedance of a correctly terminated line is independent of frequency and purely resistive, given by

$$Z_k = \sqrt{\frac{L}{C}} \quad 9.13$$

Over this range of frequencies for which the characteristic impedance  $Z_k$  of the line is purely resistive the attenuation is zero and all the power is transmitted down the line (ie across the crystals) and finally absorbed by the terminating



resistor. A termination  $R_0 = Z_t = R_L$  at the receiving end has to be provided so that any reflections at the output termination will be absorbed at the input end. It is claimed<sup>(2)</sup> that the above technique results to a bandwidth improvement of 2.5 over the simple lumped capacitance modulator. Realisation of an even wider bandwidth can be now achieved in two ways. One is to reduce the intrinsic propagation delay of the line by reducing its characteristic impedance and the terminating resistors at the generator and load ends. Unfortunately this will also increase the power requirements. Also cables with characteristic impedances less than the standard  $50\Omega$  are not commercially available. The second and most viable alternative to reduce the electrical delay is to connect each crystal or pair of crystals to an independent driver amplifier driven by a common modulating signal source. This way the crystals are driven electrically in parallel and optically in series as shown in fig 9.1 e. The bandwidth improvement is now a factor of 4 over the simple capacitance modulator but two drivers are required which makes this solution prohibitively expensive.

#### 9.2 A new bandwidth broadening technique.

From all the bandwidth broadening techniques discussed so far the most efficient and cost effective is to configure the modulator as a constant  $k$  delay line. It has already been mentioned that the upper frequency of modulation is limited by the electrical delay of the line. This delay causes a lag

of phase of the modulating signal across the crystals during the time taken for the light to travel through the crystals. For maximum retardation the electrical and optical signals should interact constructively in each crystal throughout the modulator. This can be achieved by matching the velocity of the forward light wave to the forward modulating wave. The modulator bandwidth depends on the degree of mismatch between the light and modulating velocities and can be found as follows.

Signals that are applied at the input of the transmission line modulator will be delayed and the amount of delay per section  $t_s$ , is given by<sup>(43)</sup>:

$$t_s = \frac{\beta}{2\pi f} \quad 9.14$$

The phase factor  $\beta$  is found from

$$\beta = \cos^{-1} \left[ 1 - 2 \left( \frac{f}{f_c} \right)^2 \right] \quad 9.15$$

For frequencies much less than  $f_c$ , we can assume that the delay per section is constant so that equation 9.14 can be written as

$$t_s = \frac{1}{\pi f_c} = \sqrt{LC} = RC \quad 9.16$$

As the delay becomes comparable to the period of the modulating signal the magnitude of the voltage at each crystal will be different at the same time instant. Considering a light beam that passes through the crystals and assuming also a negligible transit time, then the light beam experiences a phase retardation

$$\Delta\phi \propto (V_{C_1} + V_{C_2} + V_{C_3} + V_{C_4}) \quad 9.17$$

Introducing the phase lag arising from equation 9.16,  $\Delta\phi$  can be written as

$$\begin{aligned} \Delta\phi &= \sin\omega t + \sin(\omega t + \phi) + \sin(\omega t + 2\phi) + \sin(\omega t + 3\phi) \\ &= 2\sin(\omega t + \frac{3\phi}{2})\cos\frac{3\phi}{2} + 2\sin(\omega t + \frac{3\phi}{2})\cos\frac{\phi}{2} \\ &= 2(\cos\frac{3\phi}{2} + \cos\frac{\phi}{2})\sin(\omega t + \frac{3\phi}{2}) \\ &= 4\cos 2\phi \cos\phi \sin(\omega t + \frac{3\phi}{2}) \end{aligned} \quad 9.18$$

At DC  $\phi=0$  and maximum retardation is obtained. The -3dB bandwidth is defined as the frequency at which the phase retardation  $\Delta\phi$  is reduced by  $\sqrt{2}$  below its maximum value ie when

$$\cos\phi \cos\frac{\phi}{2} = \frac{1}{\sqrt{2}} \quad 9.19$$

This occurs when  $\phi=0.715$  rads or  $41^\circ$ .

Therefore the time delay introduced by one crystal section should not shift the wave phase by more than 0.715 rads at the highest modulating frequency, thus

$$T_{-3dB} \geq t_s \frac{2\pi}{0.715} \quad \text{or} \quad f_{-3dB} \leq \frac{0.113}{RC} \quad 9.20$$

This results to a bandwidth improvement factor of 2.8 over the lumped modulator case. This is the maximum theoretical frequency limit that can be obtained assuming constancy of the delay per section  $t_s$  with frequency. In practice a marginally less bandwidth is to be expected because  $\beta/\omega$  is not independent of frequency which can be easily understood by inspecting equation 9.15. In fact as the frequency is increased the delay is also increased.

A constant k delay line was simulated using SPICE. Figure 9.2 shows the variation of the modulating index as a function of frequency and suggests that useful modulation can be achieved up to about 55 MHz. This is to be compared with the value of 58MHz, which is the result of equation 9.20. Even though the bandwidth improvement is a factor of 2.7.

The variation of  $t_s$  with frequency can be modified considerably by permitting coupling to exist between the two inductors of the constant k section. This modification leads to the m derived delay line<sup>(45,46,47)</sup> shown in fig. 9.3 a. The phase change per section within the passband is given by

$$\cos\beta = 1 - \frac{2m^2 \left(\frac{f}{f_c}\right)^2}{1 - (1-m^2) \left(\frac{f}{f_c}\right)^2} \quad 9.21$$

For  $m=1.27$  it turns out that the variation of  $\beta$  with  $f$  is reduced and for values of  $m$  greater than 1.27, the delay per section is reduced as the frequency gets higher. It is easily understood that a significant amount of phase compensation is achieved so that a potentially higher bandwidth can be realised this way. Further to the above, in order to obtain full advantage of the phase properties of the m derived networks the line must work into a source and load impedance that is equal to the characteristic impedance of the line. Such matching will reduce reflections at the terminations. Unfortunately it is not practical to meet this requirement because the characteristic impedance of the constant k and m derived lines varies considerably over the passband. As an example the variation of the input impedance of the constant

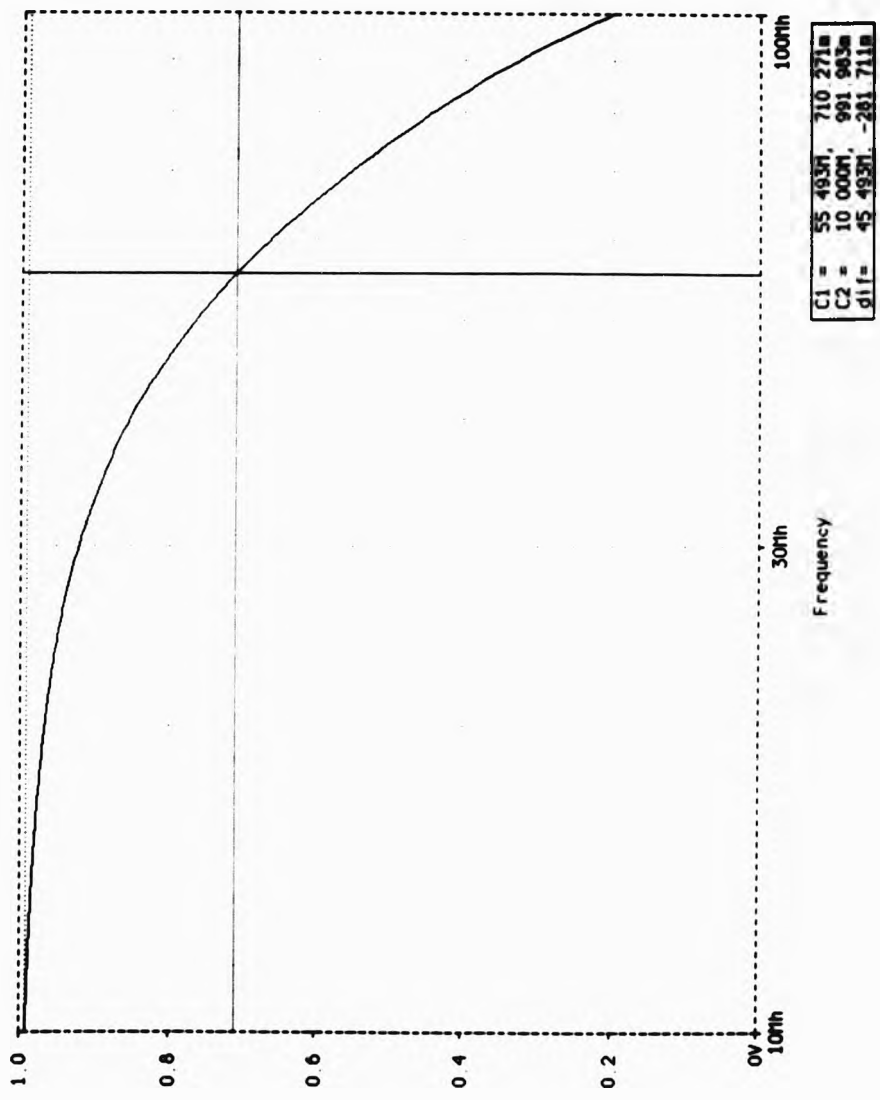


Fig. 9.2 Modulation index versus frequency.

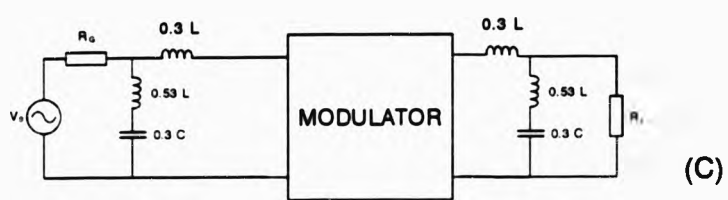
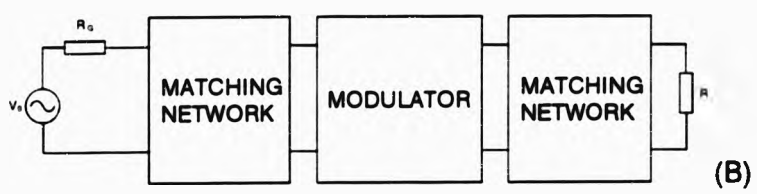
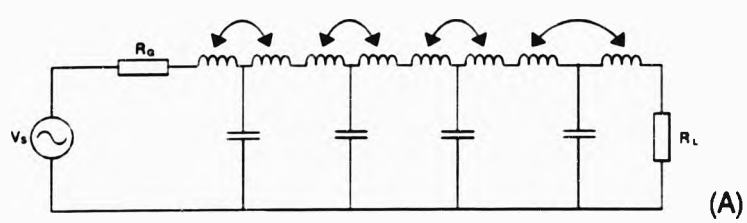


Fig. 9.3 Modulator driving configurations.

k line was plotted and is illustrated in fig. 9.4 a. Interaction and reflection losses that take place at the terminations have the result that the attenuation is not constant or zero over the modulation bandwidth but increases with the degree of mismatch between the terminating and characteristic impedance. Therefore to utilise the full potential of an m derived line modulator the line should be accurately matched over the expected bandwidth. It is possible to improve matters by introducing sections between the line and each resistive termination. A suitable network is an m derived half section with  $m=0.6$  and the principle is illustrated in fig. 9.3 b. For a modulator utilising the above principle the input impedance was constant to within 5% over 90% of the passband, fig. 9.4 b. The design equations for the half sections are

$$L_1=0.3L \quad L_2=0.53L \quad C_1=0.3C \quad 9.22$$

### 9.3 Experimental.

The four crystals were equally spaced on a nylon platform 100mm long. A step generator with a rise time of 100ps was used to drive the modulator with 250V pulses, enough to produce 50% modulation. An avalanche photodiode (APD), reverse biased at 200V through a 50Ω load resistor was used to detect the optical pulses and the output was fed to a 100MHz digital storage oscilloscope. To minimise any stray capacitances the APD was mounted on a BNC connector which was directly connected in the oscilloscope input. The rise time

k line was plotted and is illustrated in fig. 9.4 a. Interaction and reflection losses that take place at the terminations have the result that the attenuation is not constant or zero over the modulation bandwidth but increases with the degree of mismatch between the terminating and characteristic impedance. Therefore to utilise the full potential of an m derived line modulator the line should be accurately matched over the expected bandwidth. It is possible to improve matters by introducing sections between the line and each resistive termination. A suitable network is an m derived half section with  $m=0.6$  and the principle is illustrated in fig. 9.3 b. For a modulator utilising the above principle the input impedance was constant to within 5% over 90% of the passband, fig. 9.4 b. The design equations for the half sections are

$$L_1=0.3L \quad L_2=0.53L \quad C_1=0.3C \quad 9.22$$

### 9.3 Experimental.

The four crystals were equally spaced on a nylon platform 100mm long. A step generator with a rise time of 100ps was used to drive the modulator with 250V pulses, enough to produce 50% modulation. An avalanche photodiode (APD), reverse biased at 200V through a 50Ω load resistor was used to detect the optical pulses and the output was fed to a 100MHz digital storage oscilloscope. To minimise any stray capacitances the APD was mounted on a BNC connector which was directly connected in the oscilloscope input. The rise time



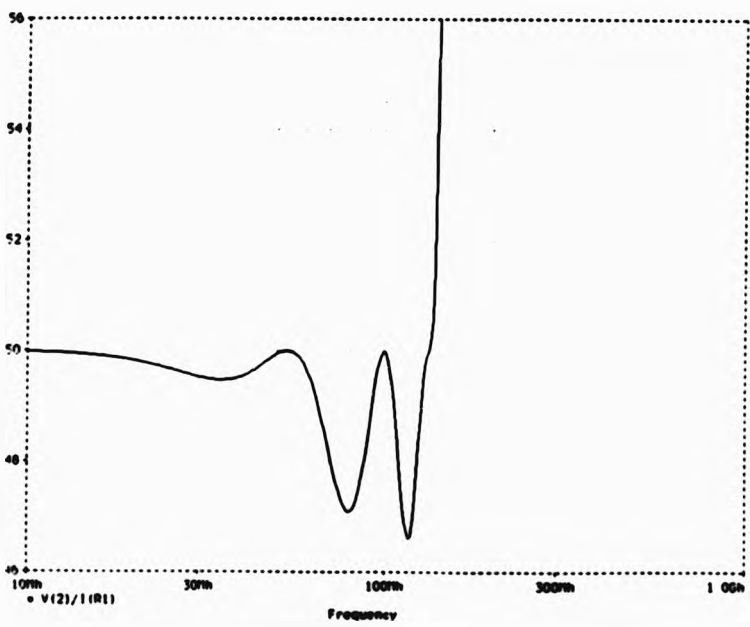
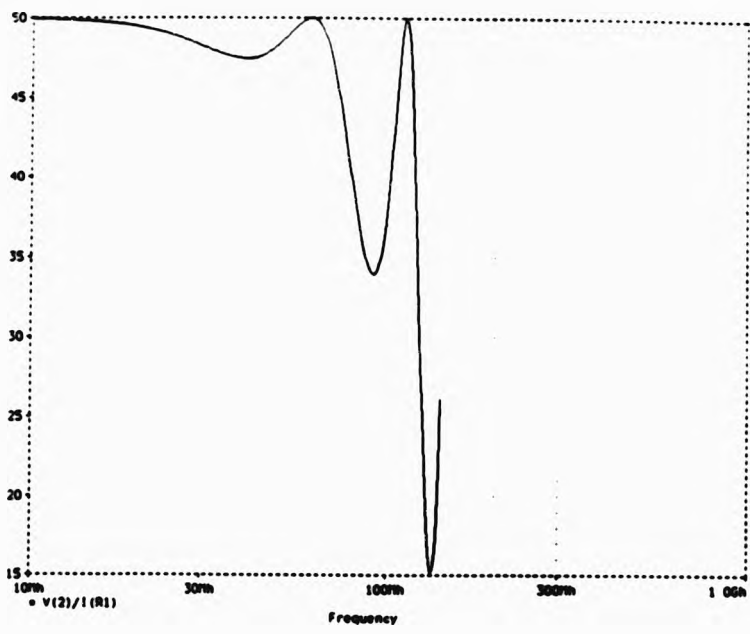


Fig. 9.4 Input impedance variation for constant k and half m derived terminated modulator.

of the system was measured to be 4.5ns which is in excellent agreement with its estimation from the oscilloscope's and APD's capacitance figures. A 5pF parasitic capacitance was also assumed to be present. Strips of copper were used to provide the necessary inductance between the crystals. The strips were preferred at this stage over the round coils to minimise inductive coupling between them so that the construction was matching as close as possible the constant k delay line. The required length of the strip was experimentally found by driving it in series with a known value capacitor. A spectrum analyzer was used to locate the resonance frequency indicated by a sharp dip until the correct value was finally obtained.

The detected pulse is shown in fig. 9.5 a and b. From the rise time of the system

$$t_s = 1.1 \sqrt{t_{CRO+D}^2 + t_M^2} \quad 9.23$$

the modulator rise time was calculated to be 7.3ns which corresponds to a bandwidth of

$$f_{-3dB} = \frac{0.35}{t_M} = 48\text{MHz} \quad 9.24$$

The strips were replaced with air cored coaxial coils suitably arranged and connected to achieve a coefficient of coupling greater than 1. Half m derived sections were also incorporated at both ends of the modulator to minimise reflections. This time the detected response was 7ns and is shown in fig. 9.5 c and d. The rise time of the modulator was again calculated using equation 9.23. A value of 5ns was obtained which is the equivalent of a 70MHz bandwidth.

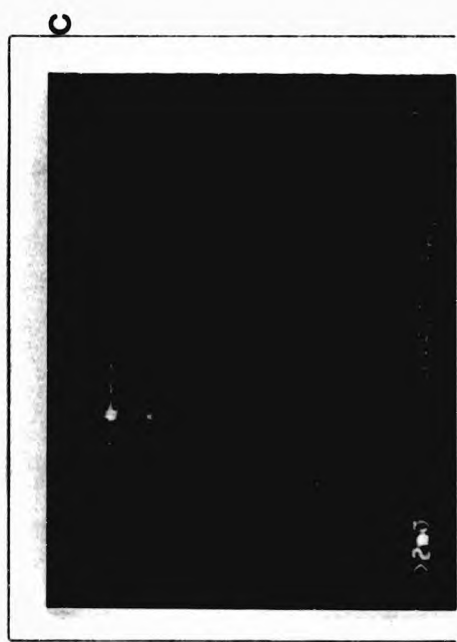
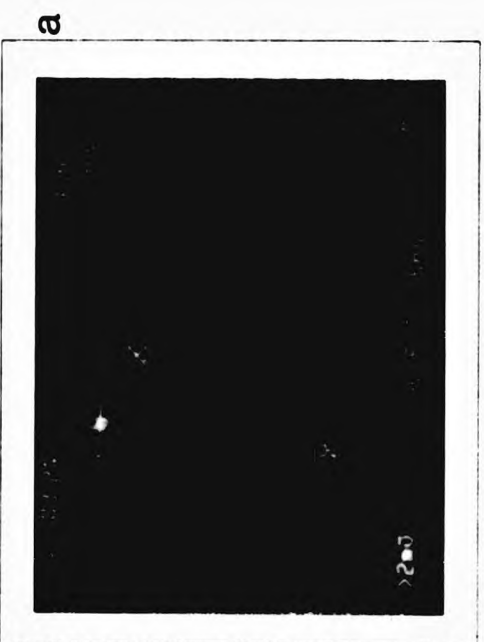
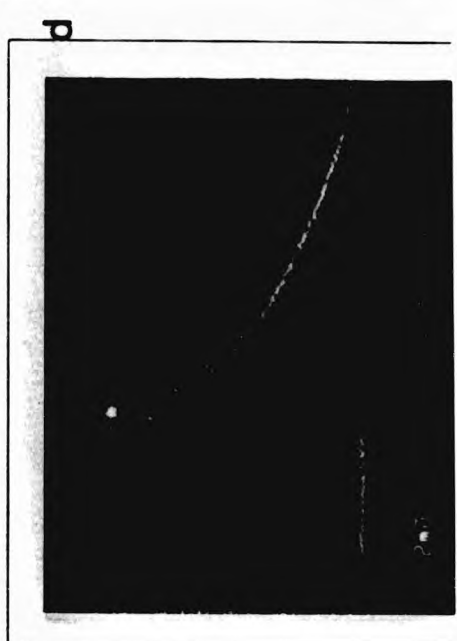
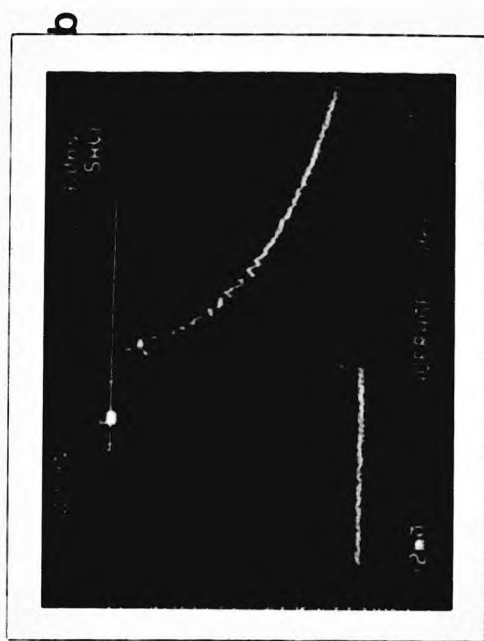


Fig. 9.5 Modulator step response.

Equation 9.23 is accurate to within 10% so it is reasonable to expect the same uncertainty for the rise time and the bandwidth.

#### 9.4 Conclusions and suggestions for further work.

The bandwidth of the modulator when configured as a constant k delay line was practically found to be 48MHz. This value is to be compared with:

(a) the value of 58MHz obtained theoretically from equation 9.20 which is the result that would be obtained if the terminating impedance was the image impedance at all frequencies and if all the frequency components in the input signal were delayed by the same amount.

(b) the value of 55MHz obtained from the SPICE simulation which takes into consideration all the variations of phase and impedance over the passband.

The results obtained experimentally and from SPICE simulation are in good agreement as expected. The constant k delay line modulator results to a practical bandwidth improvement of a 2.5 factor over the lumped modulator. It was also verified experimentally that by permitting coupling to exist between the inductors of the modulator the bandwidth can be improved considerably. The 70MHz bandwidth obtained corresponds to an improvement factor of 3.5 over the lumped modulator. It also increased the bandwidth of the constant k

modulator by 40%. It is not possible to provide an accurate justification for this improvement figure because of difficulties and uncertainties related with an accurate determination of the coupling coefficient that was achieved in practice. Formulae for the calculation of the mutual inductance between two coils critically depend on the separation and relative positions of the coils and require accuracy in all dimensions, number of turns, tapping points etc. This was not possible during the modulator construction at an experimental stage. It is well known to the RF engineers that these things are best done by trial and error. The aims of the analysis in this chapter were to push the frequency response of an electro-optic modulator beyond the limits of the today's technology and this has been theoretically justified and practically demonstrated.

Other problems that have to be considered are losses mostly on the inductors and some in the crystals and the distributed capacitance associated with the coils. Losses and mismatch both tend to reduce the power reaching the crystals. The result is that the modulation index is reduced as the frequency is increased. For a practical design a suitable value for the coupling coefficient has to be selected to achieve a certain bandwidth. When this has been determined then it has to be ascertained whether satisfactory elements can be constructed inside the modulator cavity. Experience shows that there are always economic and physical limits beyond which we can not go. Nevertheless because the inductance values we are concerned with are of the order of

a few hundred of nanohenries it seems feasible to wound all of them suitably spaced on a core inside the modulator cavity. Note that significant bandwidth improvements can be obtained only for values of  $m$  much greater than 1 which means coupling coefficients approaching unity. This suggests that the inductors of the same section only should be wound on ferrite rods with the crystal connected to the centre of the inductors to achieve the maximum possible coupling coefficient.

**CHAPTER 10 DISCUSSION, CONCLUSIONS AND SUGGESTIONS FOR FURTHER WORK.**

10.1 Discussion and conclusions.

The behaviour of a low voltage novel modulator has been analyzed in detail. This modulator differs from the existing modulators in two crucial ways. A novel crystal cut was used together with a multipath reflection technique. The basic underlying theory for this cut and the multipath reflection technique have been discussed. Based on this novel cut it was found that there are six composite modulator schemes. These schemes do not require a half wave plate and therefore the proposed modulator can be used with any optical wavelength. Temperature stability and wavelength dependence problems associated with the use of wave plates do not exist. Further to the above the proposed scheme allows multiple reflected paths and as a result the typical halfwave voltage is reduced by a factor dependent on the number of passes. Also coplanar electric fields are used which eliminate engineering problems associated with  $90^\circ$  crystal rotations and application of fields.

Initially the analysis treated all the important practical factors which limit the operation and the performance of the modulator. In essence this procedure requires that the dimensions of the crystal to be chosen so that large reductions of the half wave voltage are obtained with moderate number of passes. For the multipath reflection

technique the maximum length of the crystals obtainable from typical ADP crystal boule sizes is not a limitation since wider crystals are used which are obtainable. A half wave voltage of 65V has been obtained for seven passes and has verified the outlined principles of operation. While examining other performance characteristics it was found that the modulator was suffering from a low extinction ratio. Initially it was thought that this was the result of the alignment of the mirrors. Several months were spent in fruitless attempts to obtain an acceptable extinction ratio by readjusting the mirrors.

A study on the extinction ratio of an electro-optic modulator revealed the parameters which have an effect on the extinction ratio. Based upon this study it was found that there were three main aspects in the improvement to better extinction ratio modulator design. The first was the effect of the rays lateral displacement inside the crystals. The second was the misalignment of the crystals with respect to each other. The third and of most significance was the angle of propagation inside the crystals. These problems have been discussed and a realistic optimum design has been presented. This design is based on:

(a) a composite crystal scheme with minimum ray separation and hence minimum aperture requirement.

(b) individual crystal adjustments which enable all crystals to be positioned parallel to within 2 arc minutes.



(c) a longer modulator cavity and as a result a reduced angle of propagation.

Extinction ratios better than 2000:1 on a single pass and normal incidence reduce to between 50:1 and 150:1 for various passes in the multipath modulator. The single pass extinction ratios obtained are comparable or even better than extinction ratios obtained from longitudinal one crystal modulators and far superior from extinction ratios obtained from state of the art commercial transverse modulators. The multipass extinction ratios although on the low side they might be useful for some applications.

It has proved essential to carry out a theoretical investigation in the dependence of the extinction ratio on the angle of light propagation inside the modulator. A general analysis for double refraction at an oblique angle of incidence has been presented. The analysis shows that in general not one but two principal planes effectively exist. As a result there is a rotation in the crystal's polarisation directions which depends on the angle of incidence. The rotation of axes causes some of the resolved light components to propagate with their phase not affected by the applied electric field. These unmodulated components represent a light leakage through the analyzer which sets the maximum possible extinction ratio. Further to the above the analysis also permits an estimation of the extinction ratio as a function of the angle of incidence. The results have been found to be very close to the experimental results.

In order to fully investigate the novel modulator other performance parameters were also examined. Beam profile results indicate that the profile of the beam leaving the modulator will not be affected significantly by the number of passes, assuming the crystals' aperture is large enough to safely accommodate the beam. Finally the modulator proved to be thermally stable. However it should be noted that stability degraded with the number of passes, as expected. The practical realisation of these modulators is very feasible and should not present any additional problems to the ones encountered with current commercial electrooptic crystal modulators.

Some of the characteristics and limitations associated with the frequency response of electrooptic modulators have been also discussed. Commercial state of the art modulators offer the widest possible bandwidth from a modulator by incorporating the electro-optic crystals into a transmission line as lumped capacitors. Analysis has shown that the modulator behaves electrically as a constant  $k$  delay line. The delay line per section causes a phase lag of the modulating signal across the crystals which in turn causes a reduction of the modulation depth as the frequency is increased. To overcome this a modulator must be designed specifically to achieve the required delay specifications. It has been found that if the crystals are incorporated in a line which behaves electrically as an  $m$  derived delay line with  $m$  larger than 1 then the useful modulation bandwidth can be increased. This in effect is achieved by making the line

intentionally dispersive. This was verified experimentally by constructing such an m derived modulator. Problems associated with complexity in the construction and the uncertainties involved in achieving a certain coupling coefficient within the individual sections of the line, did not permit a tight correlation between the derived theoretical improvement factor and the experimental results obtained. Nonetheless, the feasibility of wider bandwidth electrooptic modulation, using the proposed technique, has been demonstrated.

#### 10.2 Suggestions for future work.

As far as the practical realisation of the  $(0^{\circ}, 45^{\circ}, 45^{\circ})$  cut multipath modulators is concerned there are no alignment and constructional problems. However it should be noted that at the present time extinctions of the required ratio (at least 100:1) are not feasible. Continuing research however, indicates that this situation should improve. Because the angle of propagation limits the extinction ratio in a fundamental way, a practical design is required in which one can achieve multiple reflected paths at normal incidence. For example this could be achieved by placing the crystals in a cavity where four mirrors suitably spaced and orientated make the beam travel always normal to the crystals. However this design requires four mirrors and hence more complicated adjustments.

It is believed that normal propagation can be achieved at the expense of more complicated design and optical components. Clearly this should be investigated and critically evaluated.

Further substantial work with the proposed modulator could also exist in the investigation of modulation of a white light beam. A white light beam could be divided and filtered into three colours, (red, green, blue), so that each colour would be individually modulated. At the output of the modulator the three beams could be combined with a lens to produce a spot of different colours. Such a modulator might prove useful in large area display systems, colour proofing applications etc. Alternatively three lasers at the required wavelengths could also be used for the above application.

Also, if time had allowed the author would have liked to construct  $m$  derived delay line modulators and examine their frequency response. It has to be mentioned that this can be also done using SPICE to simulate such a modulator. This way, the bandwidth, step response and the overshoot can be easily obtained for various values of  $m$ . An optimum design could then be selected and practically realised. Some of the problems associated with the construction of such a modulator have already been discussed in section 9.5.

Also principal theorems exist<sup>(48,49)</sup> on the reflection coefficient obtainable in a circuit including a prescribed parasitic element. These theorems deal with the maximum performance possibilities from an amplifier when its output is terminated at one end by a finite resistance and a capacitance in parallel. It is shown that a suitable design allows the presence of  $C$ , (the modulator capacitance), to be compensated and achieve the smallest reflection coefficient

over the widest possible bandwidth. This way the modulation bandwidth can be significantly increased. It is important to appreciate that these theorems do not in themselves provide a complete design technique, however they suggest the general framework for a practical design approximating the theoretical limits. The synthesis and construction of such a network should be extremely useful.

The design of a suitable high frequency driver would be an essential part of a complete modulation system, based on the multipath modulator.

As a matter of theoretical interest, the theory presented in chapter 7 regarding double refraction at oblique angles of incidence can be further extended. It should be possible to derive a quantitative analysis that reduces the problem of double refraction into a pure stereometry problem. Such an analysis would permit expressions for the polarisation directions and wave directions as a function of the angle of incidence, the orientation of the crystallographic z axis and the plane of incidence.

Concluding this work, the field of the electro-optics is very active and numerous applications exist requiring modulation of a light beam. The  $(0^\circ, 45^\circ, 45^\circ)$  cut modulators have the potential to contribute to the present technology leading to new application areas for low voltage, multiwavelength, high frequency modulation.

### **Acknowledgements.**

The author wishes to thank the following people and organisations.

My family for their emotional and financial support.

Dr. D. Kalymnios. For his assistance, supervision, advice, criticism and encouragement. Many thanks also for suggesting this topic.

The University of North London. For providing a studentship for the research.

G. Darmanin and Electrooptic Developments Ltd. For the free supply of the electrooptic crystals, equipment, extensive facilities and advice which made this research possible.

Dr. R. Meadows (Head of school). For encouragement and provision of facilities for this work.

R. Harley and T. Clay at the University workshop. For constructing the modulator mechanics and many valuable and insightful suggestions and criticism.

E. Papanicolaou and T. Botsicas in Athens, Greece. For constructing additional mechanics and many helpful suggestions.

David Bell (CLMS Systems and networks manager) and H. Benetatos. For kindly allowing time and use of their facilities to produce this thesis in its final form.

K. K. Cheung. For carefully preparing the diagrams and illustrations. Particularly indebted for his patience.

M. Rummeli. For his help and cooperation.

The Schilizzi Foundation. For financial support.

Dr. I. W. Rogers. For helpful discussions, commentary and criticism.

#### REFERENCES

1. J. Wilson and J. F. D. Hawkes, *Lasers: Principles and applications* Prentice Hall, New York 1987.
2. R. F. Enscoe and R.J. Kocka, *Electro-optic modulation: Systems and applications*, *Laser and applications* June 1984, pages 91-95.
3. R. G. Walker, *High speed III-V Semiconductor intensity modulators*, *IEEE Journal of Quantum Electronics*, vol. 27, no. 3, pp 654-657, 1991.
4. L. Levi, *Applied optics volume 2* page 1027, John Wiley, 1980.
5. J. Watson, *Optoelectronics*, pages 50-51, Van Nostrand Reinhold, 1989.
6. T. Nowicki, *A-O and E-O modulators, basics and comparisons*, *Electro-optical systems design* February 1974, pages 23-28.
7. J. M. Ley, T. M. Christmas and C. G. Wildey, *Light modulators and their applications*.
8. J. M. Ley, *Solid state subnanosecond light switch*, *Proc IEE*, vol 117, No 6, June 1970.
9. J. F. Nye, *Physical properties of crystals*, Oxford

Clarendon Press, 1990.

10. M. Born and E. Wolf, Principles of optics, New York, Macmillan, 1964.

11. E. E. Wahlstrom, Optical Crystallography, John Wiley & Sons, Inc., 1948.

12. Benno, Swicker and Scherrer, Electrooptische Eigenschaften der seignette-elektrischer Kristalle  $\text{KH}_2\text{PO}_4$  und  $\text{KD}_2\text{PO}_4$ , Helv Phys. Acta 16, 214, 1943.

13. B. H. Billings, The Electro-optic effect in uniaxial crystals of the type  $\text{XH}_2\text{PO}_4$ , part 1 theoretical, J. Opt. Soc. Amer, 39, p797-801, 1949.

14. W. J. Deshotel, Ultraviolet transmission of dihydrogen arsenate and phosphate crystals, J. Opt. Soc. Am., vol. 50, p865, 1960

15. F. Pockels, Lehrbuch der Kristallographie, Leipzig: Teubne, 1906.

16. B. H. Billings, The electro-optic effect in uniaxial crystals of the type  $\text{XH}_2\text{PO}_4$ , part 2, experimental. Ibid, p802-808.

17. B. H. Billings, The electro-optic effect in uniaxial crystals of the Dihydrogen Phosphate ( $\text{XH}_2\text{PO}_4$ ) type IV. Angular field of the electro-optic shutter, J. Opt. Soc. Amer, 42,



p12-20 1952.

18. R. O. Carpenter, The electro-optic effect in uniaxial crystals of the dihydrogen phosphate type. III. Measurement of coefficients. J. Opt. Soc. Amer, 40, p225-229, 1950.

19. C. Peters, Gigacycle bandwidth coherent light travelling wave phase modulator, Proc IEEE, 51, p147, 1963.

20. C. Peters, Gigacycle bandwidth coherent light travelling wave amplitude modulator, Proc IEEE, 53, p455, 1965.

21. J. M. Ley,  $V_{M2}$  and  $r_4$ , as a function of wavelength for ADP, Electronics letters, 3, p145, 1967.

22. C. H. Clayson, Low voltage light amplitude modulation, vol2, No 4, pp138, 1966.

23. J. M. Ley, Low voltage light amplitude modulation, Electronics letters, 1966, 2, No 4, p12-13.

24. J. M. Ley, Reply to Clayson on low voltage electro-optic modulation, Electronics letters, 1966, vol 2, No 4, pp139.

25. G. E. Francois and F. M. Libreht, ADP four crystal light modulator, Applied Optics, vol. 11, no. 2, 1972.

26. K. Hookabe and Y. Matsuo, Novel type of cut of KDP crystals for low voltage modulation, Electronics letters, 6, p550, 1970.

27. D. Kalymnios, Optimisation of electro-optic crystal modulators, Electronics letters, 6, 25, p804.

28. W. W. Rigrod and I. P. Kaminow, Wide band microwave light modulation, Proc IEEE, vol 51, pp137-140, 1963.

29. M. DiDomenico, JR and L. K. Anderson, Broadband electro-optic travelling wave light modulators, Bell Sys. Tech. J, vol 42, pp2621-2678, November 1963.

30. Z. V. Nesterova, Broadband UHF modulation of light, Soviet Journal of optical technology, 34, p17-23, March / April 1967, (Engl. Translation).

31. D. Kalymnios, Double field XDP modulators, Proc. Electro-optics'71 International Conference, Brighton, March 1971, p247, 1971.

32. A. C. S. Van Heel, Advanced optical techniques, North Holland Publishing Co., Amsterdam, 1967.

33. I. P. Kaminow, Strain effects in electro-optic crystal modulators, ppl. Optics, 3, p 511-515, 1964.

34. I. P. Kaminow and E. H. Turner, Electro-optic light modulators, Proc IEEE, vol 54, pp1374-1399, October 1966.

35. D. C. Doughty, X-band travelling-wave light intensity modulator using ZnS crystals, Electron. Letts, vol. 4, no. 7, 1968.

36. J. R. Mansell, Video frequency light modulator having a wide angular aperture, Proc. IEE, vol. 116, no. 5, 1969.

37. R. S. Longhurst, Geometrical and physical optics, Longman group ltd., london, 1967.

38. F. A. Jenkins and H. E. White, Fundamentals of optics, McGraw-Hill Inc., 1976.

39. C. E. Curry, Electromagnetic theory of light, Pub. by Macmillan and Co., Limited, 1905.

40. Geometry school textbook 2nd class of Lyceum, National organisation of publications of textbooks, Greece 1980.

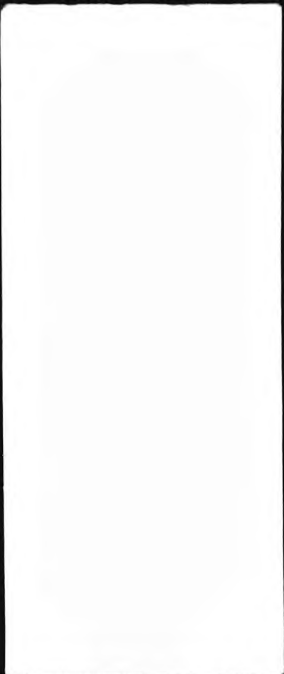
41. E. Hecht and A. Zajac, Optics, Addison-Wesley Publishing company, 1974.

42. F. S. Chen, Modulators for optical communications, Proc. IEEE, vol. 58, pp. 1440-1457, Oct. 1970.

43. M. E. Van Valkenburg, Network analysis, sec. 13-8, Prentice-Hall, Inc., Englewood Cliffs, N.J., 1955.

44. F. R. Connor, Networks, sections 4 and 5, Edward Arnold Ltd., 1972.

45. J. Millman and H. Taub, Pulse, digital and switching waveforms, McGraw-Hill, Inc., 1965.



46. J. B. Trevor, Artificial delay line-design, *Electronics*, vol. 18, pp. 135-137, June 1945.

47. I. A. D. Lewis and F. H. Wells, *Millimicrosecond pulse techniques*, Pergamon Press Ltd., 1959.

48. H. W. Bode, *Network analysis and feedback amplifier design*, D Van Nostrand, 1945.

49. E. A. Guillemin, *Theory of linear physical systems*, John Wiley and Sons, Inc., 1963.

#### ADDITIONAL REFERENCES AND BIBLIOGRAPHY

A. Yariv and P. Yeh, Optical waves in crystals, Wiley-Interscience, 1983, chapters 7 and 8.

A. Yariv, Optical electronics, Holt-Saunders International Editions, 1985.

A. Sommerfeld, Optics, Academic Press, Inc.

4. R. G. Hunsperger, Integrated optics: Theory and practice, Springer-Verlag, 1984.

Karim, Electro-optical devices and systems, PWS-Kent, 1990

J. Wilson and J. F. B. Hawkes, Optoelectronics an introduction, Prentice Hall, 1989.

S. F. Pellicor, Transmittance of some optical materials for use between 0.19 and 0.34 microns, Applied optics 1964, 3, pp361-366.

I. P. Kaminow and J. Liu, Propagation characteristics of partially loaded two conductors transmission line for broadband light modulators, Proc IEEE, 51, p 133-137, 1963.

I. P. Kaminow, Microwave modulation of the electro-optic effect in  $\text{KH}_2\text{PO}_4$ , Phys Rev. Letts, 6, p 528-529, 1961.

C. F. Buhrer, Wideband electro-optic light modulation

utilising an asynchronous travelling wave interaction, *Appl. Optics*, 4, p 545-550, 1965.

Introduction to crystal optics, pub. Cooke, Troughton & Simms Ltd. York, England.

N. H. Hartshorne and A. Stuart, *Crystals and the polarising microscope*, Edward Arnold (publishers) Ltd, 1960.

R. S. Longhurst, *Geometrical and Physical Optics*, pub. Longmans, 1964.

J. L. Putz, A wideband light modulator, *IEEE, Trans. Elect. Dev.* ED15 p 695, 1968.

M. Dore, A low drive power light modulator using a readily available material ADP, *IEEE J. Quantum Electron.*, vol. QE-3, pp. 555-560.

R. T. Denton, F. S. Chen and A. A. Ballman, Lithium Tantalate light modulators, *Journal of Applied Physics*, vol. 38, no. 4, pp. 1611-1617, 15 March 1967.

E. H. Turner, High frequency electro-optic coefficients of Lithium niobate, *Applied Physics Letters*, vol. 8, no. 11, 1 June 1966.

I. P. Kaminow, Barium titanate light modulator II, *Applied Physics Letters*, vol. 8, no. 11, 1 June 1966.

E. V. Sidnenko and I. S. Zheludev, Measurement of the electromechanical and electro-optical coefficients of an ADP single crystal using a Twyman Interferometer, Soviet Physics Crystallography, vol. 12, no. 3, Nov-Dec., 1967.

W. P. Mason, The elastic, piezoelectric, and dielectric constants of Potassium Dihydrogen Phosphate and Ammonium Dihydrogen Phosphate, Physical Review, vol. 69, no. 5 and 6, 1946.

J. H. Ott and T. R. Sliker, Linear electro-optic effects in  $\text{KH}_2\text{PO}_4$  and its isomorphs, Journal of the optical society of America, vol. 54, no. 12, 1964.

M. O. Kada and S. Ieiri, Extinction ratio of electro-optic light modulator, IEEE J. of Q.E., August 1970.

W. R. Rattman, W. E. Bicknell, B. K. Yap, and C. J. Peters, 10.2-Broadband, low drive-power electro-optic modulator, IEEE J. of Q.E., vol. QE-3, no. 11, 1967.

L. L. Steimetz, T. W. Pouliot, and B. C. Johnson, Cylindrical, ring-electrode  $\text{KD}^*\text{P}$  electro-optic modulator, Applied Optics, vol. 12, no. 7, 1973.

K. Wu, C. E. Tong and R. Vahldieck, Microwave characteristics of high-speed traveling wave electro-optic modulators on III-V semiconductors, Journal of Lightwave Technology, vol. 9, no. 10, pp. 1295-1303, 1991.

N. Theofanous, S. Tsitomeneas, G. Alexakis, A. Arapoyianni and G. Papaioannou, A high-voltage electro-optic driver with DMOS power FETs and optocoupling isolation, J. Phys. E:Sci. Instrum., 8, 667-673.

M. Bracale and A. Lombardi, The design of broadband light modulators, The Radio and Electronic Engineer, vol. 39, no. 4, 1970.

E. L. Ginzton, W. R. Hewlett, L. H. Jasberg, and J. D. Noe, Distributed amplification, Proc. IRE, vol. 36, pp. 956-969, August 1949.

W. C. Johnson, Transmission lines and networks, McGraw-Hill Book Company, New York, 1950.



**THE BRITISH LIBRARY**  
BRITISH THESIS SERVICE

**TITLE** THE DEVELOPMENT OF A CRYSTAL MODULATOR  
USING A MULTIPATH REFLECTION TECHNIQUE

**AUTHOR** Vassilis  
BOUGAS

**DEGREE** Ph.D

**AWARDING  
BODY** University of North London

**DATE** 1993

**THESIS  
NUMBER** DX178814

**THIS THESIS HAS BEEN MICROFILMED EXACTLY AS RECEIVED**

The quality of this reproduction is dependent upon the quality of the original thesis submitted for microfilming. Every effort has been made to ensure the highest quality of reproduction. Some pages may have indistinct print, especially if the original papers were poorly produced or if awarding body sent an inferior copy. If pages are missing, please contact the awarding body which granted the degree.

Previously copyrighted materials (journals articles, published texts etc.) are not filmed.

This copy of the thesis has been supplied on condition that anyone who consults it is understood to recognise that its copyright rests with its author and that no information derived from it may be published without the author's prior written consent.

Reproduction of this thesis, other than as permitted under the United Kingdom Copyright Designs and Patents Act 1988, or under specific agreement with the copyright holder, is prohibited.

C 6.

DX

178814